ANALYSIS OF AERO-ELASTIC FORCES IN LABYRINTH SEALS AND THE DESIGN OF AN EXPERIMENTAL FACILITY TO MEASURE THEM

by

KNOX TAYLOR MILLSAPS JR.

B.S. University of Florida
(1983)

SUBMITTED IN PARTIAL FULFILLMENT
OF THE REQUIREMENTS FOR THE DEGREE OF

MASTER OF SCIENCE

at the

Massachusetts Institute of Technology

1987

Signature of Author Signature Redacted
Department of Aeronautics and Astronautics
August 18, 1987

Certified by Signature Redacted
Professor Manuel Martinez-Sanchez
Thesis Supervisor

Accepted by Signature Redacted
Professor Harold Y. Wachman
Chairman, Departmental Graduate Committee

ANALYSIS OF AERO-ELASTIC FORCES IN LABYRINTH SEALS AND THE DESIGN OF AN EXPERIMENTAL FACILITY TO MEASURE THEM

by

KNOX TAYLOR MILLSAPS JR.

Submitted to the Department of Aeronautics and Astronautics on August 18, 1987 in partial fulfillment of the
requirements for the Degree of Master of Science in Aeronautics and Astronautics

ABSTRACT

The aero-elastic forces generated by labyrinth seals and their impact on rotor dynamic stability are discussed. A review of the pertinent literature is given. A lumped parameter model of the flow in a single gland seal based on the theory of Kostyuk is presented. The resulting equations are simplified by changing to a rotating coordinate system. A system of linear algebraic equations is obtained by employing small amplitude perturbation methods and assuming harmonic solutions. This system is non-dimensionalized and solved for the pressure perturbation inside the seal. Results of a design study are presented and specification on a facility to measure these self-exciting forces are given. The final mechanical design along with instrumentation requirements are presented.

Thesis Supervisor: Dr. Manuel Martinez-Sanchez

Title: Associate Professor of Aeronautics and Astronautics, Massachusetts Institute of Technology

ACKNOWLEDGMENTS

I would like to express my sincere gratitude to Professor John Dugundji and Professor Manuel Martinez-Sanchez. Their guidance and insights have led me around and through the many obstacles which have arisen. To both of them I am truly indebted.

Many thanks to Professor Gu, Visiting Professor from Xian Northwest Polytechnic, and Jean-Luc Pouvreau, who provided much help in the design of the facility.

Finally, I would like to state my appreciation for M.I.T. in general and my fellow graduate students in particular. Whether it was watching a game with Alexandros Gioulekas or discussing the finer points of turbulence with Mark Lewis, my friends always supplied personal and intellectual companionship which has made my stay at M.I.T. both rewarding and enjoyable.

This thesis is dedicated to my Mother and Father.

This work was performed under Air Force Grant AFOSR-83-0034. Dr. Anthony Amos was the technical monitor.

TABLE OF CONTENTS

Page

LIST OF ILLUSTRATIONS

NOMENCLATURE

Symbol	Description	Units/MKS
A_1	Actual area between seal knife and seal land.	m^2
C_c	Coefficient of Contraction.	[1]
C_p	Specific heat at constant pressure.	$JKg^{-1}K^{-1}$
C_v	Specific heat at constant volume.	$JKg^{-1}K^{-1}$
d	Thickness of seal in knife.	m
$D = \frac{\delta_1^*}{h}$	Nondimensional sealing gap.	[1]
D_H	Hydraulic diameter	m
e	Base of natural logarithm.	[1]
e	rms roughness of surface.	m
f	Cross sectional area of seal gland.	m^2
f_{D1}	Component of damping force in X_1 direction acting on rotor.	N
f_{D2}	Component of damping force in X_2 direction acting on rotor.	N
f_{S1}	Component of elastic force in X_1 direction acting on rotor.	N
f_{S2}	Component of elastic force in X_2 direction acting on rotor.	N
F_{X_1}	Component of elastic force in X_1 direction acting on rotor.	N
F_{X_2}	Component of elastic force in X_2 direction acting on rotor.	N
$\bar{F}_{X_2} = \frac{\delta_1^* F_{X_2}}{r\pi R_s l P^*}$	Nondimensional out of phase force.	[1]
$H = \frac{h}{R_s}$	Nondimensional height of sealing knives.	[1]
h	Height of sealing knives.	m

Symbol	Description	Units/MKS
I	Sectional moment of inertia of shaft.	m^4
I_1	Disks moment of inertia through neutral axis.	m^4
i	Imaginary base $\sqrt{-1}$.	[1]
K_S	Spring constant of shaft due to bending rigidity.	Nm^{-1}
$L = \frac{l}{R_S}$	Nondimensional distance between sealing knives.	[1]
l	Distance between sealing knives.	m
M	MACH number.	[1]
M_1	Mass of disk.	Kg
$\dot{m}_1$	Total mass flow rate over seal knife.	Kgs^{-1}
N	Number of seal chambers.	[1]
P	Static pressure inside seal gland.	Nm^{-2}
P_i	Static pressure upstream of the seal.	Nm^{-2}
P_o	Downstream static pressure.	Nm^{-2}
P^*	Static pressure inside non-whirling seal.	Nm^{-2}
q^*	Axial flow rate through non-whirling seal per unit circumferential length.	$Kgm^{-1}s^{-1}$
q_1	Flow rate per unit length of seal over first knife.	$Kgm^{-1}s^{-1}$
q_2	Flow rate per unit length of seal over second knife.	$Kgm^{-1}s^{-1}$
r	Radius of seal whirling orbit.	m
R_a	Gas constant for air.	$JKg^{-1}K^{-1}$
Re	Reynolds number.	[1]
R_s	Seal radius.	m
$S = \frac{\omega R_s}{V^*}$	Nondimension spinning frequency of shaft.	[1]

Symbol	Description	Units/MKS
T	Air temperature.	K
t	Time.	s
$\bar{t}$	Time in rotating coordinate system.	s
V	Circumferential velocity in seal gland.	ms^{-1}
V_i	Circumferential velocity upstream of the seal.	ms^{-1}
V^*	Circumferential velocity for non-whirling seal.	ms^{-1}
$\bar{V}=V-\Omega R_s$	Velocity in rotating frame.	ms^{-1}
$W = \frac{\Omega R_s}{V^*}$	Nondimensional whirling frequency.	[1]
$\tilde{w}(X)$	Assumed mode shape of shaft.	m
w_1	Axial velocity through sealing knives.	ms^{-1}
x_1, x_2, x_3	Cartesian coordinates.	m
r, θ, z	Cylindrical coordinates.	m
u, v, w	Velocity component associated with r, θ, z.	ms^{-1}
x, y, z	Orthogonal coordinates.	m

Vectors and Matrices

Symbol	Description	Units
$[A]$	Dimensional coefficients of linearized continuity and momentum equations.	$Kgm^{-1}s^{-1}$ $Kgms^{-2}$
$[B]$	Dimensionless coefficients of linearized continuity and momentum equations.	[1]
$[C]$	Damping matrix.	Kgs^{-1}
C_{ij}	Coefficient relating force in i direction due to velocity in j direction.	Kgs^{-1}
$\overline{C_{ij}} = \frac{C_{ij}V^*\delta_1^*}{\pi R_s^2 l P^*}$	Nondimensional damping coefficients.	[1]
K_{ij}	Rotordynamic spring coefficient relating for in i direction to a displacement in the j direction.	Nm^{-1}
$\overline{K_{ij}} = \frac{K_{ij}\delta_1^*}{\pi R_s l P^*}$	Nondimensional spring coefficients.	[1]
$\vec{F}_S$	Force on rotor due to its position.	N
$\vec{F}_D$	Force on rotor due to its velocity.	N
$\vec{R}$	Nonhomogeneous terms in perturbation equations.	[1]
$\vec{V}$	Flow velocity.	ms^{-1}

Greek Symbols

Symbol	Description	Units
$\alpha = \frac{\delta_2^*}{\delta_1^*}$	Seal divergence ratio.	[1]
β	Carry over factor.	[1]
$\gamma = \frac{C_P}{C_V}$	Ratio of specific heats.	[1]
$\Gamma = 1 - \frac{V_i}{V^*}$	Swirl gradient parameter.	[1]
$\Delta = \frac{q^*}{m\delta_1^* \rho^* \sqrt{R_a T}}$	Pressure difference parameter.	[1]
δ_1, δ_2	Sealing gaps between the first and second knives and seal lands respectively.	m
δ_1^*, δ_2^*	Nominal sealing gaps.	m
$\varepsilon_1, \varepsilon_2 = \frac{r}{\delta_1^*}, \frac{r}{\delta_2^*}$	Nondimensional whirling eccentricities.	[1]
$\lambda, \lambda_S, \lambda_R$	Darcy friction factors.	[1]
τ, τ_S, τ_R	Viscous shear stresses.	Nm^{-2}
κ	Thermal conductivity.	$Jm^2s^{-1}K^{-1}$
μ	Flow coefficient.	[1]
μ	Absolute viscosity.	Nm^2s^{-1}
ξ	Pressure perturbation.	[1]
$\hat{\xi}$	Complex amplitude of assumed harmonic pressure perturbation.	[1]
η	Velocity perturbation.	[1]
$\hat{\eta}$	Complex amplitude of assumed harmonic velocity perturbation.	[1]
ζ_1	Flow perturbation through first constriction.	[1]
ζ_2	Flow perturbation through second constriction.	[1]

Symbol	Description	Units
ν	Kinematic viscosity.	m^2s^{-1}
ρ	Density inside gland.	Kgm^{-3}
ρ^*	Density inside non-whirling seal.	Kgm^{-3}
θ	Angular coordinate in absolute frame.	radians
Φ	Dissipation function.	Nms^{-2}
$\psi=\theta-\Omega t$	Angular coordinate in rotating frame.	radians
ψ_η	Phase angle of maximum velocity perturbation referenced to minimum gap.	radians
ψ_ξ	Phase angle of maximum pressure referenced to minimum gap.	radians
$\sigma = \frac{\rho^* \delta_1^* V^*}{q^*}$	Swirl angle parameter.	[1]
ω_n	Shafts natural frequency.	s^{-1}
ω	Shaft rotational frequency.	s^{-1}
Ω	Shaft whirling frequency.	s^{-1}

Subscripts and Superscripts

$[\,]_1$	Condition at 1st seal constriction.
$[\,]_2$	Condition at 2nd seal constriction.
$[\,]_i$	Condition upstream of seal.
$[\,]_o$	Condition downstream of seal.
$[\,]_{RE}$	Real component of complex quantity.
$[\,]_{IM}$	Imaginary component of complex quantity.
$[\,]^*$	Condition inside non-whirling seal (zeroth order solution).
$[\,]_S$	Relating to stator surface.
$[\,]_R$	Relating to rotor surface.

CHAPTER 1

INTRODUCTION

1.1 LABYRINTH SEALS

Modern turbomachines, which include turbines, compressors, fans and pumps, must operate efficiently and be durable in order to be cost competitive. One major source of losses in turbomachines can be attributed to leakage flows that occur between stationary and rotating parts. Pressure differences between adjacent regions drive flows that inevitably degrade performance. Figure 1 shows a typical rotating half stage and where these leakage losses occur.

At low speeds it is possible to employ contact seals, which would virtually eliminate leakage. But at the large relative velocities, which are typical of current designs, the wear of the contacting materials would be prohibitive. In high speed machines non-contact seals are used with very small clearances in order to minimize the associated losses. In choosing the clearances, the designer must account for engine vibration and relative expansion between the parts due to thermal and rotationally induced stresses. All of the analyses must be done for both steady state and transient operation. A typical seal clearance may range from 0.007 cm to 0.05 cm (3-20 mils). A seal with relatively straight surfaces is referred to as an annular seal. One way to reduce the flow rate for a given pressure difference, seal length and minimum allowable gap is to have several

successive sharp sealing knives separated by large kinetic energy dissipating chambers. This is called a labyrinth seal. A leakage reduction of 50 percent or more may be realized by using multi-chamber labyrinth seals. There are several types of labyrinths varying mainly in complexity, but all are based on the same principle. Figure 2 shows an annular seal along with three common kinds of labyrinth seals. The first complete leakage analysis was done by Martin (1). Most current analyses (2,3,4), which tend to be semi-empirical, are generalizations of Martin's work. For many years these seals were designed only for their ability to minimize leakage flows. However, over the past forty years another design objective has received increasing consideration. The leakage flows over the knives and around the annular regions of the seal chambers create pressure oscillations that generate self-exciting forces. These displacement and velocity dependent self-exciting forces contribute to rotordynamic instability, which can have a very negative impact on machine durability.

1.2 ROTORDYNAMIC INSTABILITY

High speed turbomachine rotors undergo lateral vibrations which may limit their range of operation and usable life. These vibrations are broadly categorized as either forced or self-excited. Ehrich (5) and Ehrich and Childs (6) give relatively comprehensive treatments of these two distinct phenomena. Briefly, a forced or resonant vibration occurs

at the rotational speed of the shaft or some rational multiple of it. The amplitude of these vibrations will increase and decrease as the rotor speed is raised, being largest at the rotor critical frequencies. The forcing here is external to the system, in that the forcing function does not depend on the motion of the shaft. There are many sources of forced vibration, but the most common is residual unbalance. The amplitude of these vibrations can usually be limited by careful balancing and not operating too near critical frequencies.

Self-excited vibrations are a class of instability phenomena in which the motion of the rotor causes energy to be extracted from some external source. This added energy causes rotordynamic instability which is analogous to aeroelastic flutter of an airplane wing (7). Just like flutter, these instabilities do not happen at low speeds, but suddenly occur at some onset speed and progressively worsen at higher speeds. The frequency of vibration is nearly constant and corresponds to one of the shaft's natural frequencies. In practice, these instabilities are usually first seen when the rotor rpm is above the first critical and the whirl occurs at the first critical. This is referred to as sub-synchronous whirl and its presence can be very harmful since it introduces alternating flexural stresses in the shaft. An infamous example of this was the Space Shuttle Main Engine Turbopumps as reported by Childs (8) and Ek (9). A rotor may whirl in either angular

direction. It is conventional to refer to a whirl in the same direction as the shaft's spin as forward whirl. When the whirling precession is in the opposite sense as the spin: it is called a backward whirl. Figure 3 shows some of the more important characteristics of both forced and self-excited free vibration for comparison.

In order to predict the range of stable operation of a rotor-bearing system a structural model must be used which accounts for all of the important forces. A simple planar, two-degree-of-freedom model will be used to illustrate how known self-exciting forces are incorporated into a structural model and how they influence stability. In this model, due to Jeffcoat (10), all of the mass is concentrated in a single thin disk and the elasticity due to the bending rigidity is supplied by a massless shaft of spring constant K_s. Figure 4 shows such an idealized rotor with other forces acting on the disk. Let x_1 and x_2 be the displacement coordinates in the plane of the disk and $\vec{F}_s = \vec{F}_s(x_1,x_2)$ be the force on the mass due to its position. The other force acting on the rotor $\vec{F}_D = \vec{F}_D(\dot{x}_1,\dot{x}_2)$ can be recognized as a damping force since it is a function of the disk's velocity $\dot{x}_1$ and $\dot{x}_2$. If $\vec{F}_s$ is a linear function of the displacements x_1 and x_2 it can be represented in the following form,

$$\vec{F}_s = \begin{Bmatrix} f_{s1} \\ f_{s2} \end{Bmatrix} = - \begin{bmatrix} K_{11} & K_{12} \\ K_{21} & K_{22} \end{bmatrix} \begin{Bmatrix} x_1 \\ x_2 \end{Bmatrix} \tag{1.1}$$

The K's are the linear elastic coefficients which relate the forces and displacements through constants of proportionality. K_{11} and K_{22} (the diagonal entries) are called direct stiffnesses since they relate forces and displacements in the same direction. On the other hand, K_{12} and K_{21} relate the forces in one direction which result from a displacement in the other. These are referred to as cross-coupling stiffness coefficients. In a similar manner the damping forces can be related to the velocities by,

$$\vec{F}_D = \begin{Bmatrix} f_{D1} \\ f_{D2} \end{Bmatrix} = - \begin{bmatrix} C_{11} & C_{12} \\ C_{21} & C_{22} \end{bmatrix} \begin{Bmatrix} \dot{x}_1 \\ \dot{x}_2 \end{Bmatrix} \tag{1.2}$$

Now the equations of motion can be written for the mass in Figure 4 by applying Newton's second law,

$$\begin{bmatrix} M & O \\ O & M \end{bmatrix} \begin{Bmatrix} x_1 \\ x_2 \end{Bmatrix} + \begin{bmatrix} C_{11} & C_{12} \\ C_{21} & C_{22} \end{bmatrix} \begin{Bmatrix} \dot{x}_1 \\ \dot{x}_2 \end{Bmatrix} + \begin{bmatrix} K_s + K_{11} & K_{12} \\ K_{21} & K_s + K_{22} \end{bmatrix} \begin{Bmatrix} x_1 \\ x_2 \end{Bmatrix} = 0 \tag{1.3}$$

These are the equations for a coupled, damped, harmonic oscillator, which can be neatly expressed in matrix from as,

$$[M]\{x\} + [c]\{\dot{x}\} + [K]\{x\} = 0 \qquad (1.4)$$

Equations of this form are solved by substituting $\{x\}=\{a\}e^{\lambda t}$ where λ is complex. The frequency and growth or decay rate of lateral vibration are determined by the roots, $\lambda = \sigma+i\tau$, of the resulting characteristic equation for the homogeneous system. The real part of λ, σ, will determine whether small perturbations will grow or decay. A negative σ will indicate stability while, positive σ implies that oscillations will grow and instability will occur. The frequency of vibration is determined by the imaginary part of λ. In order to perform these calculations, the entries for the mass, damping, and stiffness matrices must be known. This is just as true for more complicated multi-degree-of-freedom rotor models such as those described by Nordman (11) and Dugundji (12). There are many physical phenomena which lead to damping and elastic forces on a rotor (5). Contributing to these may be bearings, seals, turbines and compressors. Since this system is linear, the contributions from each source may be summed using superposition to obtain the net [c] and [K]. This thesis will deal with the damping and elastic forces generated by the labyrinth seals only.

The forces from labyrinth seals are due to non-uniformity in the pressure within the seal glands. To find these forces, a known pressure distribution must be projected in orthogonal directions and integrated around the circumference of the seal. The net forces acting on a seal of radius R_s and

length l due to a pressure distribution $P(\theta,x_3,t)$ are,

$$F_{X_1} = - R_s \int_0^{2\pi} \int_0^l P\left(\theta,x_3,t\right) \cos\theta \, dx_3 \, d\theta \qquad (1.5)$$

$$F_{X_2} = - R_s \int_0^{2\pi} \int_0^l P\left(\theta,x_3,t\right) \sin\theta \, dx_3 \, d\theta \qquad (1.6)$$

If the pressure does not vary in the axial direction, these expressions simplify to,

$$F_{X_1} = - R_s l \int_0^{2\pi} P\left(\theta,t\right) \cos\theta \, d\theta \qquad (1.7)$$

$$F_{X_2} = - R_s l \int_0^{2\pi} P\left(\theta,t\right) \sin\theta \, d\theta \qquad (1.8)$$

Many researchers, past and present, have focused their attention on trying to understand and predict these pressure distributions $P(\theta,t)$.

1.3 LITERATURE REVIEW

It has been known since the 1940's that the circumferential variations in pressure which exist in the glands of labyrinth seals may lead to unstable rotor whirl as reported by Den Hartog (13). However, to the knowledge of the author, there was no analysis explaining the nature of these non-uniformities and how they cause whirl until the works of Thomas (14) in 1958 and Alford (15) in 1965. The analysis

proposed by Thomas tends to be lengthy and depend on a great deal of empirical correlations of losses vs. clearance. Alford assumed that the nominal sealing gap varies from chamber to chamber and that there is limited redistribution of the flow in the circumferential direction. Under these conditions, he showed that a converging seal promotes forward whirl, whereas a diverging one will tend to be stabilizing to forward whirl. Ehrich (16) performed an analysis where the seals were permitted to pivot relative to the outer casing. Vance and Murphy (17) did a similar analysis to both Alford and Ehrich which accounted for sonic choking in the last seal. While these four theories predict destabilizing forces under certain conditions, a problem exists with all of them, in that they predict no self-exciting forces in cases where they are known to exist.

In 1972 Kostyuk (18) introduced a more fundamental fluid mechanical approach to explain the aerodynamic forces in labyrinth seals. In his analysis, the equations relating the flow rate over the knives were coupled to the governing continuity and momentum equations in the circumferential direction. Iwatsubo (19,20) used a similar model but included area change terms due to the motion of the whirling shaft. He showed that these terms are important when predicting damping. Iwatsubo solved these equations by a linear perturbation analysis and assumed harmonic solutions to the resulting equations and compared these solutions to a finite difference solution.

Recently many Kostyuk-Iwatsubo type analyses for multi-chamber seals have appeared (21,22,23,24,25,26,27,28). These theories lead to 2N linear complex algebraic equations in the same number of variables for a N chamber seal. While some trends were established by doing parametric studies, no closed form solutions have been obtained that describe the influences of the various geometric and flow parameters. Computer solutions of these systems have shown some interesting trends. First, is that one of the parameters important in the generation of aerodynamic forces is the change in swirl from chamber to chamber. Second, smaller clearances, which are beneficial with regard to machine performance, have been predicted to lead to greater destabilizing forces. Some of the trends predicted by analysis have been confirmed by experimental data. Measurements of the elastic forces taken by Benckert and Wachter (29,30) show good agreement with most theories. In these experiments, the forces on the eccentric rotor were measured and then checked by integrating measured pressure distributions inside the labyrinth glands. Other researchers (31,32,33,34,35) have performed similar experiments for various geometries and flow conditions yielding an extensive data base for stiffness coefficients. There are much less data available for the damping effects of labyrinth seals since these experiments require time resolved measurements on whirling rotors. But as pointed out by Martinez (28) the damping forces can be of the same order of magnitude as the

elastic ones and can be just as important.

Childs (36) obtained data for a whirling seal with no rotation. Wright (37,38) performed experiments with both rotation and whirl but no attempt was made to control or measure the swirl entering the seal. Data was taken on straight through, convergent and divergent configurations. The trends obtained run contrary to those predicted by Alford and no direct comparison can be made to a Kostyuk-Iwatsubo type model, in which pre-swirl is of great importance. Clearly, more data on the damping characteristics are needed.

1.4 OBJECTIVES

A simplified set of equations, based on the Kostyuk-Iwatsubo model that approximate the air flow through a two constriction labyrinth seal, is derived. These equations are linearized and harmonic solutions are assumed. These equations are non-dimensionalized and the importance of individual terms is discussed. From the solution of these resulting equations, the effects of various geometric and flow parameters are presented. Based on these analytical predictions, design objectives for an experimental rig to measure aerodynamic forces, especially damping, on arbitrarily spinning and whirling labyrinth seals are set. The final mechanical design of this rig is presented along with the facility and instrumentation requirements.

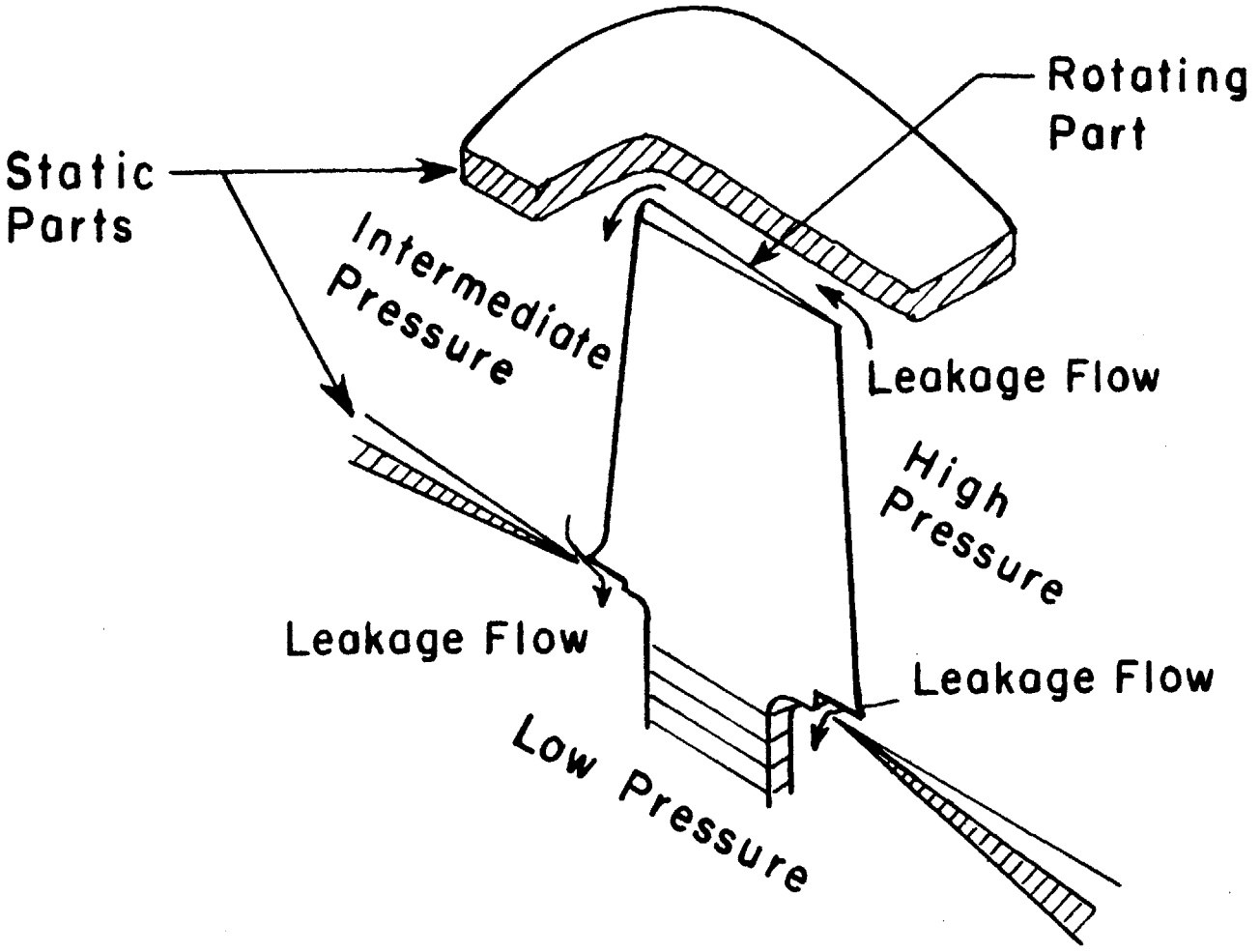

Figure 1 - Rotating half stage out of a typical turbomachine showing where leakage losses occur.

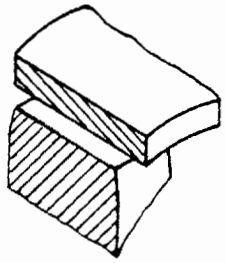

A. Annular Seal

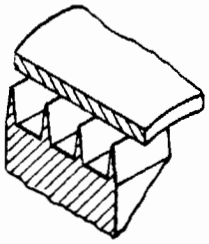

B. Simple Or Straight-Through Labyrinth

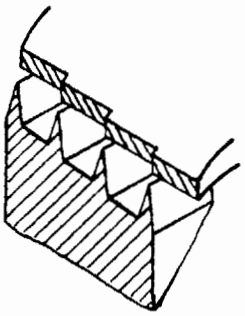

C. Stepped Labyrinth

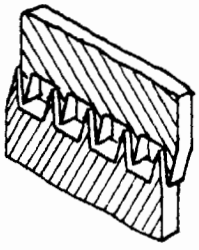

D. Interlocking Or Full Labyrinth

Figure 2 - Four commonly used seal configurations used in rotating machinery.

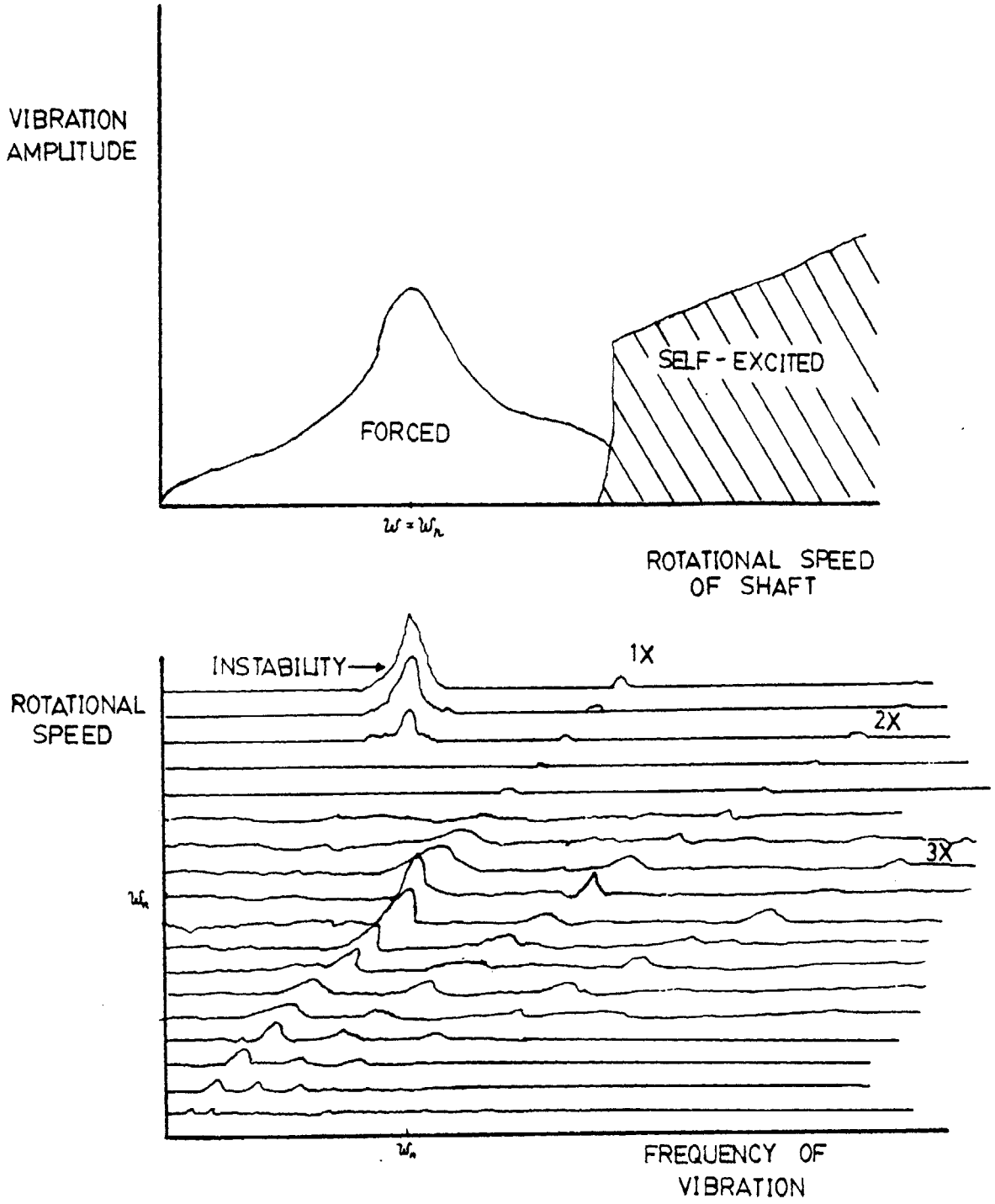

Figure 3 - Characteristics of forced and self-excited vibrations. Top: vibration amplitude vs. shaft speed. Bottom: vibration cascade showing shaft speed vs. vibration frequency.

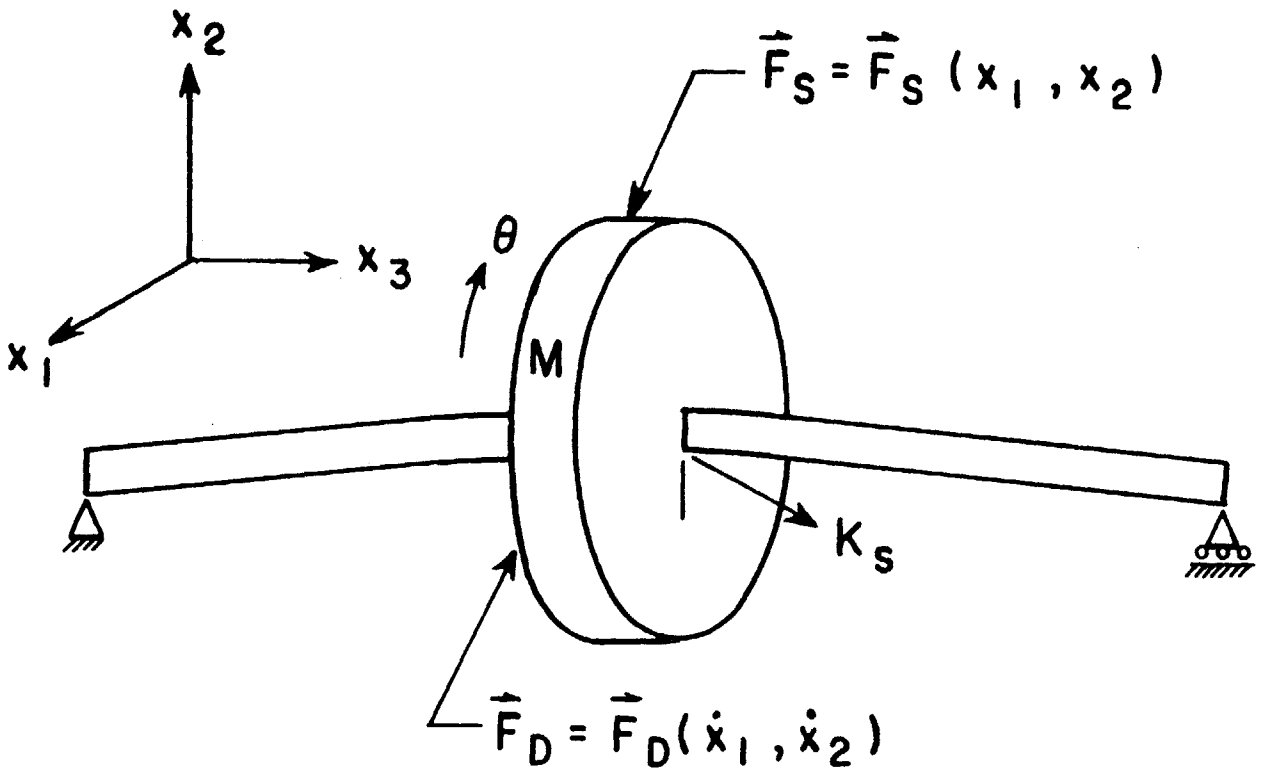

Figure 4 - Jeffcoat model of plane rotor. $\vec{F}_S$ and $\vec{F}_D$ are the forces which act due to the disks position and velocity respectively.

CHAPTER 2

MODEL FORMULATION

2.1 COMPLETE EQUATIONS OF MOTION

The air flow through a rotating, whirling labyrinth seal is three-dimensional, unsteady, compressible and turbulent with large scale separations. The equations that govern this phenomena are the Navier-Stokes equations along with the appropriate boundary conditions. These equations of continuity, momentum, energy and state in vector form are,

$$\frac{\partial \rho}{\partial t} + \nabla \cdot \rho \bar{V} = 0 \tag{2.1}$$

$$\rho \frac{D\bar{V}}{Dt} = - \nabla P + \mu \nabla^2 \bar{V} + \frac{\mu}{3} \nabla(\nabla \cdot \bar{V}) \tag{2.2}$$

$$\rho C_v \frac{DT}{Dt} = \kappa \nabla^2 T + \frac{DP}{Dt} + \Phi \tag{2.3}$$

Φ = dissipation function

$$P = \rho R_a T \tag{2.4}$$

No analytical methods are available for the solution of such a general system. Direct numerical simulation of this 3-D problem at the high Reynolds numbers which occur in real machines would require an enormous number of grid points to account for all the scales of motion (39). It would be prohibitively expensive to do parametric studies for this problem. Clearly a simplified model which yields a more tractable set of equations is highly desirable.

2.2 KOSTYUK-IWATSUBO MODEL

Kostyuk (11) introduced a lumped parameter model of the flow in labyrinth seals which considerably simplified the governing equations. In this model, it is assumed that the flow in the axial direction over the seal knives can be coupled to essentially one dimensional continuity and momentum equations in the circumferential direction.

The state variables in the seal glands are considered to be functions of angle and time only. That is, variations in pressure P, density ρ, velocity V, etc. in the radial and axial direction inside a given chamber are neglected. This type of assumption is known to be reasonably accurate when the gap between the seal knives and lands, δ, is much smaller than the characteristic dimension of the seal chamber ($\delta << l$, $\delta << h$) where l is the distance between the knives and h is the height of the glands as shown in Figure 6.

Iwatsubo (19) generalized Kostyuk's model slightly by allowing for area variations in the chamber due to the shaft whirling. The equations that will be derived are the same as presented by Iwatsubo but for a simple two constriction, single gland seal.

2.3 DERIVATION OF GOVERNING EQUATIONS

Along with the basic assumptions described previously, leading to the lumped parameter model the following simplifications will be made.

1. The inlet and exit conditions are constant and known and carry subscripts i and o respectively.
2. The working fluid, air, is ideal and colorically perfect.

$$P = \rho R_a T$$

3. All processes are adiabatic. This assumption replaces the energy equation (2.3).
4. As a consequence of 2 and 3 the mean air temperature in the gland is the same as before and after the seal.
5. Small flow changes in the circumferential direction are permitted and are assumed to be isentropic.
6. The amplitude of the whirling motion of the shaft is small compared with the nominal seal clearance.
7. The shear stresses exerted on the fluid inside the gland follow a Darcy Friction law. This is expressed as

$$\tau = \frac{1}{8} \lambda \rho \bar{V}_{rel}^2$$

where τ is the shear stress, λ the Darcy friction factor, ρ the fluid density, and V_{rel} is the relative velocity between the average fluid core flow and the nearest solid surface.

Figure 5 shows a cutaway of the seal along with the cylindrical coordinate system and associated velocity components. Figure 6 is a cross section out of Figure 5 giving the geometry and pertinent flow parameters. The labyrinth gland has dimensions l x h and is at radius R_s.

The sealing clearance into and out of the gland are δ_1 and δ_2 respectively. Of course these gaps vary with angle and time due to the rotor whirl. The initial pressure and circumferential velocity before the seal are P_i and V_i respectively. The temperature T and exit Pressure P_o are both constant and given.

The last of the parameters to be specified describe the motion of the seal relative to the outer casing. Figure 7, which shows an axial and side view, gives the necessary kinematic information. The rotor spins at ω and the whirl is of amplitude r and at angular velocity Ω. The problem is to find the unknown pressure P, velocity V and density ρ inside the seal gland. The first equations to be derived relate the flow rates in and out of the gland to the geometry, air properties and pressure differences across the sealing strips.

The total mass influx to the seal chamber $\dot{m}_1$ is,

$$\dot{m}_1 = \rho_1 A_1 w_1 \tag{2.5}$$

where ρ_1 and w_1 are the density and axial velocity respectively at the minimal area. A_1 is the effective area which is the actual area multiplied by a contraction coefficient. The mass inflow per unit circumferential length of seal q_1 is,

$$q_1 = \rho_1 \delta_1 \mu w_1 \tag{2.6}$$

where μ is the empirically obtained contraction coefficient for the flow. Exact expressions for ρ_1 and w_1 are given in Appendix A but an approximation for q_1 based on the mean density between the chambers will be derived and used. The error incurred in the prediction of mass flow rate is less than five percent for axial Mach numbers less than 0.6. Using Bernoulli's equation and assuming that the axial velocity is negligible far upstream, a relation is obtained for the axial velocity w, at the seal gap.

$$w_1 = \sqrt{\frac{2}{\rho_1} (P_i - P)} \tag{2.7}$$

where P_i and P are the pressures before and after the constriction. The density at the throat ρ_1 is assumed to be the average of the density before and in the gland. This density can be expressed in terms of pressure using the ideal gas law as

$$\rho_1 = \frac{1}{2} (\rho_i + \rho) = \frac{1}{2R_a T} (P_i + P) \tag{2.8}$$

Substituting (2.7) and (2.8) into (2.6) yields the first governing equation

$$q_1 = \frac{\delta_1 \mu}{\sqrt{R_a T}} \left(P_i^2 - P^2\right)^{1/2} \tag{2.9}$$

Similarly, the mass efflux from the gland per unit seal

length q_2 is

$$q_2 = \frac{\delta_2 \mu}{\sqrt{R_a T}} \left(P^2 - P_o^2\right)^{1/2} \tag{2.10}$$

Throughout, μ will be assumed to have the constant value of 0.65 and no carry-over effect will be accounted for. For a brief discussion of these assumptions see Appendix A.

The next relationship to be presented is the continuity equation governing the flow in the circumferential direction inside the seal gland. Figure 8 shows a control volume with the various mass fluxes crossing the associated control surfaces and the mass accumulation within the control volume. Equating the change in mass to the net inflow and rearranging yields the following continuity equation

$$\frac{\partial(\rho f)}{\partial t} + \frac{1}{R_s} \frac{\partial}{\partial \theta} (\rho f V) + q_2 - q_1 = 0 \tag{2.11}$$

where f is the gland's cross-sectional area normal to the velocity V.

The final relation will be the momentum equation in the θ-direction. Figure 9 shows a control volume with the momentum fluxes, shear stresses and the θ-pressure gradient. Using Newton's second law that the time rate of change of the momentum is equal to the applied forces yields

$$\frac{\partial}{\partial t}(\rho f V) + \frac{1}{R_s}\frac{\partial}{\partial \theta}(\rho f V^2) + q_2 V - q_1 V_i + \tau_s l$$

$$- \tau_R (1+2h) + \frac{f}{R_s}\frac{\partial P}{\partial \theta} = 0 \qquad (2.12)$$

The shear stress exerted on the fluid by the stator, τ_s can be approximated by a Darcy friction law. Using the following formula, the shear stress is given by

$$\tau_s = \frac{1}{8}\rho\lambda_s V \cdot |V| = \frac{1}{8}\rho\lambda_s V^2 \cdot \mathrm{sgn}(V) \qquad (2.13)$$

where λ_s is the friction factor for the stator. Note that the absolute value or sgn is used to insure that the shear stress always retards relative motion. The force exerted by the rotor wall is expressed in a similar manner. But the rotor wall has an absolute velocity of ωR_s, so that the relative velocity is $V-\omega R_s$. Hence, the stress exerted on the fluid by the rotor is

$$\tau_R = \frac{1}{8}\lambda_R(V-\omega R_s)\cdot|V-\omega R_s| = \frac{1}{8}\rho\lambda_R(V-\omega R_s)^2\cdot\mathrm{sgn}(\omega R_s - V) \qquad (2.14)$$

where λ_R is the friction factor for the rotor. The friction factors λ_s and λ_R depend on many factors (see Appendix A for details) but here they will be assumed to be functions of the steady state Reynolds numbers Re_s^* and Re_R^*. Re_s^* and Re_R^* are defined by using the hydraulic diameter D_H, Mean relative velocity V and kinematic viscosity ν as

$$Re_s^* = \left| \frac{V \cdot D_H}{\nu} \right| \tag{2.15}$$

and

$$Re_R^* = \left| \frac{(\omega R_s - V) \cdot D_H}{\nu} \right| \tag{2.16}$$

The friction factors are now computed from these, and are,

$$\lambda_s = 0.3164 \; Re_s^{*-0.25} \tag{2.17}$$

$$\lambda_R = 0.3164 \; Re_s^{*-0.25} \tag{2.18}$$

An iteration scheme must be used to calculate these since the velocity and friction factors are coupled in a non-elementary manner. If λ_s and λ_R are given the appropriate sign, depending on the relative velocities, the absolute values or sgn may be dropped from equations (2.13) and (2.14). Combining all of this, the original momentum equation (2.12) becomes

$$\frac{\partial}{\partial t}(\rho f V) + \frac{1}{R_s} \frac{\partial}{\partial \theta} (\rho f V^2) + q_2 V - q_1 V_i + \frac{1}{8} \rho \lambda_s l V^2$$

$$- \frac{1}{8} \rho \lambda_R (1+2h)(V-\omega R_s)^2 + \frac{f}{R_s} \frac{\partial P}{\partial \theta} = 0 \tag{2.19}$$

The sealing clearances δ_1, and δ_2, which vary due to the rotor center executing a circular orbit of amplitude r and angular velocity Ω can be written (Referring to Figure 7) in terms of the nominal clearances δ_1^*, and δ_2^*, r, θ and

Ω for δ_1^*, $\delta_2^* << R_s(25)$ as

$$\delta_1 = \delta_1^* - r\cos(\theta-\Omega t) \tag{2.20}$$

$$\delta_2 = \delta_2^* - r\cos(\theta-\Omega t) \tag{2.21}$$

The gland cross-sectional area f can be expressed in terms of δ_1 as

$$f = l(h+\delta_1) \tag{2.22}$$

The equations presented above are consistent with those of Iwatsubo. However, it will be found to be beneficial to recast these equations in terms of rotating coordinates.

2.4 TRANSFORMATION TO ROTATING COORDINATES

One of the difficulties that would be encountered in dealing with the equations as they stand is that all state variables are functions of time and space and both temporal and spatial partial derivatives appear in the continuity and momentum equations. This state of affairs can be removed by changing to a more convenient frame of reference. Since the sealing clearance distribution travels around at an angular frequency of Ω it would be natural to chose a reference frame which rotates at Ω, yielding a problem which does not contain time explicitly. This is true provided the whirling motion is uniform and circular, and also that the seal has cylindrical symmetry. Referring to Figure 7, let ψ be

defined as the counter clockwise angle from the minimum gap. By using this and noting that no time scaling is necessary the new rotating coordinates $(\psi,\bar{t})$ may be written in terms of the old ones (θ,t) as

$$\psi = \theta - \Omega t \tag{2.23}$$

$$\bar{t} = t \tag{2.24}$$

By using this independent variable transformation $\frac{\partial}{\partial\theta}$ and $\frac{\partial}{\partial t}$ can be replaced by

$$\frac{\partial}{\partial\theta} = \frac{\partial\psi}{\partial\theta}\frac{\partial}{\partial\psi} + \frac{\partial\bar{t}}{\partial\theta}\frac{\partial}{\partial\bar{t}} = \frac{\partial}{\partial\psi} \tag{2.25}$$

$$\frac{\partial}{\partial t} = \frac{\partial\psi}{\partial t}\frac{\partial}{\partial\psi} + \frac{\partial\bar{t}}{\partial t}\frac{\partial}{\partial\bar{t}} = -\Omega\frac{\partial}{\partial\psi} + \frac{\partial}{\partial\bar{t}} \tag{2.26}$$

Also introducing velocity $\bar{V}$ relative to this new coordinate system as

$$\bar{V} = V - \Omega R_s \tag{2.27}$$

By noting that all of the state variables have become functions of ψ only

$$P(\theta,t) \rightarrow P(\psi) \tag{2.28a}$$

$$\rho(\theta,t) \rightarrow \rho(\psi) \tag{2.28b}$$

$$\vdots \qquad\qquad \vdots$$

there is no longer any explicit dependence on $\bar{t}$ so that

$\frac{\partial(\,)}{\partial \bar{t}} = 0$ and the partial derivatives with respect to ψ, $\frac{\partial}{\partial \psi}$ may be replaced by ordinary derivatives $\frac{d}{d\psi}$. Using this information the original governing equations (2.11) and (2.19) can be rewritten as,

$$\frac{d}{d\psi}\left[\rho f \bar{V}\right] + R_s\left(q_2 - q_1\right) = 0 \tag{2.30}$$

$$\frac{d}{d\psi}\left[\rho f \bar{V}\left(\bar{V}+\Omega R_s\right)\right] + \frac{R_s}{8}\,\rho\left[\lambda_s 1 (\bar{V}+\Omega R_s)^2 - \lambda_R (1+2h)(\omega R_s - (\bar{V}+\Omega R_s)^2)\right]$$

$$+ R_s q_2\left(\bar{V}+\Omega R_s\right) - R_s q_1\left(\bar{V}_i+\Omega R_s\right) + f\,\frac{dP}{d\psi} = 0 \tag{2.31}$$

The leakage equations for q_1 and q_2 are invariant but δ_1 and δ_2 simplify to

$$\delta_1 = \delta_1^* - r\cos\psi \tag{2.32}$$

$$\delta_2 = \delta_2^* - r\cos\psi \tag{2.33}$$

and by defining eccentricity ratios $\varepsilon_i = \frac{r}{\delta_i^*}$ the non-dimensional gap distributions may be given as

$$\frac{\delta_1}{\delta_1^*} = 1 - \varepsilon_1\cos\psi \tag{2.34}$$

$$\frac{\delta_2}{\delta_2^*} = 1 - \varepsilon_2\cos\psi \tag{2.35}$$

The continuity (2.30) and momentum (2.31) equations along with the auxiliary leakage and gap distribution relations

form a system of two coupled nonlinear ordinary differential equations and will be used in the following chapters for the theoretical prediction of the labyrinth seal forces.

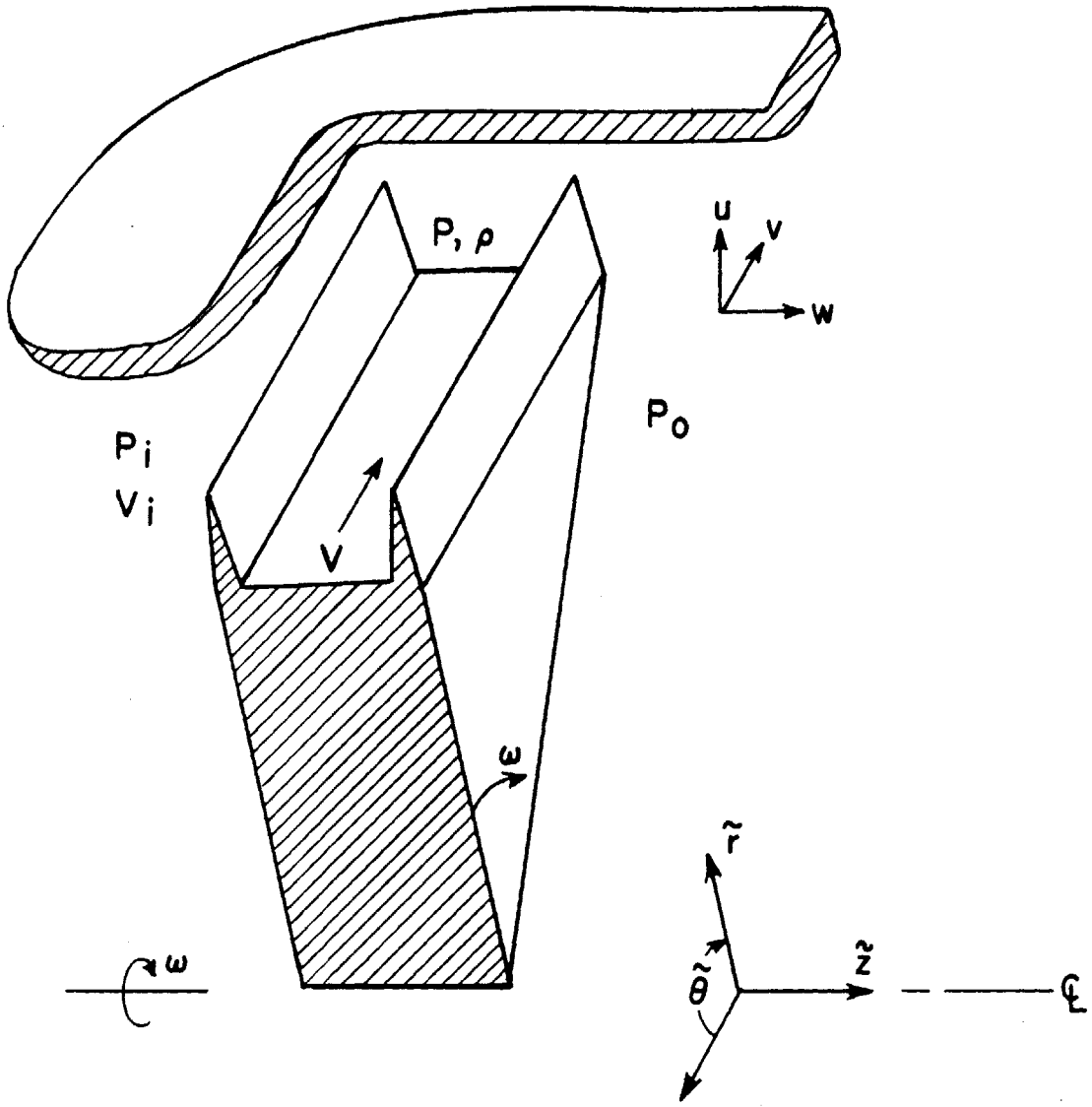

Figure 5 - Cutaway section of a single gland labyrinth seal.

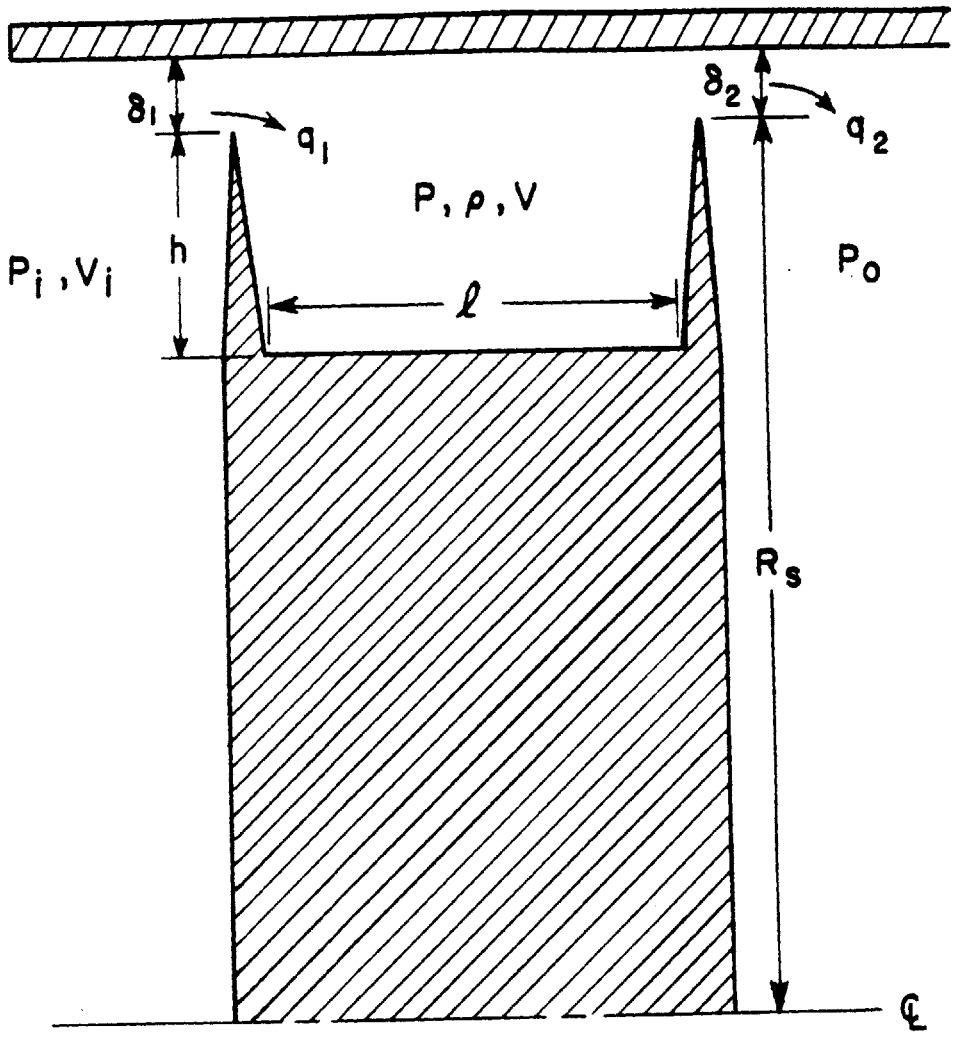

Figure 6 - Cross section of seal out of Figure 5. The geometry and flow variables are given.

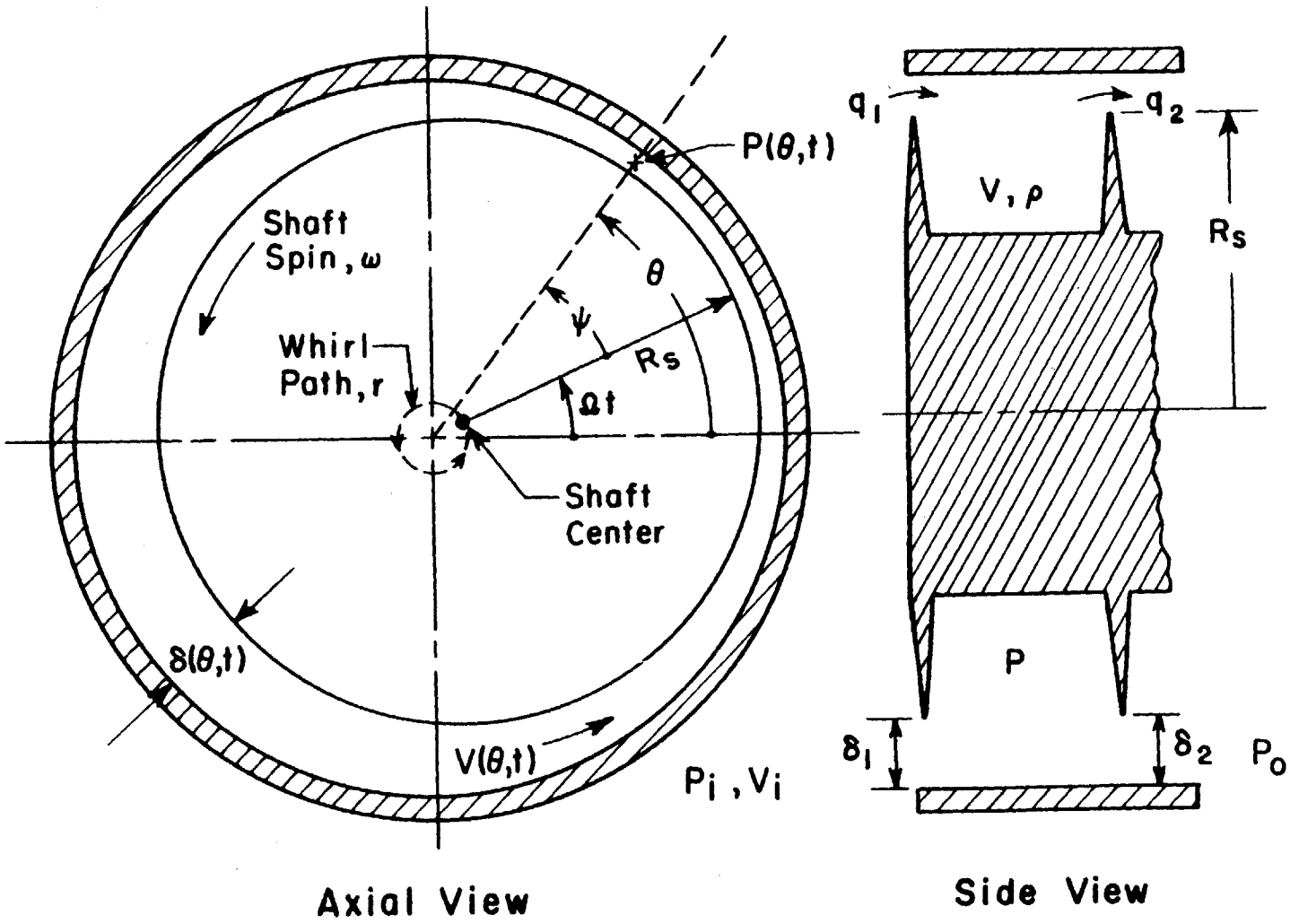

Figure 7 - Axial and side view of single chamber seal showing the geometry and kinematics of the whirling seal.

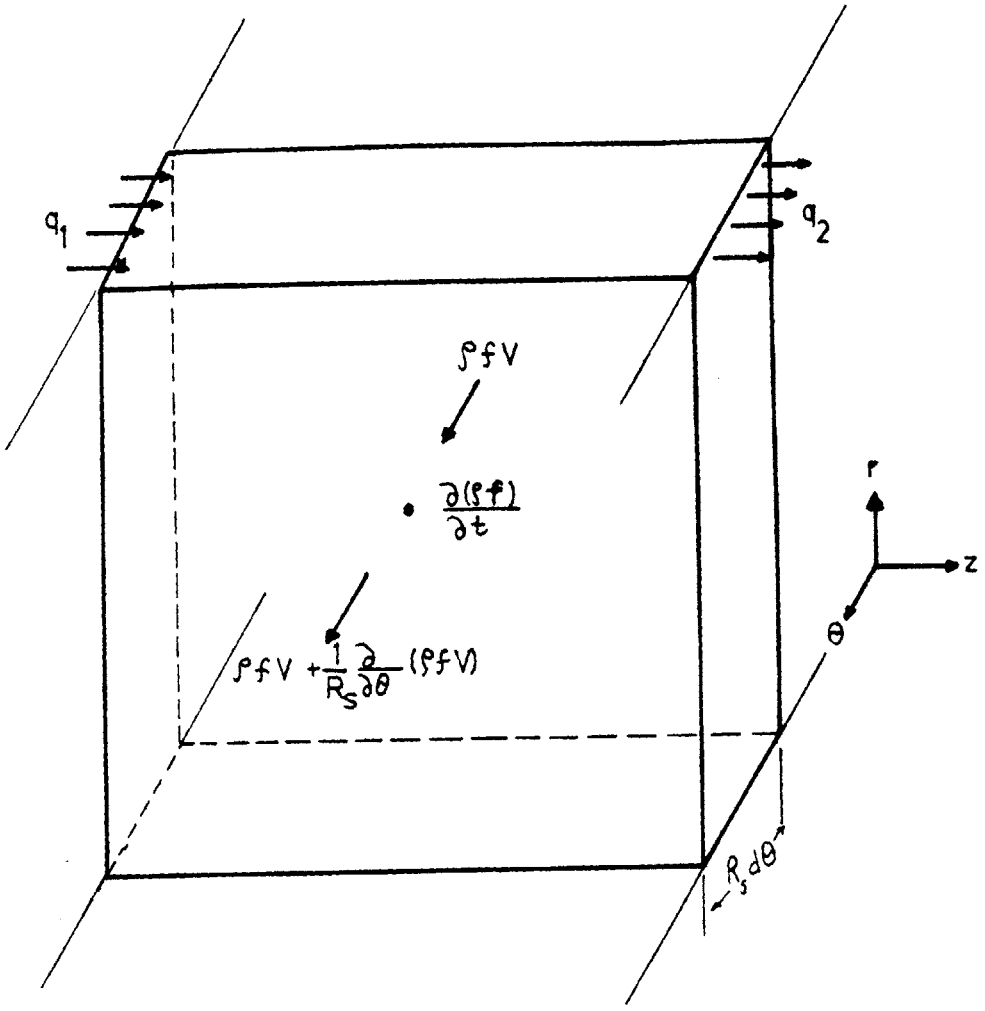

Figure 8 - Control volume for the derivation of the continuity equation.

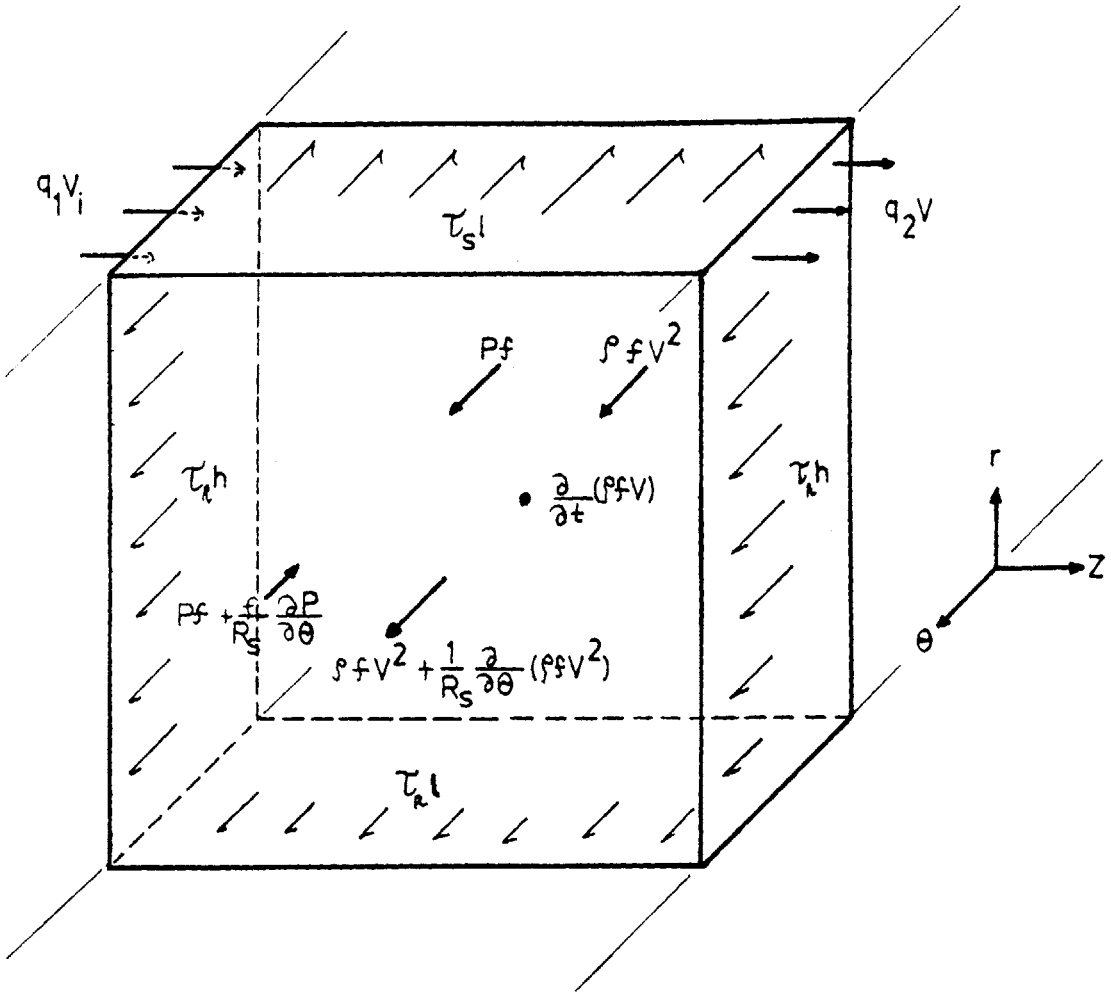

Figure 9 - Control volume for the derivation of the momentum equation.

CHAPTER 3

LINEARIZATION OF GOVERNING EQUATIONS

3.1 INTRODUCTION

Even though the equations derived in the last chapter are much simpler than the full Navier Stokes equations they still contain nonlinearities and hence are difficult to integrate in closed form. Many mathematical methods for approximating the solution are available. The system could be numerically integrated by any one of several methods. This would appear to be a straightforward approach. But the periodicity boundary conditions on both pressure and velocity tend to be difficult to impose for either a time marching shooting scheme or a finite difference method. Also, some valuable physical insight is lost by numerical simulation. Instead of numerically solving the equations a linear perturbation technique will be used. To do this, first the equations are solved with the shaft in the centered position to obtain a zeroth order solution. Next, small amplitude perturbation expressions are substituted into the governing equations which are then linearized. Harmonic solutions for the perturbation are assumed and the resulting system of linear algebraic equations is presented.

3.2 ZEROTH ORDER SOLUTION

The first step will be to obtain a zeroth order solution. To do this, the rotor is assumed to be centered with respect

to the outer casing. In this non-whirling condition all variables are independent of angle and time (e.g. $\frac{\partial}{\partial\theta} = \frac{\partial}{\partial\psi} = \frac{\partial}{\partial t} = 0$). Let any starred variable (ρ^*, V^*, P^*, $\bar{V}^*$, etc.) represent these uniform zeroth order solutions. Under these assumptions the original equations greatly simplify to

$$q_2^* - q_1^* = 0 \tag{3.1}$$

$$\frac{1}{8}\rho^*\left(\lambda_s 1 V^{*2} - \lambda_R(1+2h)(V^*-\omega R_s)^2\right) + q_2^* V^* - q_1^* V_i = 0 \tag{3.2}$$

The value of P^* can be found from (3.1) by using the flow rate equations (2.9) and (2.16) as follows

$$\frac{\delta_2^*\mu}{\sqrt{R_a T}}\left(P^{*2}-P_o^2\right)^{1/2} - \frac{\delta_1^*\mu}{\sqrt{R_a T}}\left(P_i^2-P^{*2}\right)^{1/2} = 0 \tag{3.3}$$

Solving for P^* gives

$$P^* = \left(\frac{\delta_1^{*2}P_i^2 + \delta_2^{*2}P_o^2}{\delta_1^{*2} + \delta_2^{*2}}\right)^{1/2} \tag{3.4}$$

The steady state flow rate per unit circumferential length is $q_1^* = q_2^* = q^*$ and is given by

$$q^* = \frac{\delta_2^*\mu}{\sqrt{R_a T}}\left(P^{*2}-P_o^2\right)^{1/2} \tag{3.5}$$

ρ^* is found from $P^* = \rho^* R_a T$. Finally V^* must be determined.

The initial guess for V^* is V_i then λ_s and λ_R are obtained from (2.17) and (2.18) respectively. Then the quadratic equation for V^* from (3.2) is solved for an updated V^*.

$$\frac{1}{8}\rho^*\left[\lambda_s 1-\lambda_R(1+2h)\right]V^{*2} + \left[q^* + \frac{1}{4}\rho^*\lambda_R(1+2h)\omega R_s\right]V^* - \left[q^*V_i + \frac{1}{8}\rho^*\lambda_R(1+2h)\omega^2 R_s^2\right] = 0 \qquad (3.6)$$

With this value of V^* new estimates for λ_s and λ_R can be obtained. This iteration process is continued until a convergent solution for V^* is obtained.

3.3 PERTURBATION EXPANSIONS

Once the zeroth order solution for the equilibrium, non-whirling rotor has been obtained the state variables inside the labyrinth gland for the case of the small amplitude whirling rotor can be expressed in terms of the following perturbation expressions.

$$P = P(\psi) = P^*(1+\xi(\psi)) = P^* + \xi P^* \qquad (3.7)$$

$$V = V^*(1+\eta) \qquad (3.8)$$

$$q_1 = q^*(1+\zeta_1) \qquad (3.9)$$

$$q_2 = q^*(1+\zeta_2) \qquad (3.10)$$

The flow rate perturbation ζ_1 can be eliminated in favor of the pressure perturbation ξ using (2.9), (3.7) and $|\xi|<<1$ as follows

$$\frac{q_1}{q^*} = \frac{\frac{\mu\delta_1}{\sqrt{R_a T}}\left(P_i^2 - P^2\right)^{1/2}}{\frac{\mu\delta_1^*}{\sqrt{R_a T}}\left(P_i^2 - P^{*2}\right)^{1/2}} = \frac{\delta_1}{\delta_1^*}\left(\frac{P_i^2 - P^{*2} - 2\xi P^{*2}}{P_i^2 - P^{*2}}\right)^{1/2}$$

$$= \frac{\delta_1}{\delta_1^*}\left(1 - \frac{2\xi P^{*2}}{P_i^2 - P^{*2}}\right)^{1/2} \simeq \frac{\delta_1}{\delta_1^*}\left(1 - \frac{\xi P^{*2}}{P_i^2 - P^{*2}}\right) \qquad (3.11)$$

This can be rewritten as

$$q_1 = \frac{q^*\delta_1}{\delta_1^*}\left(1 - \frac{\xi P^{*2}}{P_i^2 - P^{*2}}\right) \qquad (3.12)$$

Similarly ζ_2 can be eliminated in the expression for q_2, here q_2 is expressed in terms of ξ as

$$q_2 = \frac{q^*\delta_2}{\delta_2^*}\left(1 + \frac{\xi P^{*2}}{P^{*2} - P_o^2}\right) \qquad (3.13)$$

Several relationships will prove useful in manipulating the equations. From the assumption that all the flow processes in the circumferential direction are isentropic, the pressure and density variations can be related by

$$\frac{\partial\rho}{\partial\psi} = \frac{1}{\gamma R_a T}\frac{\partial P}{\partial\psi} = \frac{\rho^*}{\gamma P^*}\frac{\partial P}{\partial\psi} \qquad (3.14)$$

or in terms of the perturbation variables

$$\frac{\partial \rho}{\partial \psi} = \frac{1}{\gamma R_a T} P^* \frac{\partial \xi}{\partial \psi} = \frac{\rho^*}{\gamma} \frac{\partial \xi}{\partial \psi} \tag{3.15}$$

which implies

$$\rho = \rho^* \left(1 + \frac{\xi}{\gamma}\right) \tag{3.16}$$

Also from (3.7) and (3.8)

$$\frac{dP}{d\psi} = P^* \frac{d\xi}{d\psi} \tag{3.17}$$

$$\frac{dV}{d\psi} = \frac{d\bar{V}}{d\psi} = V^* \frac{d\eta}{d\psi} \tag{3.18}$$

The perturbation expressions (3.7) and (3.18) are inserted into the continuity equation (2.30). Note that q_1 and q_2 are replaced by (3.12) and (3.13) respectively. By doing this, one obtains terms of zeroth, first and second order. Each order is considered separately. The zeroth order relation, $q_2^* - q_1^* = 0$, of course, contains no new information. The second order terms are neglected since they are much smaller than first order ones when $r << \delta_1^*, \delta_2^*$. The first order terms yield the following linearized perturbation equation

$$\left\{\rho^*\left(\bar{V}^* + \Omega R_s\right) hl \frac{d\eta}{d\psi} + \rho^* \bar{V}^* \frac{df}{d\psi} + \frac{\rho^* \bar{V}^* hl}{\gamma} \frac{d\xi}{d\psi}\right\} - q^* R_s \left\{\frac{r}{\delta_2^*} - \frac{r}{\delta_1^*}\right\} \cos\psi$$

$$+ \xi q^* \left\{\frac{P^{*2}}{P^{*2} - P_o^2} + \frac{P^{*2}}{P_i^2 - P^{*2}}\right\} R_s = 0 \tag{3.19}$$

Analogously, the linearized, perturbation momentum equation that results from (2.31) is

$$\left\{\rho^* h1\bar{V}^* V^* \frac{d\eta}{d\psi} + \rho^* h1 V^{*2} \frac{d\eta}{d\psi} + \rho^* \bar{V}^* V^* \frac{df}{d\psi} + \frac{\rho^* h1 \bar{V}^* V^*}{\gamma} \frac{d\xi}{d\psi}\right\}$$

$$+\left(\frac{R_S \rho^*}{8\gamma}\right)\left[\lambda_S 1 V^{*2} - \lambda_R (1+2h)(\omega R_S - V^*)^2\right]\xi + P^* h1 \frac{d\xi}{d\psi}$$

$$+R_S q^* \left(\frac{V^* P^{*2}}{P^{*2} - P_o^2} + \frac{V_i P^{*2}}{P_i^2 - P^{*2}}\right) \xi$$

$$+\left\{\left(\frac{R_S \rho^* V^*}{4}\right)\left[\lambda_S 1 V^* + \lambda_R (1+2h)(\omega R_S - V^*)\right] + \left(R_S q^* V^*\right)\right\} \eta$$

$$-\left\{R_S q^* \left(\frac{V^*}{\delta_2^*} - \frac{V_i}{\delta_1^*}\right) r \cos\psi\right\} = 0 \qquad (3.20)$$

3.4 HARMONIC SOLUTIONS

It has already been assumed that the clearances and area are periodic functions of the whirling angle ψ. Now the perturbations in pressure and velocity are also assumed to consist of a first harmonic in ψ. That is, the fluid properties can be represented mathematically by simple sinusoidal functions with unknown amplitudes and phases. Physically, this is a very special case. More generally one would expect that the form of the solution could consist of the sum of any number of harmonic functions with period $2\pi n$ (n = integer). Solu-

tions of this type could be allowed because they maintain constructive interference. Since the problem is now linear there are no interactions among the various harmonic components. Therefore each can be treated separately. The reason that one would like to consider the first harmonic only can clearly be seen by examining equations (1.7) and (1.8). The contribution to the aeroelastic forces F_{X_1} and F_{X_2} from any component other than the first harmonic vanishes due to orthogonality. These other harmonics will not be treated here explicitly, but it should be noted that in the closely related problem of high cycle fatigue (HCF) of the sealing knives they can be important. Discussions of this problem along with the common aerodynamic approaches used are given in the papers by Abbot (40), Srinivasan and Dennis (41) and Lewis and Platt (42). The basic model to be used for the prediction of stiffness and damping coefficients appears to be equally applicable to the problem of HCF. Returning to the problem at hand, it will prove convenient, for manipulation purposes, to express these assumed harmonic solutions in complex exponential notation. The pressure and velocity perturbations ξ and η are represented as,

$$\xi = R_e\left[\hat{\xi}\, e^{-i\psi}\right] \tag{3.21}$$

$R_e[\,]$ = real part of

$$\eta = R_e\left[\hat{\eta}\, e^{-i\psi}\right] \tag{3.22}$$

Here $\hat{\xi}$ and $\hat{\eta}$ are complex constants which contain both amplitude and phase information because they can be represented in the complex plane as shown in Figure 10 as

$$\hat{\xi} = \hat{\xi}_{RE} + i\hat{\xi}_{IM} \tag{3.23}$$

$$\hat{\eta} = \hat{\eta}_{RE} + i\hat{\eta}_{IM} \tag{3.24}$$

Again referring to Figure 10 the amplitudes and phases are given by

$$|\hat{\xi}| = \left(\hat{\xi}_{RE}^2 + \hat{\xi}_{IM}^2\right)^{1/2} \tag{3.25}$$

$$|\hat{\eta}| = \left(\hat{\eta}_{RE}^2 + \hat{\eta}_{IM}^2\right)^{1/2} \tag{3.26}$$

$$\psi_\xi = \tan^{-1} \frac{\hat{\xi}_{IM}}{\hat{\xi}_{RE}} \tag{3.27}$$

$$\psi_\eta = \tan^{-1} \frac{\hat{\eta}_{IM}}{\hat{\eta}_{RE}} \tag{3.28}$$

Where ψ_ξ and ψ_η are the angles ahead of the minimum gap where the maximum perturbation in pressure and velocity respectively occur. Care must be taken in assigning the appropriate ψ's. Usually the principle value is taken, $-\pi/2 < \psi < \pi/2$ but in this case ψ should be defined on $[-\pi,\pi]$. On this interval $\tan^{-1}$ is multivalued therefore the ψ's should be chosen such that $\hat{\xi}_{IM}$, $\hat{\eta}_{IM} > 0 \Rightarrow \psi > 0$ and

$\hat{\xi}_{IM}$, $\hat{\eta}_{IM} < 0 \Rightarrow \psi < 0$. The derivatives of ξ and η are

$$\frac{d\xi}{d\psi} = \frac{d}{d\psi}\left\{\hat{\xi}e^{-i\psi}\right\} = -i\hat{\xi}e^{-i\psi} \tag{3.29}$$

$$\frac{d\eta}{d\psi} = -i\hat{\eta}e^{-i\psi} \tag{3.30}$$

The variation of the area can be represented in this notation as

$$\frac{df}{d\psi} = R_e\left[-irle^{-i\psi}\right] \tag{3.31}$$

Substituting these into equation (3.19) rearranging, noting that $\bar{V}^* = V^* - \Omega R_s$, and eliminating the phasor $e^{-i\psi}$ yields the following linearized perturbation equation of continuity

$$\left\{\left(\frac{\rho^* hl}{\gamma}\right)\bar{V}^* i - q^* R_s\left(\frac{P^{*2}}{P^{*2}-P_o^2} + \frac{P^{*2}}{P_i^2-P^{*2}}\right)\right\}\hat{\xi}$$

$$+\left\{\rho^* V^* hli\right\}\hat{\eta} = \left\{\rho^*\bar{V}^* li - q^* R_s\left(\frac{1}{\delta_2^*} - \frac{1}{\delta_1^*}\right)\right\} r \tag{3.32}$$

and assuming harmonic solutions yields the following linearized momentum equation when applied to equation (3.20),

$$\left\{\frac{\rho^*\bar{V}^* V^* hli}{\gamma} - \frac{R_s q^* V^* P^{*2}}{P^{*2}-P_o^2} - \frac{R_s q^* V_i P^{*2}}{P_i^2-P^{*2}} - \left[\left(\frac{R_s\rho^*}{8\gamma}\right)\left[\lambda_s lV^{*2}\right.\right.\right.$$

$$\left.\left.\left. - \lambda_R(1+2h)(\omega R_s - V^*)^2\right] + hlP^* i\right\}\hat{\xi} + \left\{\rho^* V^*\left(\bar{V}^* + V^*\right)hli\right.$$

$$- R_s q^* V^* - \left(\frac{R_s \rho^* V^*}{4}\right)\left(\lambda_s 1 V^* + \lambda_R (1+2h)\cdot(\omega R_s - V^*)\right)\Bigg\} \hat{\eta}$$

$$= \left\{\rho^* \bar{V}^* V^* 1 i - R_s q^* \left(\frac{V^*}{\delta_2^*} - \frac{V_i}{\delta_1^*}\right)\right\} r \qquad (3.33)$$

These two linear algebraic equations contain the complex perturbation variables $\hat{\xi}$ and $\hat{\eta}$ as unknowns on the left hand side with known parameters (zeroth order quantities and whirling amplitude) on the right hand side. These equations may be written, employing matrix notation, as

$$\begin{bmatrix} A_{11} & A_{21} \\ A_{21} & A_{22} \end{bmatrix} \begin{Bmatrix} \hat{\xi} \\ \hat{\eta} \end{Bmatrix} = \begin{Bmatrix} R_1 \\ R_2 \end{Bmatrix} r \qquad (3.34)$$

The next chapter will deal with the solution of this system for the various cases. The equations will be non-dimensionalized and some physical interpretation will be attached to the various terms in the equations.

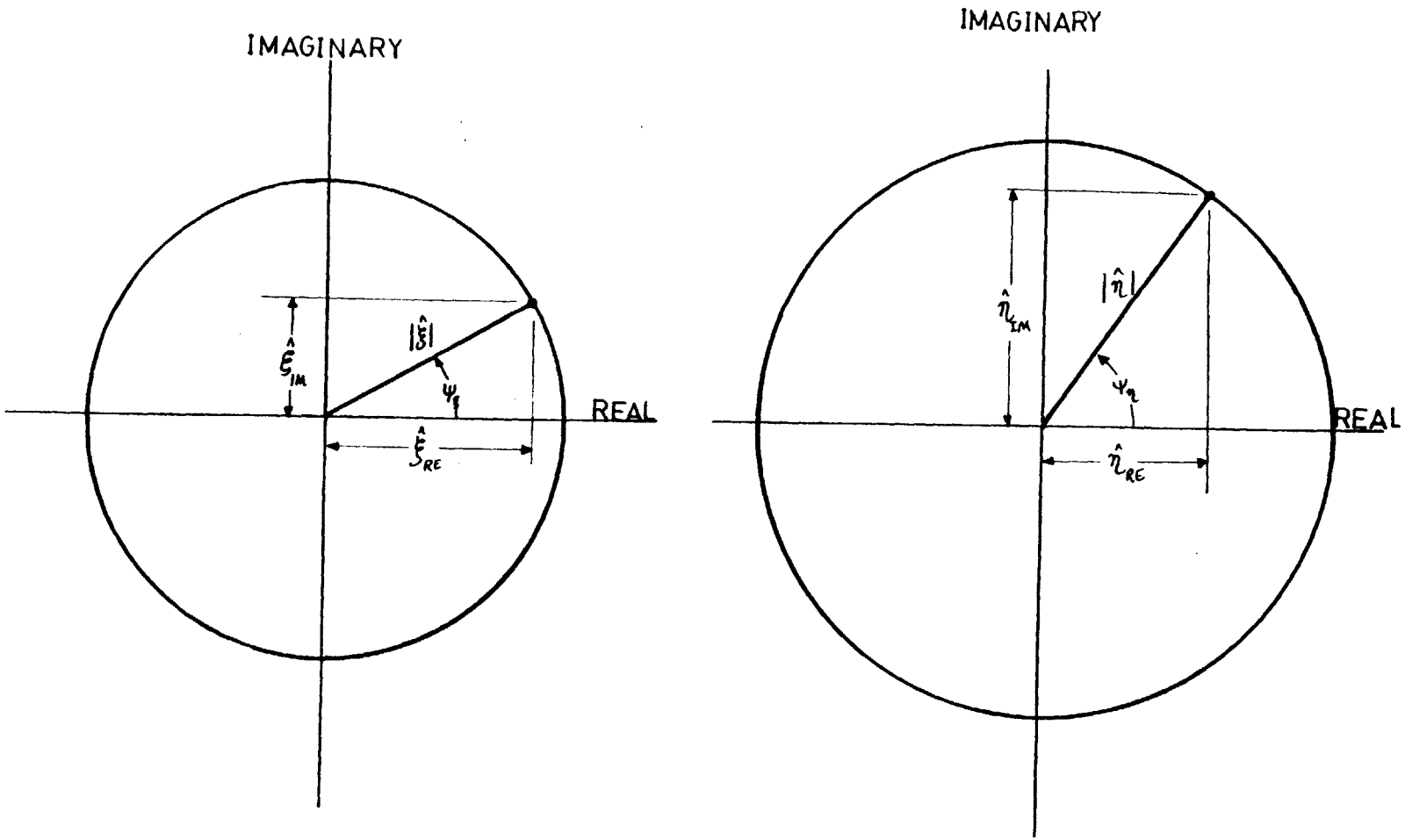

Figure 10 - Complex plane representation of the complex amplitudes of the pressure and velocity perturbations.

CHAPTER 4

NON-DIMENSIONALIZATION AND SOLUTION OF GOVERNING EQUATIONS

4.1 NON-DIMENSIONALIZATION OF GOVERNING EQUATIONS

As presented in the previous chapter, the equations governing the pressure and velocity perturbations for the case of a small amplitude whirling rotor are,

$$\begin{bmatrix} A_{11} & A_{12} \\ A_{21} & A_{22} \end{bmatrix} \begin{Bmatrix} \hat{\xi} \\ \hat{\eta} \end{Bmatrix} = \begin{Bmatrix} R_1 \\ R_2 \end{Bmatrix} r \tag{4.1}$$

It will prove advantageous to recast this system in an equivalent non-dimensional form. When the equations are non-dimensionalized the following geometric, kinematic and flow parameters naturally emerge,

Geometric

$$\varepsilon_1 = \frac{r}{\delta_1^*} \qquad \varepsilon_2 = \frac{r}{\delta_2^*} \qquad \alpha = \frac{\delta_2^*}{\delta_1^*} = \frac{\varepsilon_1}{\varepsilon_2}$$

$$H = \frac{h}{R_s} \qquad L = \frac{l}{R_s} \qquad D = \frac{\delta_1^*}{h} \tag{4.2}$$

Kinematic

$$W = \frac{\Omega R_s}{V^*} \qquad S = \frac{\omega R_s}{V^*}$$

Flow

$$\Delta = \frac{q^*}{\mu \delta_1^* \rho^* \sqrt{R_a T}} \qquad \sigma = \frac{\rho^* \delta_1^* V^*}{q^*} \qquad \Gamma = 1 - \frac{V_i}{V^*}$$

The physical interpretation of some of the parameters, especially the geometric ones, is straightforward while that of others is not. A brief discussion of some of these is in order in light of the central role they will play in subsequent treatments. The ratio of $\frac{\delta_2^*}{\delta_1^*} = \alpha$ indicates the degree to which the seal converges or diverges. $\alpha = 1$ means straight through, $\alpha < 1$ indicates convergence and $\alpha > 1$ implies divergence. The two kinematic parameters, S and W, relate the velocity of the seal surface and gap variation phase speed respectively, to the average circumferential flow velocity inside the gland. It will be found that S is only important in the determination of Γ. Δ is the non-dimensional flow rate, which characterizes the axial pressure difference from inlet to exit. This can be seen if Δ is written as

$$\Delta = \frac{q^*}{\mu \delta_1^* \rho^* \sqrt{RT}} = \left(\left(\frac{P_i}{P^*} \right)^2 - 1 \right)^{1/2} \tag{4.3}$$

σ is proportional to the swirl inside the gland and is a measure of the angle at which the air leaves through the second knife edge.

Finally, Γ is a parameter which measures the axial gradient in swirl. It conveys the degree to which viscous shear forces change the swirl in the seal chamber. If $\Gamma=0$, the inviscid case, the air enters and leaves the gland with the same circumferential velocity. To a first approximation, from Eq. (3.2),

$$V^* \simeq V_i - \frac{\rho^*}{8q^*}\left[\lambda_s 1\ V_i^2 - \lambda_R(1+2h)(V_i-\omega R_s)^2\right] \qquad (4.4)$$

or in nondimensional terms,

$$\Gamma \simeq -\frac{\lambda}{8}\frac{L\sigma}{DH}\left[\mathrm{sgn}(V_i)-\mathrm{sgn}(\omega R_s-V_i)(1+2\,\frac{H}{L})(1-S)^2\right] \qquad (4.5)$$

The continuity Equation (3.32) has dimensions of $[MT^{-1}]$ and will be divided by $R_s q^*$ to yield the following non-dimensional continuity equation.

$$\left\{\frac{\rho^* V^* \delta_1^*}{q^*}\cdot\frac{1}{\gamma}\cdot\frac{1}{R_s}\cdot\frac{h}{\delta_1^*}\left(1-\frac{\Omega R_s}{V^*}\right)i - \frac{\delta_1^{*2}\rho^{*2}R_a T\mu^2}{q^{*2}}\left(1+\frac{\delta_2^{*2}}{\delta_1^{*2}}\right)\right\}\hat{\xi}$$

$$+\left\{\frac{\rho^* V^* \delta_1^*}{q^*}\cdot\frac{1}{R_s}\cdot\frac{h}{\delta_1^*}\,i\right\}\hat{\eta}=\left\{\frac{\rho^* V^* \delta_1^*}{q^*}\cdot\frac{1}{R_s}\cdot\left(1-\frac{\Omega R_s}{V^*}\right)i-\left(\frac{\varepsilon_2}{\varepsilon_1}-1\right)\right\}\frac{r}{\delta_1^*} \qquad (4.6)$$

In terms of the non-dimensional parameters of (4.2) this equation can be simply written as

$$\left\{\frac{\sigma L}{\gamma D}\,(1-W)i\,-\,\frac{1\,+\,\alpha^2}{\Delta^2}\right\}\,\hat{\xi}\,+\,\left\{\frac{\sigma L i}{D}\right\}\,\hat{\eta}$$

$$=\,\{\sigma L(1-W)i+(1\,-\,\frac{1}{\alpha})\}\;\varepsilon_1 \qquad (4.7)$$

The momentum equation could be dealt with directly. However, a simpler form will result by subtracting from it the continuity equation times V^*. This conservation form of the momentum equation can now be non-dimensionalized by dividing by $R_s q^* V^*$. In terms of primitive variables this equation can be written as,

$$\left\{\left(1\,-\,\frac{V_i}{V^*}\right)\left(\frac{P^{*2}}{P_i^2-P^{*2}}\right)\,-\,\frac{\rho^* V^* \delta_1^*}{8\gamma q^* \delta_1^*}\left[\lambda_s 1\,-\,\lambda_R(1+2h)\left(\frac{\omega R_s}{V^*}\,-\,1\right)^2\right]\right.$$

$$\left.+\,\left(\frac{\rho^{*2}\mu^2\delta_1^{*2}R_a T}{q^{*2}}\right)\left(\frac{1}{\mu^2}\right)\left(\frac{1h}{R_s\delta_1^*}\right)\left(\frac{q^*}{V^*\rho^*\delta_1^*}\right)\right\}\,\hat{\xi}$$

$$+\,\left\{\frac{\rho^* V^* \delta_1^*}{q^*}\cdot\frac{h1}{R_s\delta_1^*}\cdot\left(1\,-\,\frac{\Omega R_s}{V^*}\right)i\,-\,1\,-\left(\frac{\rho^* V^* \delta_1^*}{4q^*\delta_1^*}\right)\left[\lambda_s 1\,+\,\lambda_R(1+2h)\right.\right.$$

$$\left.\left.\left(\frac{\omega R_s}{V^*}\,-\,1\right)\right]\right\}\,\hat{\eta}\,=\,\left\{\frac{V_i}{V^*}\,-\,1\right\}\,\frac{r}{\delta_1^*} \qquad (4.8)$$

Again this equation can be written more compactly in terms of the non-dimensional parameters as,

$$\left\{\frac{\Gamma}{\Delta^2} - \frac{\sigma L}{8\gamma DH}\left[\lambda_s - \lambda_R\left(1 + \frac{2H}{L}\right)(S-1)^2\right] + \frac{L}{\Delta^2\sigma\mu^2 D}\, i\right\}\hat{\xi}$$

$$+ \left\{\frac{\sigma L}{D}(1-W)i - 1 - \frac{\sigma L}{4HD}\left[\lambda_s + \lambda_R\left(1 + \frac{2H}{L}\right)(S-1)\right]\right\}\hat{\eta} = -\Gamma\varepsilon_1 \qquad (4.9)$$

A matrix equation for (4.5) and (4.7) analogous to (4.1) can be written with non-dimensional coefficients as,

$$\begin{bmatrix} B_{11} & B_{12} \\ B_{21} & B_{22} \end{bmatrix}\begin{Bmatrix} \hat{\xi} \\ \hat{\eta} \end{Bmatrix} = \begin{Bmatrix} Z_1 \\ Z_2 \end{Bmatrix}\varepsilon_1 \qquad (4.10)$$

This system will now be solved.

4.2 SOLUTION OF EQUATIONS

Two distinct possibilities arise when considering the solution of (4.8). First, for r=0 the determinant of B must vanish for non-trivial solutions to exist. This case would correspond, within the approximation of this model to a standing acoustic mode in the labyrinth gland. When one attempts to solve the implicit relationship which results from Det $B_{ij}=0$ for one of the parameters (e.g. $\Gamma=\Gamma(\sigma,W,S,A...)$) only complex roots can be found, which are physically unreal. Even when friction terms are neglected, $\hat{\xi}=0$, $\hat{\eta}=0$ are the only solutions. This state of affairs could be predicted directly from considering the 1-D acoustic wave equation inside the annulus with the appropriate monopole source distribution term (43). Any standing mode started within the annulus would quickly die

from the induced pressure perturbations generating extra flow losses over the seal knives. This has been shown indirectly by Ingard (44) while considering the acoustic-elastic instability problem experienced by labyrinth seals.

The other case of $r \neq 0$, $\det B \neq 0$ is the physically important one. By eliminating $\hat{\eta}$ the pressure perturbation $\hat{\xi}$, is given by

$$\hat{\xi} = \left\{ \left[\sigma L(1-W)i + \left(1 - \frac{1}{\alpha}\right) \right] \cdot \left[\frac{\sigma L}{D}(1-W)i - 1 \right] - \frac{\sigma L}{4HD}\left[\lambda_s + \lambda_R \left(1 + \frac{2H}{L}\right)(S-1) \right] + \Gamma \frac{\sigma L i}{D} \right\} \varepsilon_1 /$$

$$\left\{ \left[\frac{\sigma L}{\gamma D}(1-W)i - \frac{1+\alpha^2}{\Delta^2} \right] \left[\frac{\sigma L}{D}(1-W)i - 1 - \frac{\sigma L}{4HD}\left[\lambda_s + \lambda_R \left(1 + \frac{2H}{L}\right)(S-1) \right] \right] - \left[\frac{\sigma L i}{D} \right] \left[\frac{\Gamma}{\Delta^2} - \frac{\sigma L}{8\gamma DH}\left[\lambda_s - \lambda_R \left(1 + \frac{2H}{L}\right)(s-1)^2 \right] + \frac{L}{\Delta^2 \sigma \mu^2 D} i \right] \right\} \tag{4.11}$$

For some configurations and flow conditions certain terms can be neglected from this expression. However, for a wide range of parameters, typical of modern designs, only the shear stress perturbations can always be eliminated with the knowledge that they are at least an order of magnitude smaller than the other remaining terms. Dropping the shear stress terms yields the following simplified expression for $\hat{\xi}$.

$$\hat{\xi} = \left\{\left[\sigma L(1-W)i + \left(1 - \frac{1}{\alpha}\right)\right]\left[\frac{\sigma L}{D}(1-W)i-1\right] + \frac{\Gamma\sigma L}{D}\, i\right\} \varepsilon_1 /$$

$$\left\{\left[\frac{\sigma L}{\gamma D}(1-W)i - \frac{1+\alpha^2}{\Delta^2}\right]\left[\frac{\sigma L}{D}(1-W)i-1\right]\right.$$

$$\left. - \left[\frac{\sigma L i}{D}\right]\left[\frac{\Gamma}{\Delta^2} + \frac{Li}{\Delta^2 \sigma \mu^2 D}\right]\right\} \qquad (4.12)$$

From $\hat{\xi}$, the amplitude and phase information can be extracted as shown in (3.20) through (3.27). One can not say directly if a given magnitude and phase will destabilize a rotor system because as pointed out in Chapter 1, the knowledge of many different forces is needed to determine the system dynamics. For the kind of calculations presented in Chapter 1 the coefficients C_{ij} and K_{ij} are needed. Representative calculations of these will be presented later. However, for the facility design and later comparisons with experimentally obtained data the amplitude and phase representation will prove more useful. From the phase alone one can infer if the net pressure force acting on the rotor has a tendency to add or subtract energy from the through flowing fluid for a given whirl direction. If there was a small amplitude forward whirl ($\Omega > 0$) and a phase lag of the peak pressure with respect to the narrowest gap ($\psi_\xi < 0$), then a component of the force on the rotor would be in the same direction as the velocity since $F_{X_2} \sim -\psi_\xi$. This means that energy is being added to the rotor and this is potentially destabilizing. The same type of argument may be used for forward ($\Omega > 0$) or backward ($\Omega < 0$) whirl with the phase

either leading ($\psi_\xi > 0$) or lagging ($\psi_\xi < 0$)the eccentric motion. If the product of $\psi_\xi \Omega < 0$ then a small whirl will tend to grow. However, when $\psi_\xi \Omega > 0$ no instability will occur. Figure 11 shows the regions of stability/instability for the four separate combinations of Ω and ψ_ξ. The situation is slightly more complicated in terms of the non-dimensional whirl, since $W > 0$ can imply either, $\Omega > 0$ or $\Omega < 0$, depending on the sign of V^*. For these variables the stability criterion is

$$\psi_\xi V^* W < 0 \Rightarrow \text{instability} \qquad (4.13)$$

$$\psi_\xi V^* W > 0 \Rightarrow \text{stability} \qquad (4.14)$$

Unfortunately, this general case is still too complicated to permit straightforward physical interpretation. Hence a few simpler cases will be considered first in order to illuminate the influences of the various terms separately before returning to a more general case.

4.3 THREE SPECIAL CASES

By examining the numerator of (4.12) it can be seen that several terms act as sources driving the perturbations. These terms are σ, $(1-W)$, $(1 - 1/\alpha)$ and Γ. Setting one or more of these to zero it is possible to investigate the effects of the remaining terms. The first special case to be considered treats the dependence of the aerodynamic forces on α, the seal convergence/divergence. This is the

so-called "Alford Seal Effect". To do this, σ is set to zero. This implies V^* is zero since the remaining terms contained in σ are positive definite. Also $\frac{L^2}{\mu^2 D^2}$ is set to 5 for concreteness. This is approximately the seal geometry of the turbine tip shroud for the space shuttle main engine hydrogen turbopumps. Using these simplifications and rearranging, the normalized pressure perturbation can be written as a function of α as,

$$\frac{\hat{\xi}}{\varepsilon_1 \Delta^2} = \frac{\frac{1}{\alpha} - 1}{\alpha^2 + 6} \tag{4.15}$$

Two items deserve comment. First this is a real function which implies that the force generated is in phase with the displacement. This is contrary to what was predicted by Alford (15). This discrepancy arises because Alford did not allow for circumferential flow whereas this theory does. The acoustic waves that redistribute the flow may not be ignored. Second the force is not whirl dependent. This specific phenomenon contributes to the direct elastic coefficients only. Figure 12 shows a graph of $\frac{\hat{\xi}}{\varepsilon_1 \Delta^2}$ vs α. From this, it is seen that a convergent seal, $\alpha < 1$, produces a negative direct force, since F_{X_1} is proportional to $-\hat{\xi}$. This would usually be beneficial since it tends to stiffen the rotor/bearing system, hence driving up the critical frequencies. This behavior is similar to the Lomakin (45) effect found in annular seals. However, the

magnitude of the forces is usually smaller and the physical mechanism does not appear to be the same. A divergent seal, $\alpha > 1$ produces a force that resists the shafts propensity to return to a centered position after some small deflection. This force reaches a maximum when $\alpha = 2.16$. In the more general case to be described later α will contribute to the cross force on the rotor and hence α will influence motor stability. The force generated for either convergent or divergent configuration is proportional to Δ^2. Even though this will not be exactly true in the general case, it will serve as a semi-quantitative guide.

The second case of interest is of a straight through seal (α=1) configuration when the steady state swirl velocity is close to the gap variation phase speed (e.g. $V^* \simeq \Omega R_s \Rightarrow$ W~1). Letting L=D, dropping the appropriate terms and rationalizing gives the following expression for the pressure perturbation per unit eccentricity.

$$\frac{\hat{\xi}}{\varepsilon_1} = \frac{\Delta^2 \Gamma\sigma}{\left(2 + \frac{1}{\mu^2}\right)^2 + \sigma^2\Gamma^2}\left[-\sigma\Gamma + \left(2 + \frac{1}{\mu^2}\right)i\right] \qquad (4.16)$$

For most reasonable choices of parameters $|\sigma\Gamma| << |2 + \frac{1}{\mu^2}|$ therefore (4.16) may be simplified to

$$\frac{\hat{\xi}}{\varepsilon_1 \Delta^2} = \frac{\Gamma\sigma i}{\left(2 + \frac{1}{\mu^2}\right)} \qquad (4.17)$$

Since the right hand side is purely imaginary the pressure maximum is $\pm$ 90° out of phase depending on the sign of $\Gamma\sigma$. This would imply that a very destabilizing condition may exist if Γ and σ have opposite signs for $\Omega > 0$ or the same signs with $\Omega < 0$. This can be put in more physical terms by combining (4.14) and (4.17). From this, instability occurs if

$$(V^* - V_i)\ \Omega < 0 \tag{4.18}$$

Recall that $V^* = \Omega R_s$ for this case. Therefore the condition becomes

$$\Omega^2 R_s < V_i \Omega \tag{4.19}$$

If the shaft spin ω is assumed positive then two cases need to be considered. $\Omega > 0$, forward whirl, and $\Omega < 0$, backward whirl. Dividing (4.19) by Ω and replacing ΩR_s by V^* yields the condition for forward whirl namely,

$$V_i > V^* \tag{4.20}$$

This condition states that if the preswirl of the air entering the seal is in the same direction as the seal rotation and is admitted at a higher absolute value, the aerodynamic forces will tend to promote a forward whirl instability. For backward whirl, $\Omega < 0$, (4.19) becomes,

$$V^* > V_i \tag{4.21}$$

This is the opposite condition as prescribed in (4.20).

However, any $V^* > 0$ must be excluded since $W = 1$ implies that V^* and Ω must have the same sign. This means that if the preswirl V_i, is in the opposite direction as the shaft spin backward whirl is driven. The physical mechanism feeding the instability for these two cases is easily identified. The reason V^* is different from V_i is due to the presence of friction forces. But by Newton's Third Law the change in swirl must be accompanied by a reaction torque on the rotor surfaces. It is this reaction which drives the whirl when $V^* \simeq \Omega R_s$. This phenomena will be present in the general case but other factors will also contribute. The magnitude of this transverse force scales like $\Delta^2 \Gamma \sigma P^*$ which in terms of primitive variables gives,

$$\frac{F_{X_2}}{\varepsilon_1} \sim \Delta^2 \Gamma \sigma P^* \sim \left(P_i^2 - P_o^2\right)^{\frac{1}{2}} \left(V^* - V_i\right) \qquad (4.22)$$

A larger pressure difference and/or level generates greater forces. However one cannot eliminate this term without doing away with the need for the seal. Figure 13 shows the amplitude and phase of $\frac{\hat{\xi}}{\varepsilon_1}$ as a function of Γ, treating σ as a parameter.

In the last of the special cases the simplest type of whirl dependent behavior will be investigated. To do this some terms are eliminated by setting $\alpha=1$, $\Gamma=0$, and $L=D$. The condition of $\Gamma=0$ implies that friction is totally neglected

even in the zeroth order approximation. This is a reasonable assumption when either the nominal seal clearances are quite large or when V_i is nearly equal to the asymptotic value of swirl that would be obtained after many such identical chambers. The resulting expression for $\frac{\hat{\xi}}{\Delta^2\varepsilon_1}$ after rationalizing is quite complicated, but for the case of $|\sigma(1-W)| << 1$ it simplifies to

$$\frac{\hat{\xi}}{\Delta^2\varepsilon_1} = \frac{-\sigma L(1-W)i}{\left(2 + \frac{1}{\mu^2}\right)} \tag{4.23}$$

Again the net force is $\pm 90°$ out of phase with the displacement but in this case the magnitude is proportional to $\sigma(1-W)$. Figure 14 shows the amplitude and phase of $\frac{\hat{\xi}}{\Delta^2\varepsilon_1}$ as a function of W using σ as a parameter. It should be noted that at W=1 the forces become small and there is a phase reversal. Substituting (4.23) into the stability relation (4.13) and canceling all unnecessary terms yields

$$(1-W)\ W > 0 \Rightarrow \text{instability} \tag{4.24}$$

This condition is satisfied when $W < 1$, which in terms of primitive variables implies $|V^*| > |\Omega R_s|$. This suggests a useful design criterion to avoid labyrinth seal induced rotor whirl. Make sure the critical bending frequency of the shaft, ω_n, is above V^*/R_s for all seal chambers. These three cases have shown certain types of limiting behavior for special conditions. Now the more general case when all

terms contribute and interact will be treated.

4.3 THE GENERAL CASE: DESIGN STUDY

In the general case none of the terms in equation (4.10) will be neglected. Certain terms will be set and the amplitude and phase behavior of $\frac{\hat{\xi}}{\varepsilon_1}$ as a function of the non-dimensional whirl frequency W, varying one other parameter at a time will be investigated. This type of parametric study was undertaken about several baseline points which were physically realistic. The ultimate goal of this study was to determine what values and ranges of values for the various parameters are needed in order to corroborate this theory, especially with respect to the damping forces. After many iterations a final baseline design was obtained that was consistent with the primary goal and with certain auxiliary conditions such as available facilities, cost, mechanical stress limitations, etc. These will be discussed in more detail in the next chapter. A reasonable and consistent set of geometric and flow related parameters was found to be

$$\alpha = 1.0 \qquad H = 0.05 \qquad L = 0.15 \qquad D = 0.05$$

$$\Delta = 0.8 \qquad \sigma = 0.3 \qquad \Gamma = 0.05 \qquad -1 \leq W \leq 3 \tag{4.25}$$

[A set of primitive variables which correspond to these will be presented in the next chapter.]

The expression for $\frac{\xi}{\varepsilon_1}$ presented in (4.12) becomes somewhat lengthy when rationalized but it can be readily simplified for $|\sigma(1-W)|<<1$ as was done for the case $\Gamma=0$, $\alpha=1$, and $L=D$. The resulting expression is

$$\frac{\hat{\xi}}{\varepsilon_1 \Delta^2} = \frac{\left[-\left(1 - \frac{1}{\alpha}\right) - \frac{\sigma^2 L^2}{D}(1-W)^2\right] + \frac{\sigma L}{D}\left[\Gamma+(1-W)\left(-D+1-\frac{1}{\alpha}\right)\right]i}{1 + \alpha^2 + \frac{L^2}{D^2\mu^2}} \tag{4.26}$$

This expression will be used later to obtain approximate closed form expressions for the rotordynamic coefficients C_{ij} and K_{ij}. When $\alpha=1$, as in the baseline, this simplifies to

$$\frac{\hat{\xi}}{\varepsilon_1 \Delta^2} = \frac{\frac{-\sigma^2 L^2}{D}(1-W)^2 + \sigma L\left[\frac{\Gamma}{D} - (1-W)\right]i}{\left[2 + \frac{L^2}{D^2\mu^2}\right]} \tag{4.27}$$

When $W=0$, the imaginary component hence the out of phase force can be written as

$$\sigma L\left[\frac{\Gamma}{D} - 1\right]i \tag{4.28}$$

From this, it can be seen that when $\Gamma=D$ the imaginary part vanishes, hence a phase crossover occurs. Recall in the baseline case $\Gamma=D=0.05$.

Figure 15 shows the amplitude and phase of $\frac{\hat{\xi}}{\varepsilon_1}$ vs W for the baseline case. The amplitude is a minimum ($\sim 1.0 \times 10^{-3}$ P^*) around W=0.4 and increases on both sides, reaching a maximum ($\sim 6.0 \times 10^{-3}$ P^*) at W=3.0. The phase is positive when $W > 0$ and negative when $W < 0$. If $\sigma < 0$ just the sign of ψ_ξ is reversed. Since V^* is changed this seal also always provides stabilizing forces because $\psi_\xi V^* W$ is always positive.

The first two parametric variations from the baseline will involve the effects of convergence and divergence of the seal. Figure 16 shows the amplitude and phase of $\frac{\hat{\xi}}{\varepsilon_1}$ vs W for the baseline (α=1.0) along with three other cases of diverging seals (α=1.025, 1.05, 1.1). The amplitude of the perturbations tend to be larger for diverging seals. As the seal divergence becomes greater the phase charges sign at lower nondimensional whirl frequencies.

This is true regardless of the sign of σ. This implies that diverging seals tend to destabilize rotors in the direction opposite that of the inlet swirl. Alternatively if a rotor has a tendency to whirl in the direction of inlet swirl, as was the case with $\Gamma \simeq 0$, then a slightly diverging seal may enhance rotor stability.

Figure 17 shows the amplitude and phase of $\frac{\hat{\xi}}{\varepsilon_1}$ vs W for 3 converging seals along with the baseline (α = 1.0, 0.975, 0.95, 0.9). The amplitude behavior shows similar trends to

those of the diverging ones, increasing away from $\alpha=1$. However, the phase shows the opposite trend moving the phase crossover to higher whirl frequencies as α increases. converging seals promote whirl in the same direction as inlet swirl. These seals appear to be very stabilizing to whirl in the other direction, since the amplitude is greater and the phase is around $-\pi/2$.

The next parameter to be presented which influences the forces is Δ. As mentioned earlier Δ is a measure of the through flow pressure gradient. Figure 18 shows the amplitude and phase of $\frac{\hat{\xi}}{\varepsilon_1}$ vs W for $\Delta=0.3$, 0.5, 0.7 and 0.9. The shapes of the amplitude curves do not change much. They appear to be a self similar family of curves which scale as Δ^2 just as in all three special cases plus the small $\sigma(1-w)$ approximations given in (4.26) and (4.27). This suggest that the experimental data should be reduced by presenting $\frac{\hat{\xi}}{\varepsilon_1 \Delta^2}$ vs W. As a consequence of this the phase is invariant to Δ. This situation changes somewhat when $\sigma(1-W) > 1$.

The influence of Γ on the pressure perturbations can be observed by referring to Figure 19. Here $\frac{|\xi|}{\varepsilon_1}$ and ψ_ξ are plotted vs W for four different values of Γ (0.05, 0.01, -0.01, -0.05). The behavior for $|\Gamma| << 1$ approaches very well the case of $\Gamma=0$ in that the minimum pressure occurs along with a phase reversal at W=1. As Γ becomes more positive the minimum amplitude moves to lower whirl frequencies along with the phase cross over. Conversely, as

Γ becomes more negative the minimum amplitude and phase cross over proceed to higher frequencies. The phase behavior shows the combination of the two phenomena presented in special case 2 and 3. The reaction torque may either increase or decrease the range of stable operation depending on the direction in which it acts. As was shown by using (4.28), when Γ=D these two types of forces cancel. Γ can be changed by altering the relative size of rotor and stator surfaces and/or treating these surfaces in an attempt to control the friction factors λ_S and λ_R. D is probably easier to specify.

The last parameter to be investigated is σ. Figure 20 shows the amplitude and phase of $\frac{\hat{\xi}}{\varepsilon_1}$ vs W for $\sigma = \pm 0.1, \pm 0.3, \pm 0.5, \pm 0.7$. The amplitude is a very strong function of $\sigma(1-W)$. This cannot be seen from (4.26) since higher order terms in $\sigma(1-w)$ were neglected in that approximation. The sign of σ does not influence that magnitude of $\frac{\hat{\xi}}{\varepsilon_1}$ however the phase is reflected about the $\hat{\xi} = 0$ axis. This does not alter the regions of stability since both σ and W change signs with V^*. This suggest that the usual definitions of forward and backward whirl, being referenced to the shaft spin, are not very meaningful with reference to labyrinth seal induced rotor whirl. Here it is more illuminating to refer to the physical whirl direction a being with in the same or opposite sense as the mean swirl in the seal.

4.5 ROTORDYNAMIC COEFFICIENTS

As mentioned the rotordynamic coefficient C_{ij} and K_{ij} are needed as inputs to a general purpose rotordynamic stability/response program and can be obtained from the amplitude and phase information. The first step is to integrate the pressure distribution and obtain the net force components in the direction of the minimum gap and 90° ahead of it. From (1.7) and (1.8) these forces may be written as

$$F_{X_1} = -R_s l \int_o^{2\pi} P(\psi)\cos\psi d\psi = -R_s l \int_o^{2\pi} |\hat{\xi}|P^*\cos(\psi-\psi_\xi)d\psi$$

$$= -\pi R_s l |\hat{\xi}|P^*\cos\psi_\xi \qquad (4.29)$$

and

$$F_{X_2} = -\pi R_s l |\hat{\xi}|P^*\sin\psi_\xi \qquad (4.30)$$

By the definition of C and K, F_{X_1} and F_{X_2} can be decomposed into components in phase with the motion (real) and $\pi/2$ ahead (imaginary) in the whirl direction. When the real and imaginary parts are equated the forces per unit eccentricity can be expressed as

$$\frac{F_{X_1}}{r} = -K_{xx} + \Omega C_{xy} \qquad (4.31)$$

$$\frac{F_{X_2}}{r} = -K_{xy} - \Omega C_{xx} \qquad (4.32)$$

The data can be more conveniently presented by using the following non-dimensional rotordynamic coefficients defined by

$$\overline{K_{ij}} = \frac{K_{ij}\delta_1^*}{\pi R_s l P^*} \qquad \overline{C_{ij}} = \frac{C_{ij}V^*\delta_1^*}{\pi R_s^2 l P^*} \tag{4.33}$$

with these definitions, recalling that $W = \frac{\Omega R_s}{V^*}$ and using (4.31) and (4.32) it is possible to relate these as,

$$Re\left(\frac{\hat{\xi}}{\varepsilon_1}\right) = \frac{|\hat{\xi}|\cos\psi_\xi}{\varepsilon_1} = \overline{K_{xx}} - W\,\overline{C_{xy}} \tag{4.34}$$

$$Im\left(\frac{\hat{\xi}}{\varepsilon_1}\right) = \frac{|\hat{\xi}|\sin\psi_\xi}{\varepsilon_1} = \overline{K_{xy}} - W\,\overline{C_{xx}} \tag{4.35}$$

where $\overline{K_{xx}}$, $\overline{C_{xy}}$, etc. are themselves functions of W in general.

The $\overline{C}$'s and $\overline{K}$'s are calculated by inserting neighboring valu of W into these and solving the resulting simultaneous equations. This is called the local secant method and can be done for all W in the range of interest $\Delta W=0.1$ is used for the calculations. Note from the symmetry of the physical system

$$\begin{aligned} \overline{K_{xx}} &= \overline{K_{yy}} & \overline{C_{xx}} &= \overline{C_{yy}} \\ \overline{K_{xy}} &= -\overline{K_{yx}} & \overline{C_{xy}} &= -\overline{C_{yx}} \end{aligned} \tag{4.36}$$

Approximate closed form expressions for the coefficients may be obtained by decomposing (4.26) into real and imaginary components and substituting these into (4.34) and (4.35). By inserting W=0 and W=1 the following expressions for $\overline{K_{xx}}$, $\overline{K_{xy}}$, $\overline{C_{xy}}$ and $\overline{C_{xx}}$ are extracted by this global secant method.

$$\overline{K_{xx}} = \Delta^2 \cdot \frac{-(1 - \frac{1}{\alpha}) - \frac{\sigma^2 L^2}{D}(1-W)^2}{1 + \alpha^2 + (\frac{L}{\mu D})^2} \tag{4.37}$$

$$\overline{K_{xy}} = \frac{\Delta^2 \sigma L}{D} \frac{\Gamma - D + 1 - \frac{1}{\alpha}}{1 + \alpha^2 + (\frac{L}{\mu D})^2} \tag{4.38}$$

$$\overline{C_{xx}} = \frac{\Delta \sigma L}{D} \frac{D - (1 - \frac{1}{\alpha})}{1 + \alpha^2 + (\frac{L}{\mu D})^2} \tag{4.39}$$

$$\overline{C_{xy}} = \frac{-2\Delta^2 \sigma^2 L^2}{D} \frac{(1 - W)}{1 + \alpha^2 + (\frac{L}{\mu D})^2} \tag{4.40}$$

Stability criteria similar to those given for the phase can be presented for these coefficients. The non-dimensional force $\overline{F}_{X_2}$ acting out of phase with the rotor displacement is

$$\frac{\delta_1^* F_{X_2}}{r\pi R_s l P^*} = \frac{\overline{F_{X_2}}}{\varepsilon_1} = - \overline{K_{xy}} - W \overline{C_{xx}} \tag{4.41}$$

Only the cross stiffness and direct damping influence

stability. If $\overline{C_{xx}} = 0$ then $\overline{K_{xy}} > 0$ promotes whirl in the negative direction whereas $\overline{K_{xy}} < 0$ creates whirl in the positive sense. For $\overline{C_{xx}} > 0$ the damping forces must remove more energy than the elastic ones add to maintain stable operation.

$$|W\overline{C_{xx}}| > |\overline{K_{xy}}| \quad \Rightarrow \quad \text{stability} \tag{4.42}$$

However from (4.39) it can be seen that $\overline{C_{xx}}$ need not be positive. In fact when α is greater than $\frac{1}{1-D}$, $\overline{C_{xx}}$ becomes negative which is potentially very destabilizing. One very important consequence of the closed form relations (4.38) and (4.39) is that by properly choosing Γ, α and D the magnitude and signs of $\overline{C_{xx}}$ and $\overline{K_{xy}}$ can be prescribed to enhance stable operation.

Figure 21 shows these coefficients vs W for the baseline case. They follow the closed form expressions well especially for $0 \leq W \leq 2$. This is to be expected since they were derived for $|\sigma(1-W)| << 1$. The high level of stabilization this seal provides is reflected by $\overline{K_{xy}} \sim 0$ and $\overline{C_{xx}} > 0$.

Figure 22 shows the coefficients vs W for $\alpha = 1.1$. These are changed significantly from the baseline and the reduction of stability is reflected by the negative $\overline{C_{xx}}$.

Figure 23 presents $\overline{K_{ij}}$ and $\overline{C_{ij}}$ vs W for $\Gamma = -0.05$. The decreased range of stable operation as was shown in Figure

19 is predicted by the down and shift of $\overline{K_{xy}}$.

Finally Figure 24 shows these rotordynamic coefficients vs W for $\sigma = 0.6$. The magnitudes are much greater as expected. They also differ more from the closed form expressions for a given W since $|\sigma(1-W)|$ is larger.

4.6 SUMMARY

The equations derived in Chapter 3 were nondimensionalized and solved for the pressure perturbation $\hat{\xi}$. Three special cases were investigated showing limiting behavior. A design study was undertaken to determine what range of parameters would be needed in order to experimentally verify this type of theory. The amplitude and phase behavior of $\hat{\xi}$ vs W was investigated using α, Γ, Δ and σ as parameters. Closed form expressions for the rotordynamic coefficients, when $|\sigma(1-W)|<<1$, were derived. From the phase or $\overline{K_{xy}}$ and $\overline{C_{xx}}$ it was seen that Γ, D and α change a seals stability characteristics. It appears that by designing "custom tailored" seals rotor whirl may be eliminated. For a straight seal, $\alpha=1$, $\Gamma=D$ was optimum. However, when $V_i > \omega R_s$, and $\Gamma < 0$ this cannot be accomplished. Therefore α must be tailored. From a practical point of view α must be precisely controlled and it could be very expensive to hold such tight machine tolerances. In theory this could be extended to multichamber seals but the simple closed form solutions would have to be abandoned. Iterative methods would be

needed since α enters into the equations nonlinearly and a N chamber seal yields 2N complex algebraic equations similar to (4.1).

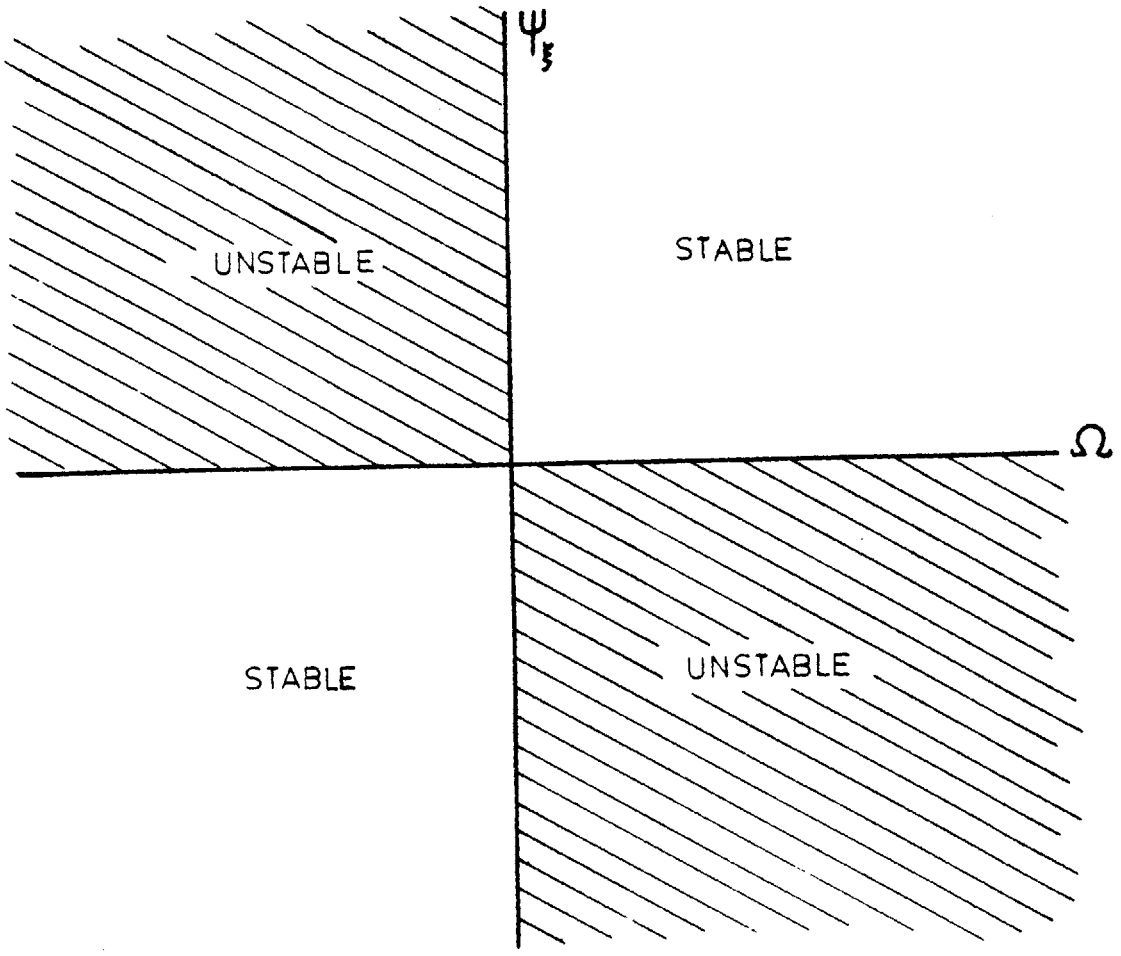

Figure 11 - Stability/instability regions in terms of the gap relative phase ψ_ξ and the rotor whirling frequency Ω.

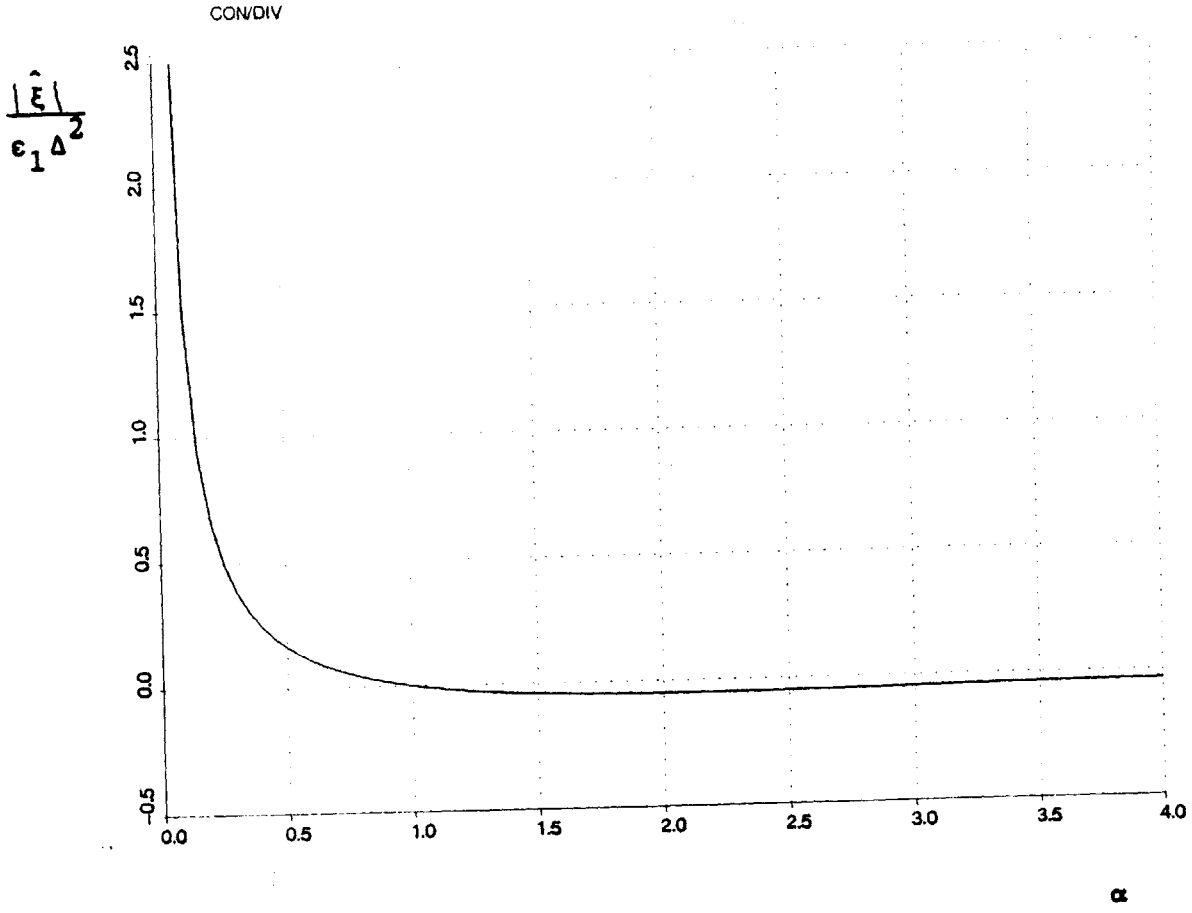

Figure 12 - Normalized amplitude of the pressure perturbation $\left|\frac{\hat{\xi}}{\varepsilon_1 \Delta^2}\right|$ vs. the seal divergence ratio α.

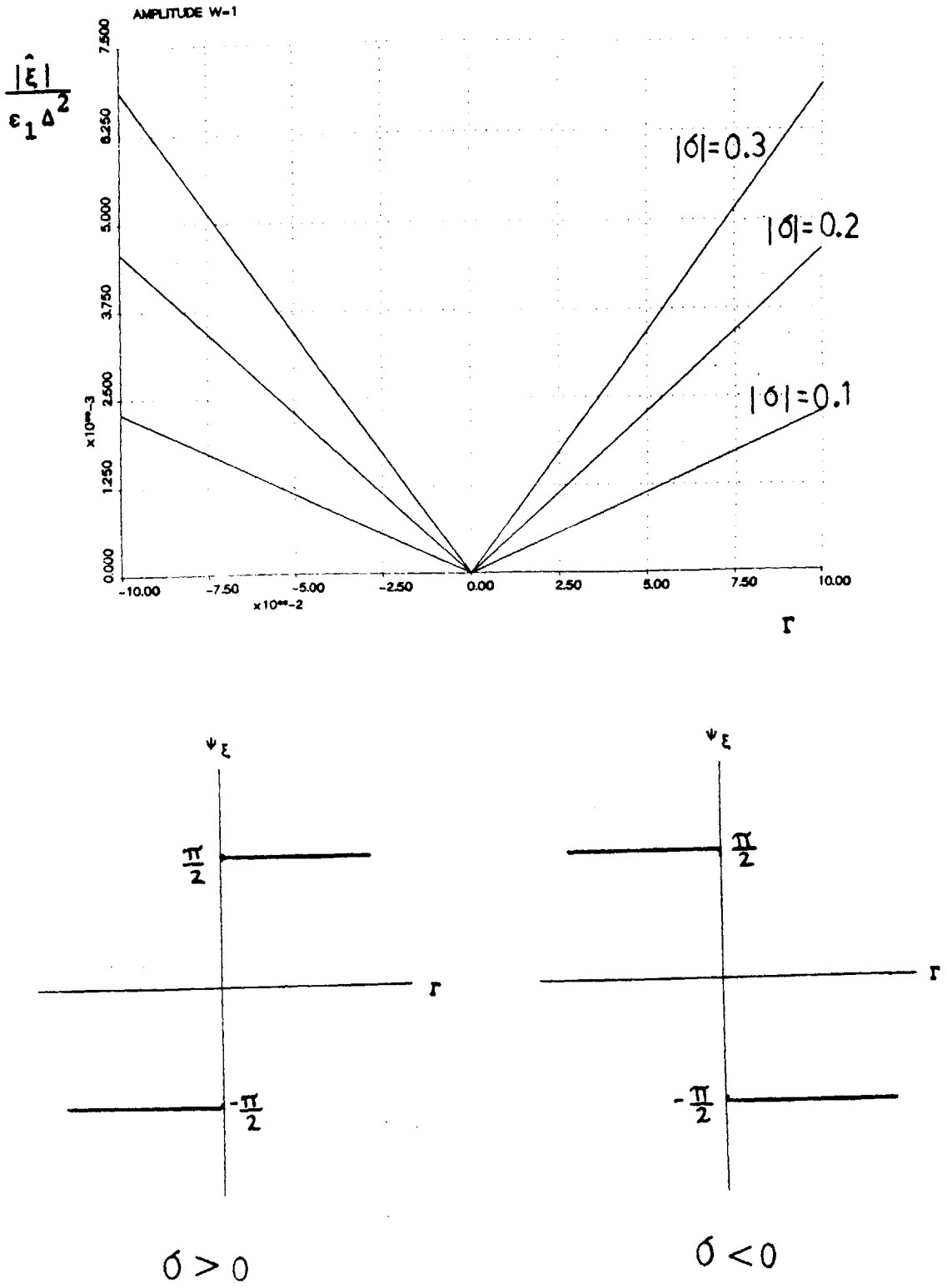

Figure 13 - Amplitude and phase of normalized pressure perturbation vs. the swirl gradient parameter Γ for different values of σ.

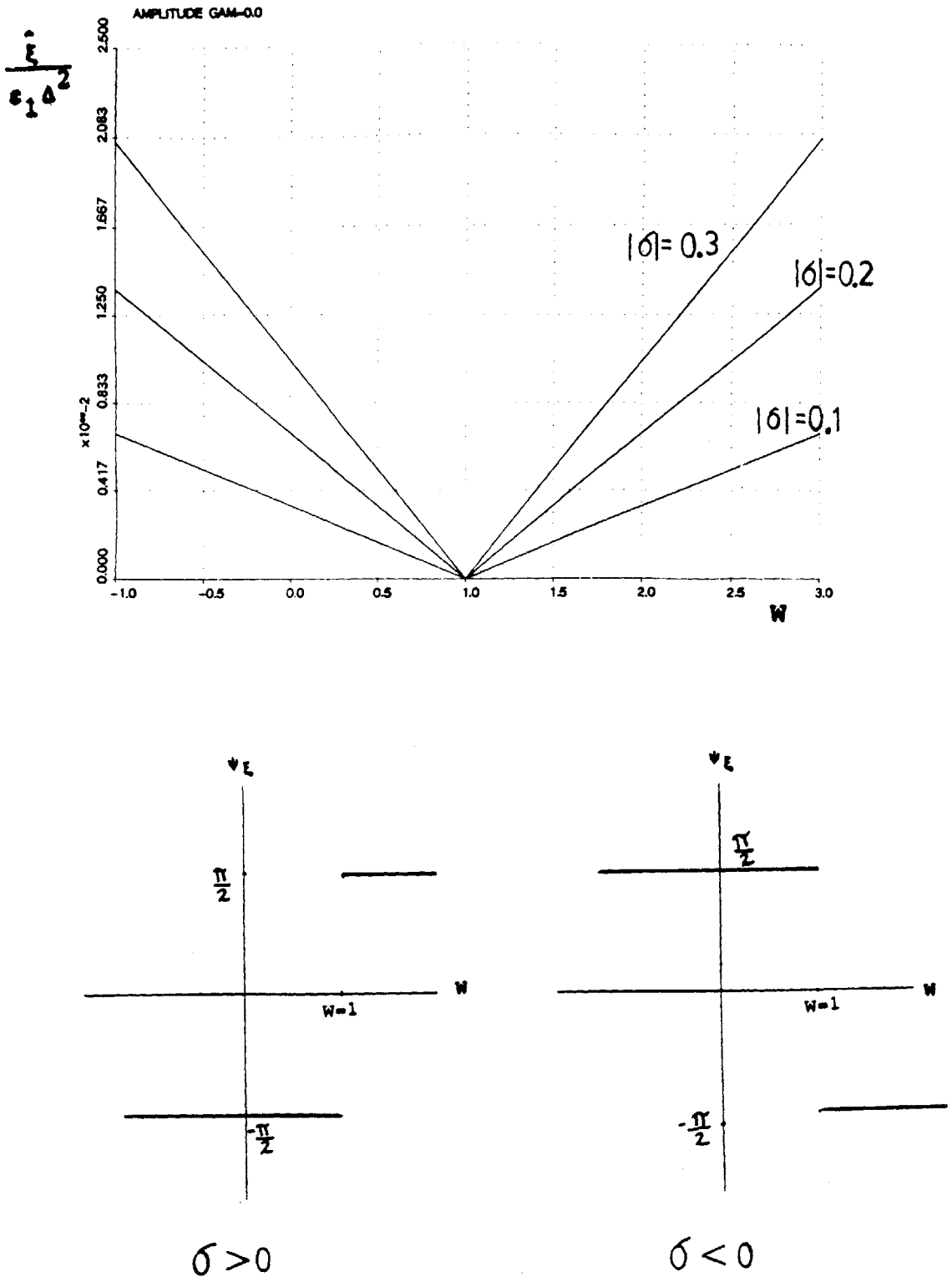

Figure 14 - Amplitude and phase of normalized pressure perturbation vs. non-dimensional whirl frequency for different values of σ.

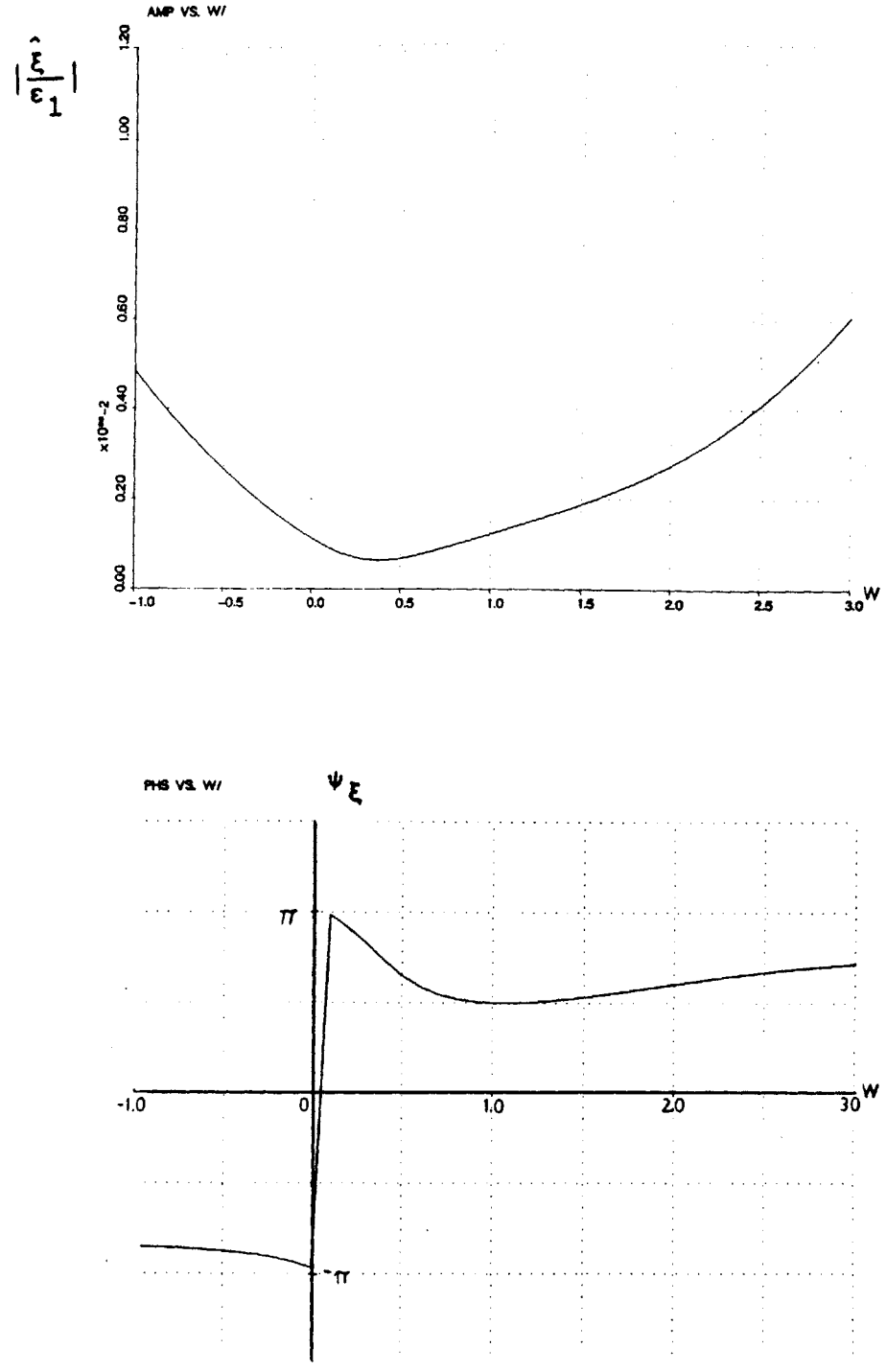

Figure 15 - Amplitude and phase of normalized pressure perturbation vs. non-dimensional whirl W for the baseline configuration.

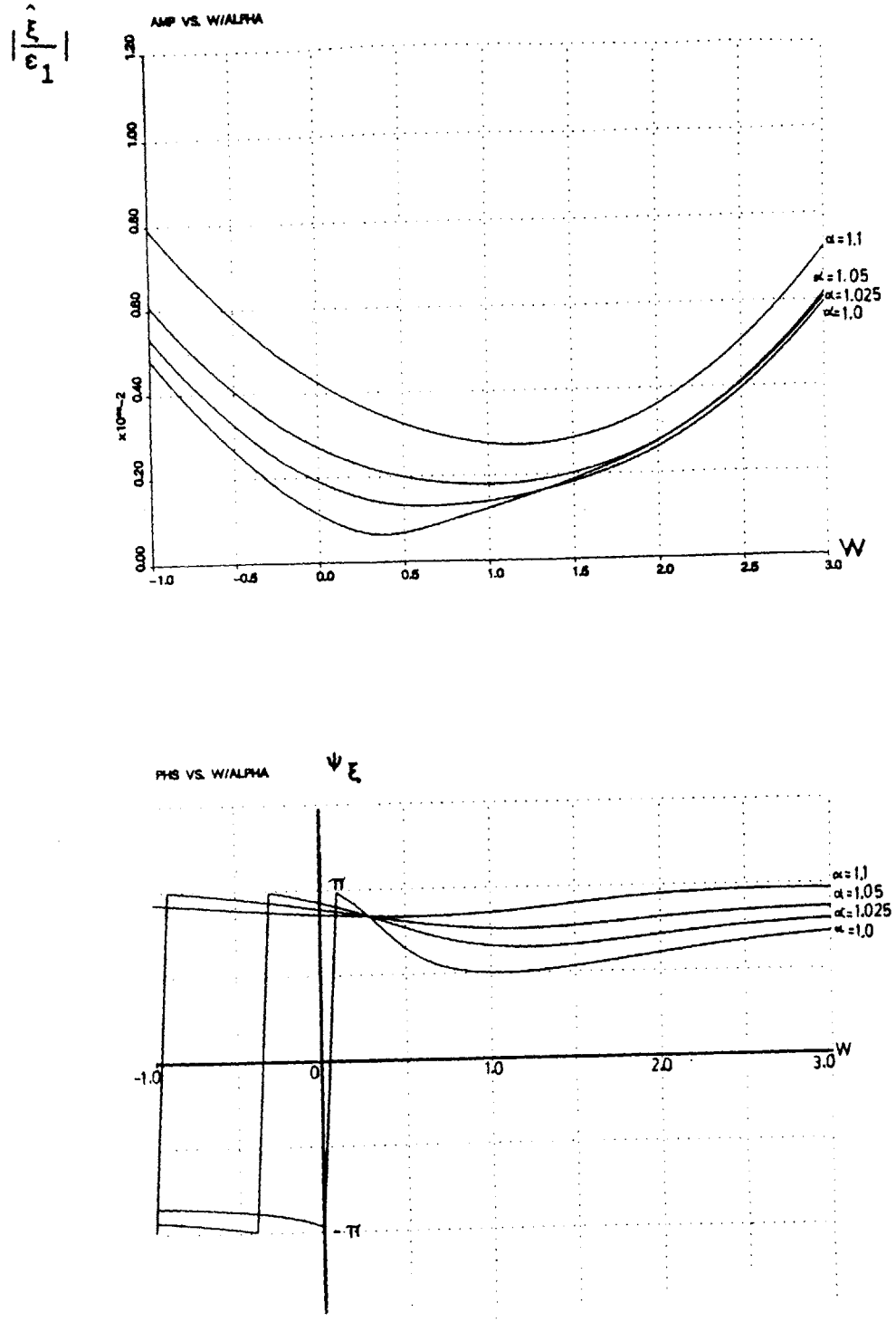

Figure 16 - Amplitude and phase of normalized pressure perturbation vs. non-dimensional whirling frequency W. Three different diverging seals are compared to the baseline case.

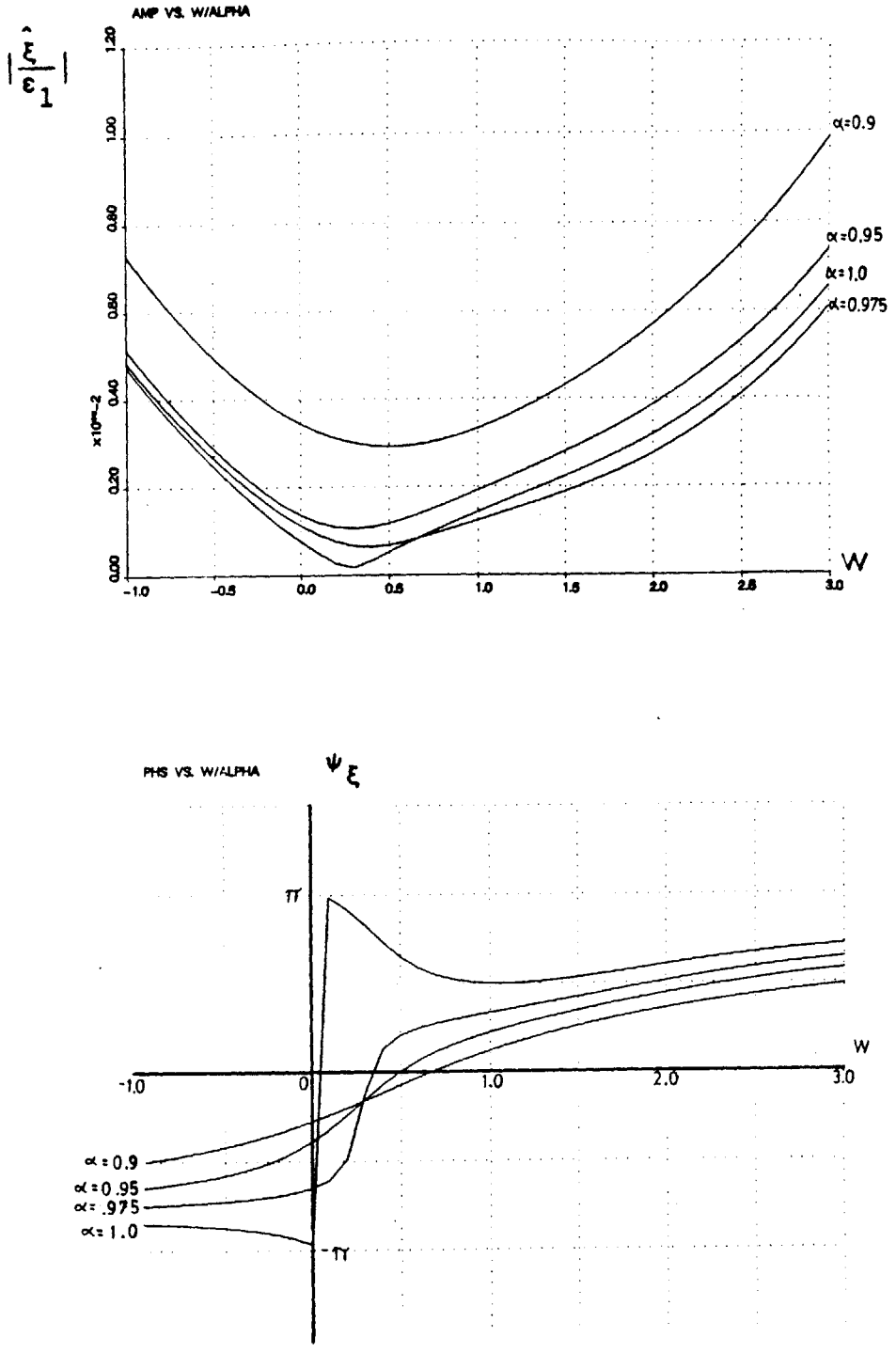

Figure 17 - Amplitude and phase of normalized pressure perturbation vs. non-dimensional whirling frequency W. Three different converging seals are shown along with the baseline.

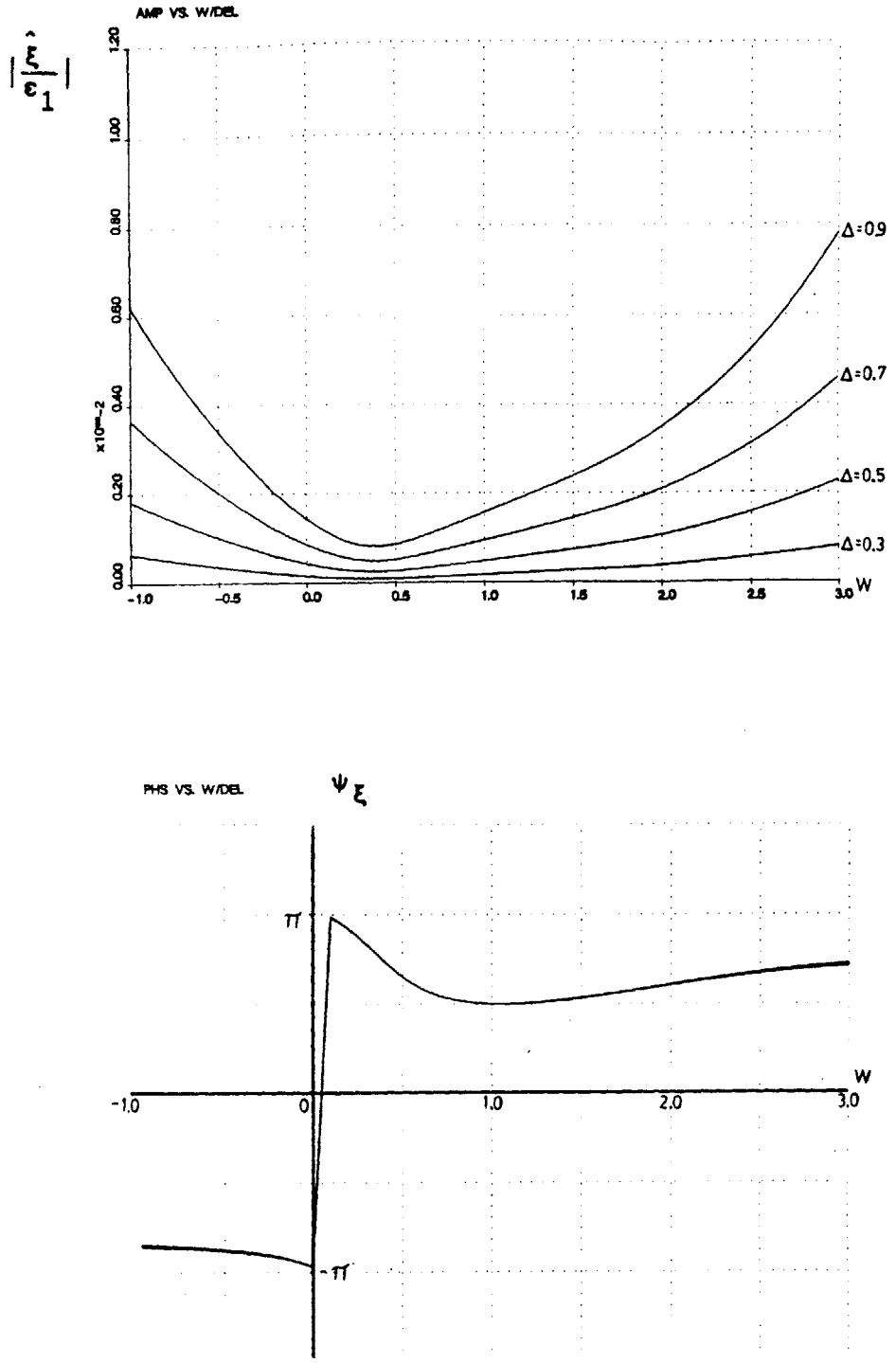

Figure 18 - Amplitude and phase of normalized pressure perturbation vs. non-dimensional whirling frequency W, using Δ=0.3, 0.5, 0.7, and 0.9. All other parameters are the same as baseline.

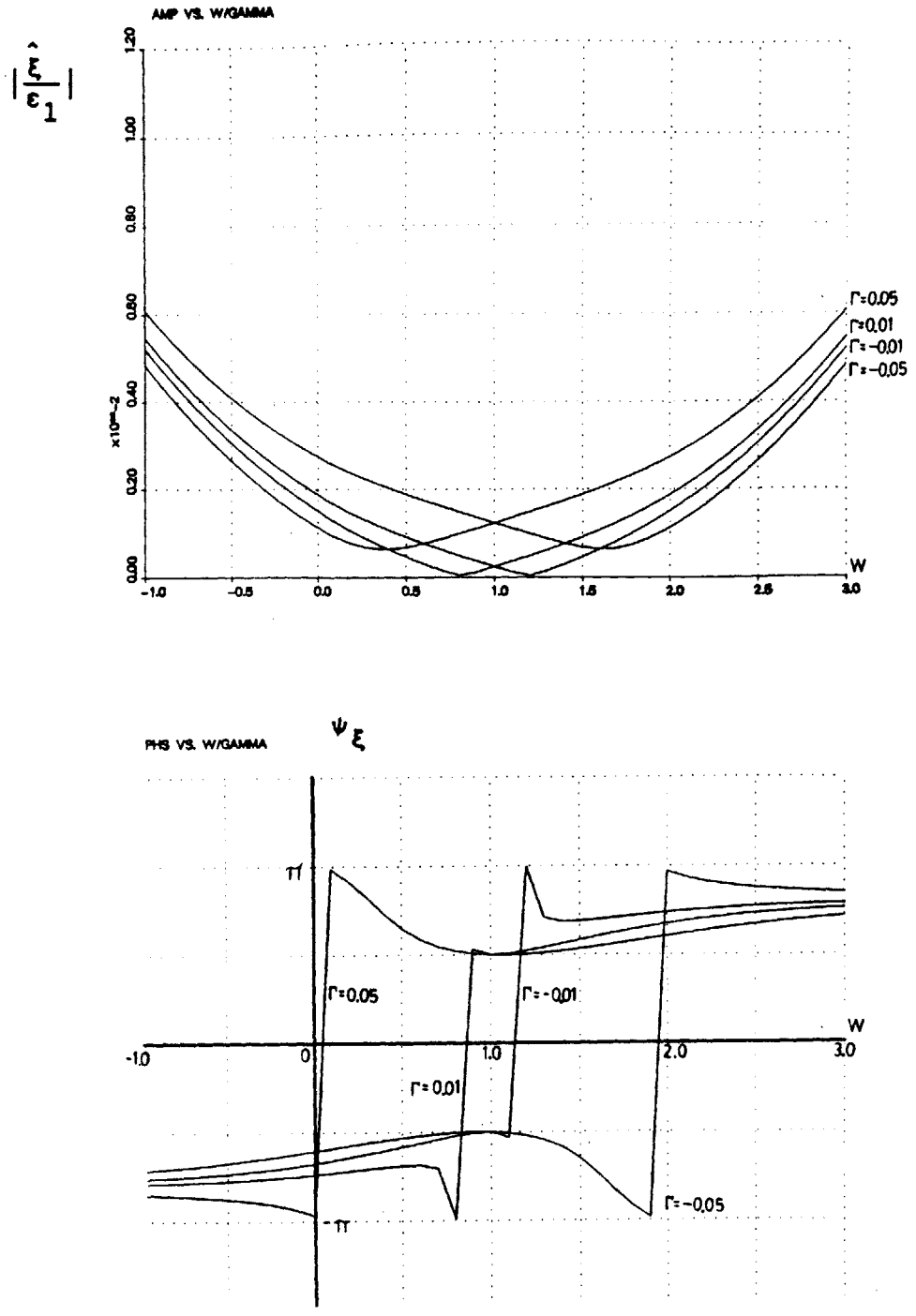

Figure 19 - Amplitude and phase of normalized pressure perturbations vs. non-dimensional whirling frequency W, using Γ=0.05, 0.01, -0.01, and -0.05. All other parameters are the same as baseline.

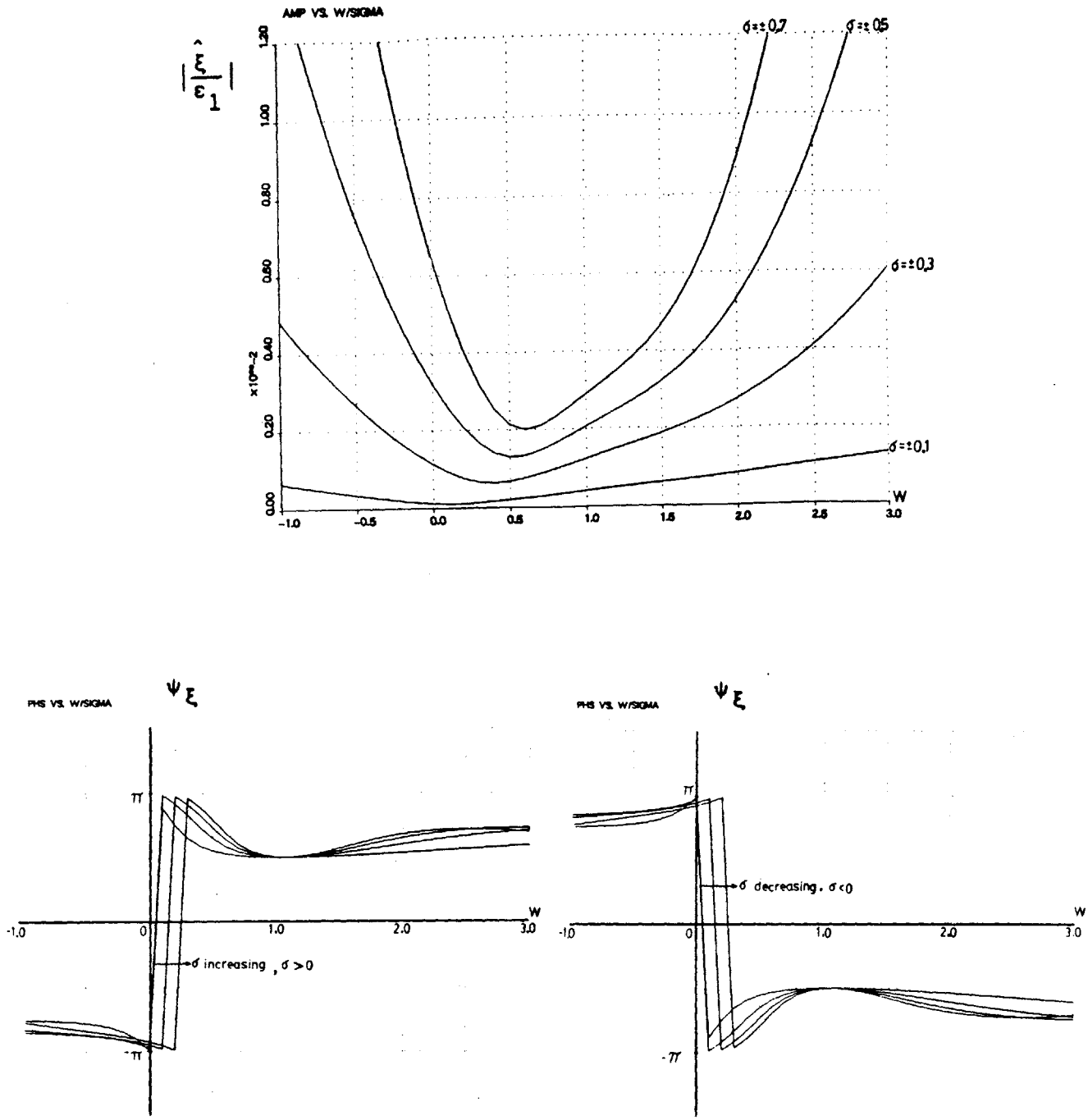

Figure 20 - Amplitude and phase of normalized pressure perturbation vs. non-dimensional whirling frequency W, using σ=0.01, 0.1, 0.2, and 0.4. All other parameters are the same as baseline.

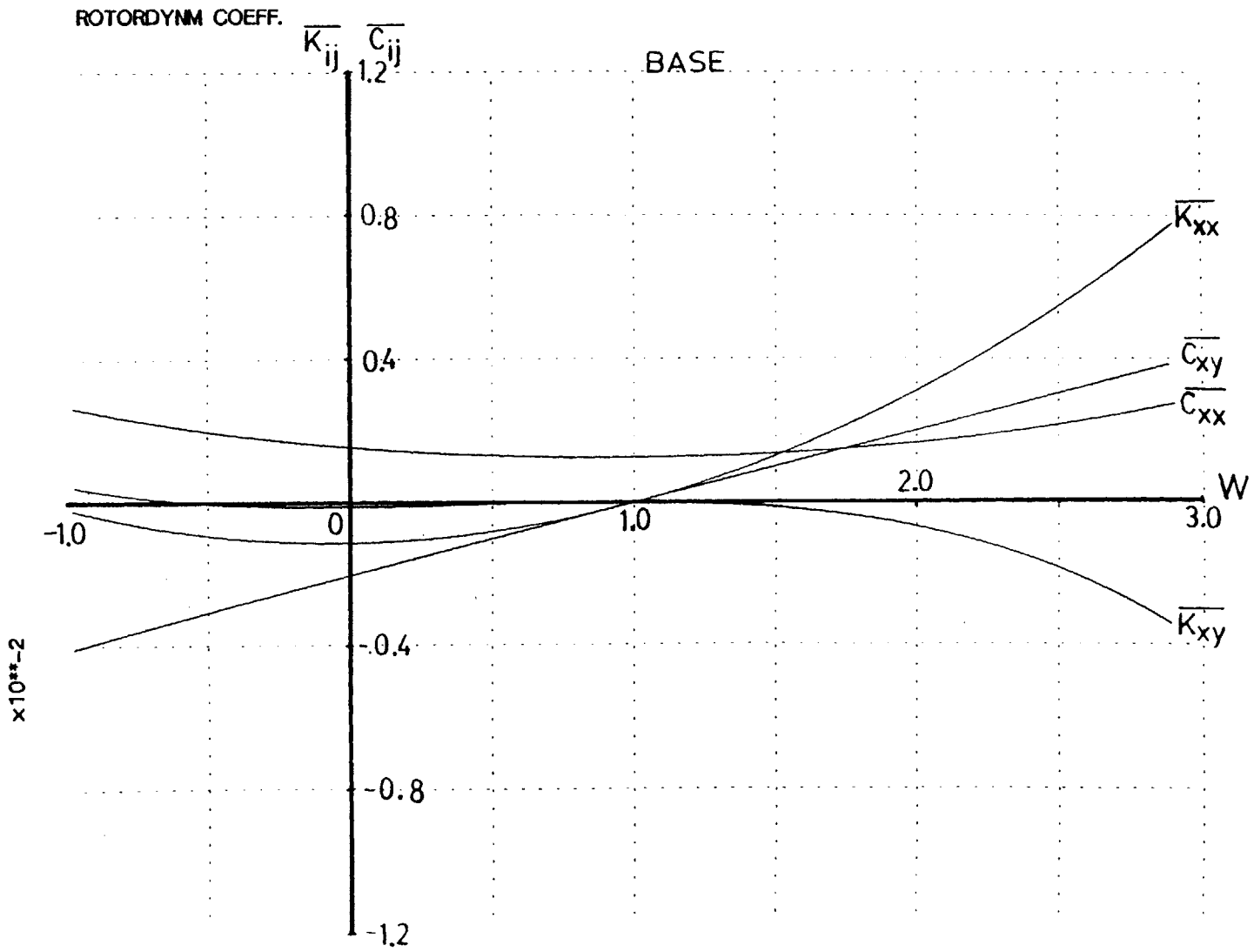

Figure 21 - Non-dimensional rotordynamic coefficients $\bar{K}_{ij}$ and $\bar{C}_{ij}$ vs. non-dimensional whirling frequency W for baseline configuration.

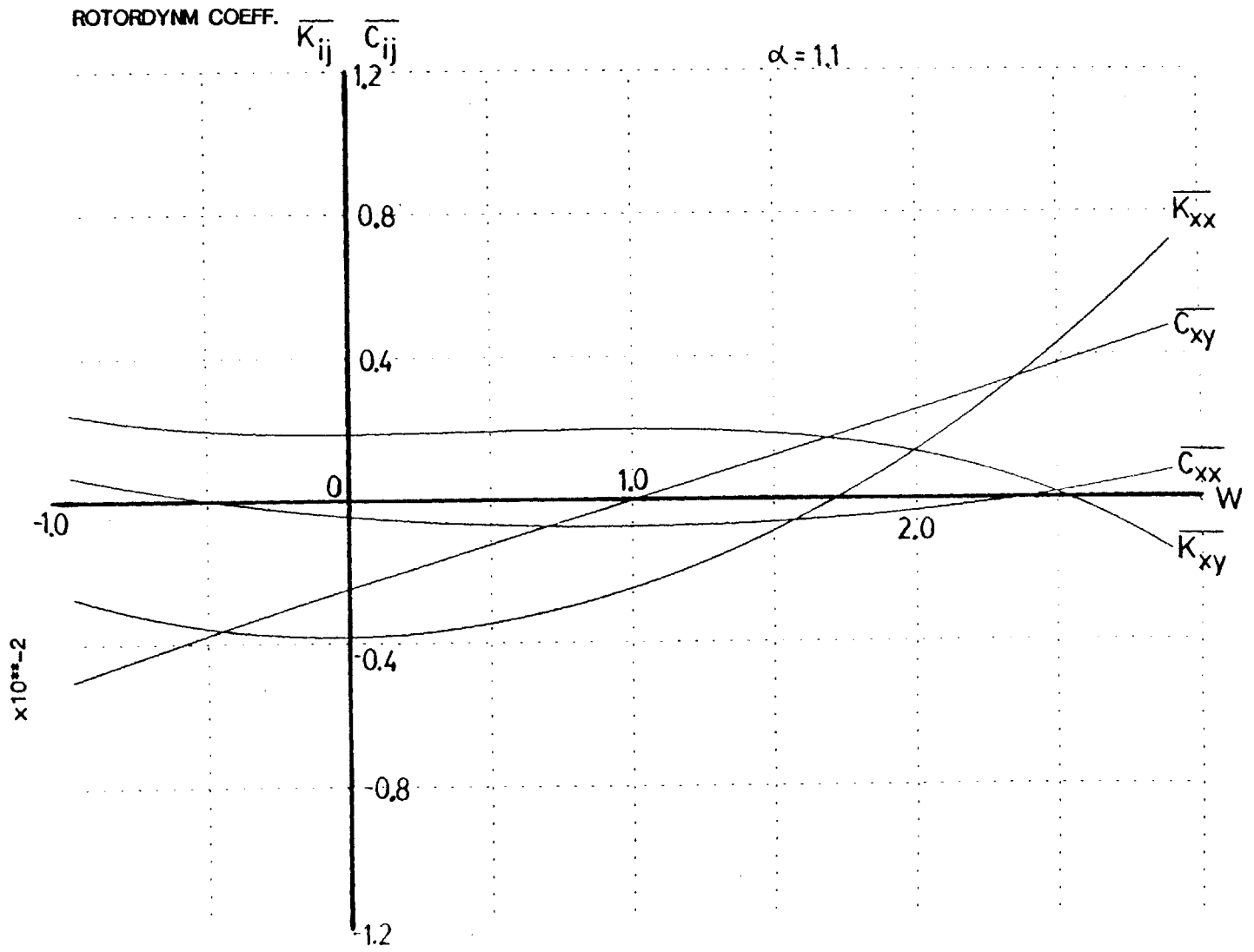

Figure 22 - Non-dimensional rotordynamic coefficients K_{ij} and $\bar{C}_{ij}$ vs. non-dimensional whirling frequency W for $\alpha = 1.1$.

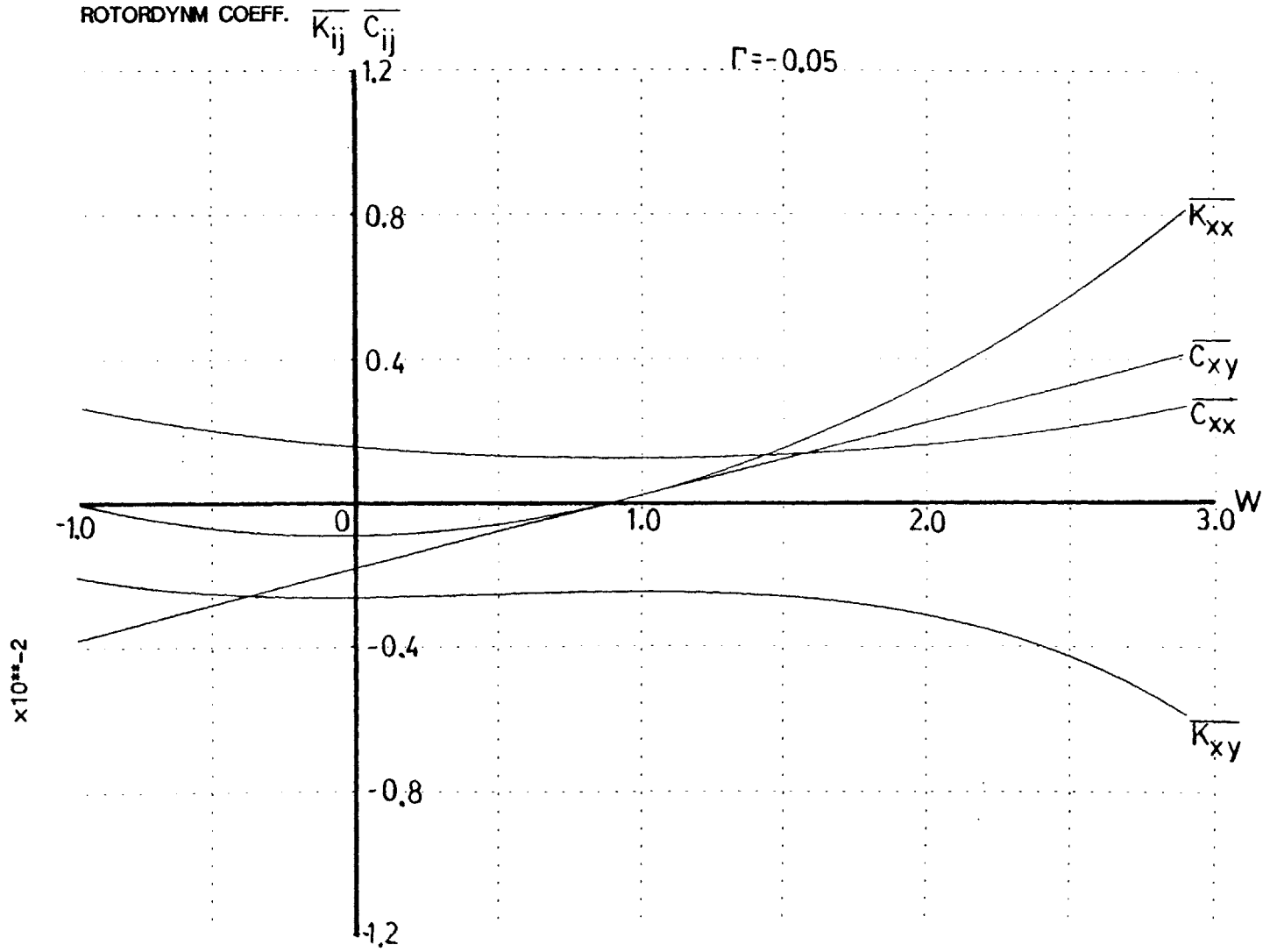

Figure 23 - Non-dimensional rotordynamic coefficients K_{ij} and $\bar{C}_{ij}$ vs. non-dimensional whirling frequency W for $\Gamma = -0.05$.

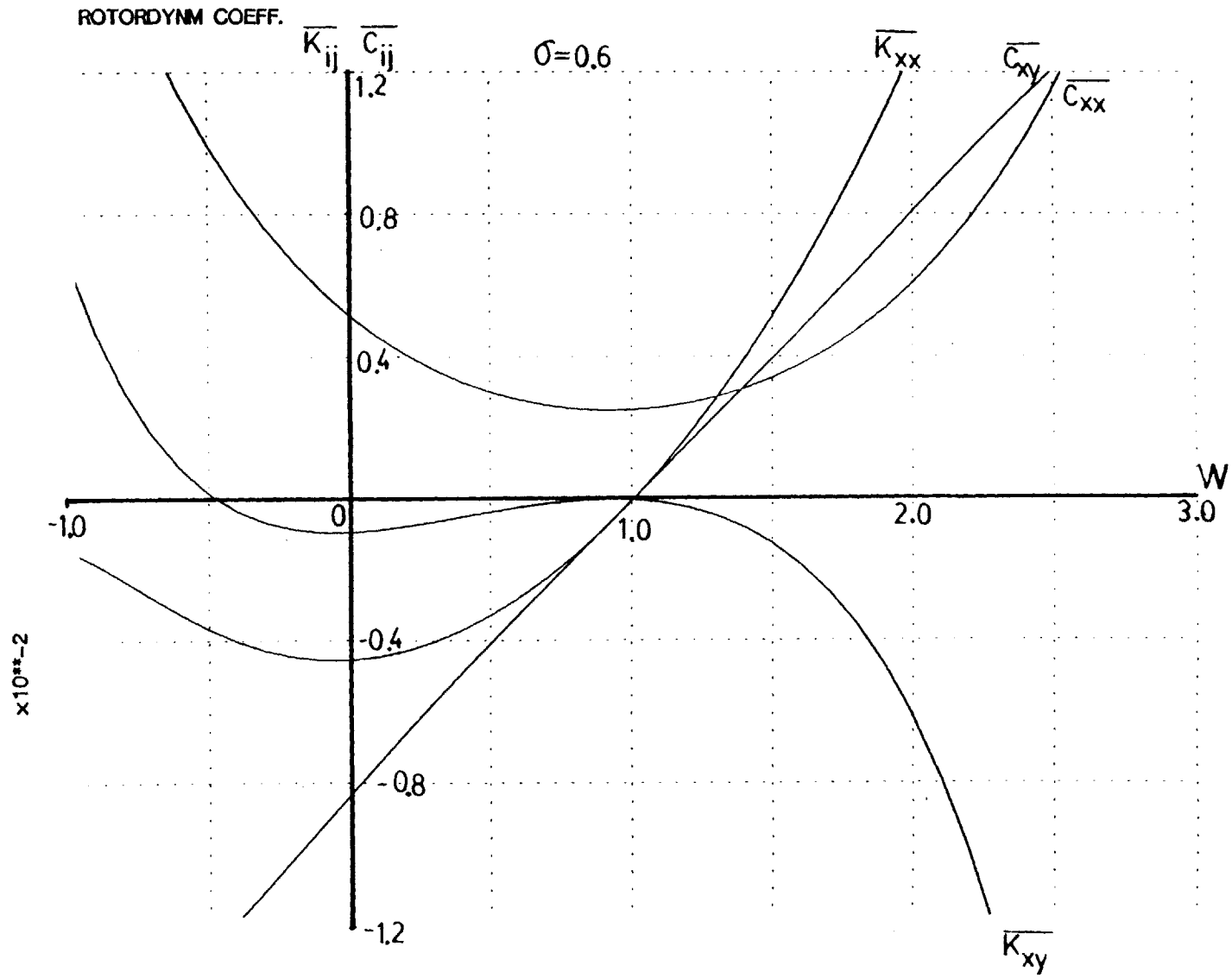

Figure 24 – Non-dimensional rotordynamic coefficients K_{ij} and $\bar{C}_{ij}$ vs. non-dimensional whirling frequency W for $\sigma = 0.4$.

CHAPTER 5

FACILITY DESIGN

5.1 DESIGN REQUIREMENTS

Many interacting constraints were considered when setting the design requirements for the Labyrinth Seal Testing Facility (LSTF). First and foremost it was necessary to determine what range of values for the various non-dimensional parameters discussed in the previous chapter must be obtained in order to corroborate the Kostyuk-Iwatsubo theory especially with regard to the damping forces. Even with these parameters set many families of designs were possible by scaling the geometric as well as flow related quantities. Certain constraints were imposed in order to minimize facility cost while still maintaining a high level of flexibility in operating conditions. The following is a list of design goals along with a brief discussion of each.

1. Flexibility

It is desirable to have a facility that can operate under as many conditions as possible. The theory provides guidelines as to what to expect but until after the experiments are conducted it is impossible to determine if the theory is very accurate.

2. Minimize Facility Size

The major purpose of this is to reduce facility cost since the cost goes up very rapidly with the linear dimensions. For geometrically similar designs this means the seal radius R_s should be kept as small as possible. This has many additional benefits such as reducing the flow rate of air and limiting stresses on rotating parts. However, the facility should not be made to small as to render the measurements difficult.

3. Limit Air Flow to 0.3 Kg/sec @ 600 Kpa

Many different sources of pressurized air were considered. Both steady state and transients mode operation were investigated as to their feasibility. A decision was made to use the MIT-GTL oil free compressor as the air source. This facility can deliver 0.3 Kg/sec of air at a pressure up to 600 Kpa. If necessary this compressor can be employed in conjunction with supply tanks with a total capacity of 500 ft^3 (14 m^3). In this configuration a mass flow rate of 1 Kg/sec can be obtained for 1 min under blow down conditions.

4. Maintain the Reynolds Numbers Above Certain Critical Values

There are two different Reynolds Numbers of importance in this problem. The gap Reynolds Number (defined as $Re_g = \frac{\delta_1^* w}{\nu}$) and the circumferential flow Reynolds number used in

Chapter 2 to obtain the friction factors (defined as $Re^* = V^*_{rel} \cdot D_H/\nu$). It is not possible to maintain similarity between the experiment and real machines for either without employing extraordinary measures (e.g. large scale, high pressures, exotic fluid, etc.). However, it probably is not necessary to obtain an exact match as long as there are maintained above certain threshold values. For the gap it is known that the flow over the knives is fairly Reynolds number independent above a critical value of 10^4 (46). For typical machines Re^* may exceed 10^6, whereas it would be very difficult to increase it much above 10^5 for this experiment. It should be noted that this is well into the turbulent regime. Hence the behavior should be similar. Within the limits of this theory, the only difference should be that with a moderate Reynolds number the seal surfaces would be hydrodynamically smooth. For the much higher Reynolds number the friction factors would be substantially increased since the surfaces would be hydrodynamically rough. These arguments would apply to normally machined surfaces (rms e ~ 150mm). If "casing treatments" were used, as done by some manufactures, the situation would be substantially altered.

Under these guidelines and considering instrumentation limitations a preliminary design was obtained. The initial seal geometry was fixed as in the last chapter with the following values of the non-dimensional geometric

parameters.

$$\alpha = 1.0 \qquad H = 0.05 \qquad L = 0.15 \qquad D = 0.05 \tag{5.1}$$

This represents a family of designs scaling linearly in real dimensions with the seal radius R_s. All other seal dimensions, except R_s, can be discretely altered by replacing the test seal. Allowing for variable R_s was though to be unnecessary as well as prohibitively expensive. The facility was scaled with a compromise seal radius of $R_s = 0.15M$. With this, the geometry of the seal for the baseline case, referring to Figure 6, is

$$\begin{aligned} R_s &= 0.15m & \delta_1^* &= 0.0006m \\ h &= 0.0075m & \delta_2^* &= 0.0006m \\ l &= 0.0225m \end{aligned} \tag{5.2}$$

For this fixed geometry, the range of the kinematic and flow parameters was found in the design study to be

$$\begin{aligned} -2 \le W \le 3 \\ 0.2 \le \Delta \le 0.9 \\ -0.1 \le \Gamma \le 0.1 \\ 0.7 \le \sigma \le -0.7 \\ -3.0 \le S \le 3.0 \end{aligned} \tag{5.3}$$

From these it is possible to calculate the ranges for each

of the physical controllable variables using the zeroth order calculation of Chapter 3. For simplicity, the air temperature and exit pressure, T and P_o respectively, will be set to the ambient conditions. With this, the remaining variables must be able to vary within the following limits.

Inlet Pressure	120 Kpa $\leq P_i \leq$ 350 Kpa
Pre-Swirl	-35 m/s $\leq V_i \leq$ 35 m/s
Spin Angular Velocity	-600 rads/sec $\leq \omega \leq$ 600 rads/sec
Whirl Angular Velocity	-300 rads/sec $\leq \Omega \leq$ 300 rads/sec
Whirl Eccentricity	$0 \leq r \leq$ 0.6mm

These requirements are of two separate kinds. The first two prescribe the inlet conditions of the air entering the labyrinth. The second three impose restrictions on the kinematics of the seal. It is useful to think of the problem in these terms since the actual mechanical design will be divided into the rotating machinery which controls the spinning-whirling motion of the seal and the air supply which admits the air into the seal at the proper pressure and relative angle.

5.2 ROTATING MACHINERY

The rotating machinery must have the capability to spin the test seal at speeds up to 6000 rpm while independently forcing it to execute an exact whirling motion up to 3000

rpm either in the same (simulating forward whirl) or opposite (simulating backward whirl) direction as the spin. The simplest type of machine able to accomplish such a complicated motion is one with an inner shaft mounted eccentrically, in bearings inside a rotating intermediate housing. This rotating housing is in turn placed in bearing supported by a fixed outer housing. Figure 25 shows a schematic of this type of mechanism. Since the shaft is not centered in the intermediate housing, a rotation of this case causes the shaft's center to proceed about the centroid of the outer housing producing the desired whirl. The inner bearings allow relative rotation of the shaft inside the rotating housing permitting any spin to proceed independently of the whirling motion. It should be noted that a given asymmetry in the rotating housing produces a characteristic whirling amplitude. Therefore, several variations on this basic design were investigated to allow for variable whirling eccentricity. One straightforward method is to machine separate rotating housings. This option was discarded due to the great expense. Another alternative is to have small replaceable bearing sets with a different set for each desirable eccentricity. The third option, which was the path taken, is to have an eccentric rotating housing containing a "counter-eccentric" bearing seat insert which can be rotated and fixed to obtain any desired whirl eccentricity within a given range. Figure 26 shows a cross section of the rotating housing, along with the eccentric

insert. With the parts located in the relative positions shown, the inner and outer surfaces are concentric, yielding a whirl amplitude of zero. However, when the insert is rotated relative to the housing the surfaces become eccentric. By adjusting these parts by the proper amount the whirling amplitude may be precisely controlled.

To obtain a detailed mechanical design for the rotating machinery, based on this concept, several auxiliary factors should be considered.

1. Design such that all critical frequencies fall outside the range of normal operation.
2. Choose the bearing types and sizes consistent with loads and speeds to obtain a maximum machine life.
3. Minimize the mechanical and thermal stresses. A factor of safety of 3 was used for all parts.
4. The machine should be easy to assemble and disassemble.
5. Each part should be easy to machine.
6. Use materials consistent with part and overall facility requirements.
7. Maximum durability at a minimum cost.

After a preliminary design was proposed, subsequent working designs were altered to be consistent with the above criteria. After many iterations a final mechanical design was obtained that met all requirements. Appendix C contains explanations and representative calculations on how the first three requirements were met.

Figure 27 shows an assembly cross section of the rotating

rig final design. The test seal, which can be easily replaced, is attached by 8 #8-36 UNC tap screws to the disk (part #9). This disk is in turn secured onto the inner shaft (part #1) by a N-07 lock nut. This shaft is driven by an inline flexible coupling and is supported eccentrically by two precision radial ball bearings (BC-207 Class 7) inside the rotating housing assembly (parts 2,3,4,5). The eccentricity can be adjusted by removing the shaft and bearing and repositioning the eccentric inserts (parts #3). These outer bearing seats are then secured by tightening the set of radially inward screws. This entire whirl controlling assembly is driven by a NX3-V3 V-Belt and is contained inside the outer housing by two radial ball bearings (BC-224 Class 5). These bearings are separated by part 5 and are kept in place by a N-24 lock nut and a bearing plate (part #8). The outer housing contains two drilled/tapped holes over each bearing and 90° apart for 4 accelerometers to be mounted. These are mainly for the purpose of machine health monitoring. The entire rig is supported by a welded steel stand (part #11).

If the region behind the disk were maintained at atmospheric pressure the resulting net axial force, which would be taken by the bearings, could reach several tons at the higher flow rates at which this machine will operate. No bearings of this size can operate at high speeds under such bearing loads. To remedy this situation, the volume between the disk and the pressure cap (part #7) will be pressurized to

minimize the thrust loads. To supply the air for this purpose a line is run through the housing and into the cap. Auxiliary facing Labyrinth Knives form of seal against the back of the disk hence minimizing leakage and increasing the counter thrust on the disk.

Detailed mechanical drawings of all the parts contained in the rotating rig are presented in Figures 28-38. Dimensions, materials and handling are all specified along with other necessary information.

The materials that were specified were used in order to increase facility functionality at a minimum cost. The inner rotating parts (1,2,3,4) of the machine, which must be taken apart and reassembled every time the eccentricity is to be changed had to be made of a very hard material for durability considerations. For these parts case hardenable 8620 steel was chosen and hardened to Rockwell 56 to a depth of 50-60 mils. This allows sufficient hardness for the bearings to be press fit many times while keeping the core material quite ductile, hence preventing cycle fatigue. The remaining parts except for the disks were made of various types of 10XX free machining mild steels. These steels were chosen for low cost. The disks are made of 6061-T6 aluminum alloy. This material was chosen for many reasons. First, it is one of the lightest metals available. This reduces the radial bearing loads during whirling and raises the critical frequencies both in bending and in pitching.

Heavier steel disks would not be as good in these regards. Also the yield stress/density ratio, which is an important figure of merit for materials used in rotating disks, is quite high. Only very expensive materials, such as those used in jet engines, are much better in this respect. However, the threads into the disks would get fouled quickly if made of aluminum. Therefore, 8-36 free running inserts were used for test seal attachments.

This machine will require dynamic balancing of both the shaft and the rotating housing. First the shaft should be balanced. The simplest way to accomplish this is to remove it and place it on a portable balancing machine. It may not require any added mass since the machining tolerances were quite small and it is nominally symmetric about the axis of rotation. With this done, the shaft is placed back in the housing, and balancing of the entire disk-shaft-housing assembly may proceed. Due to the eccentricity of the shaft and inner bearings, the combined centroid of this assembly is not concentric with the outer bearings. It may be as much as 1350 g·cm off at maximum eccentricity. If this were not compensated an intolerable vibration level would result. First, a rough balancing operation is undertaken by placing large counter weights on the ends of the rotating housing. The mass required at the given radius is a function of the eccentricity and is easily calculated. With these counter masses placed on both ends of the housing a finer balancing may be obtained by iteratively using very small masses and

checking the vibration level with the accelerometers.

5.3 AIR SUPPLY

The other major component of the Labyrinth seal testing facility is the air supply. The purpose of the air supply is to admit the air to the test seal at the proper pressure and angle. It also will serve as the mounting place for most of the instrumentation. As in the case of the rotating machinery, certain auxiliary objectives should be considered when designing this component. These are:

1. Easy adjustment of the inlet air angle.
2. This component should be easily separated from the rotating rig.
3. No natural frequencies should lie in the range of operation.
4. Limit stresses on all parts. Again a factor of safety of 3 was used.
5. Maximum durability at a minimum cost.

The pressure entering the seal can be controlled in many ways. First the pump pressure ratio can be controlled directly and there are throttles in various places along the piping. Finally the flow rate can be controlled at the entrance to the plenum.

Several methods were investigated to produce and control the swirl, maintaining circumferential uniformity, entering the test seal. It would have been preferable to have a mechanism that could be adjusted to obtain the different

swirl velocities. Designs of this kind were considered and discarded. Variable vanes of the size required would be extremely difficult to manufacture and no other design of this type could guarantee controllability and uniformity of the plenum swirl. In the design chosen the air is accelerated and turned to add the proper amount of swirl by a set of fixed vanes. Different vane assemblies, with different blade angles, need to be inserted to obtain different amounts of swirl.

Figure 39 shows an assembly cross section of the air supply/ test section. The air enters part 1 through a two inch pipe and is directed radially outward into the annular prevane plenum. The air is next accelerated and turned through a ring of fixed flat vanes (part #2). Parts 1 and 4 can be easily detached and different vane assembly can be inserted. The air is then dumped into the test plenum (between parts #3 and 4) with the proper amount of tangential momentum. Only minor losses in the circumferential component of velocity are experienced due to friction, but major pressure losses do occur because of the rapid expansion. Part 4 of the air supply serves as the seal land and test section and is rigidly attached to the rotating rig. Most of the facility instrumentation will be contained in this part as will be described in the next chapter. After the air flows through the test section it is discharged through openings in the pressure cap. This is an open loop facility.

5.4 FACILITY LAYOUT AND AUXILIARY EQUIPMENT

Figure 40 shows a side view schematic of the facility layout. The combined rotating rig-air supply/test section is held in place by the rig support. This support is in turn bolted into a welded steel stand. This stand is set on four high damping vibration isolators. The mass of the stand and spring constant/damping characteristics of the isolations were chosen to minimize the vibration. A three degree of freedom model containing one bouncing and two pitching modes was employed. See Appendix B for details. The V-belt, which drives the whirl producing rotating housing, is connected to a variable speed d.c. motor through a 6" diameter pulley. The shaft is connected to an inline d.c. motor by a flexible coupling. As mentioned previously, the air is supplied by the MIT Gas turbine Lab oil free air compressor.

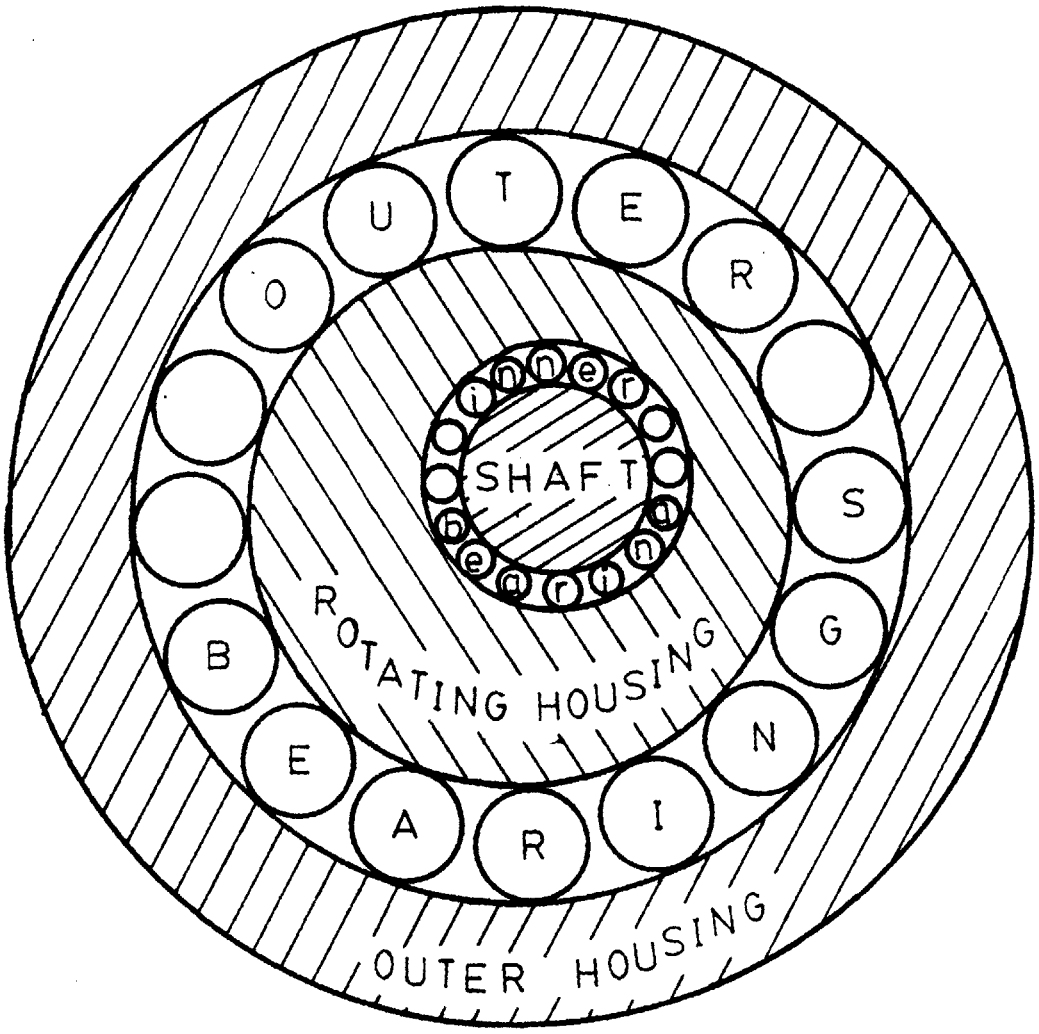

Figure 25 - Mechanism for producing spinning/whirling shaft.

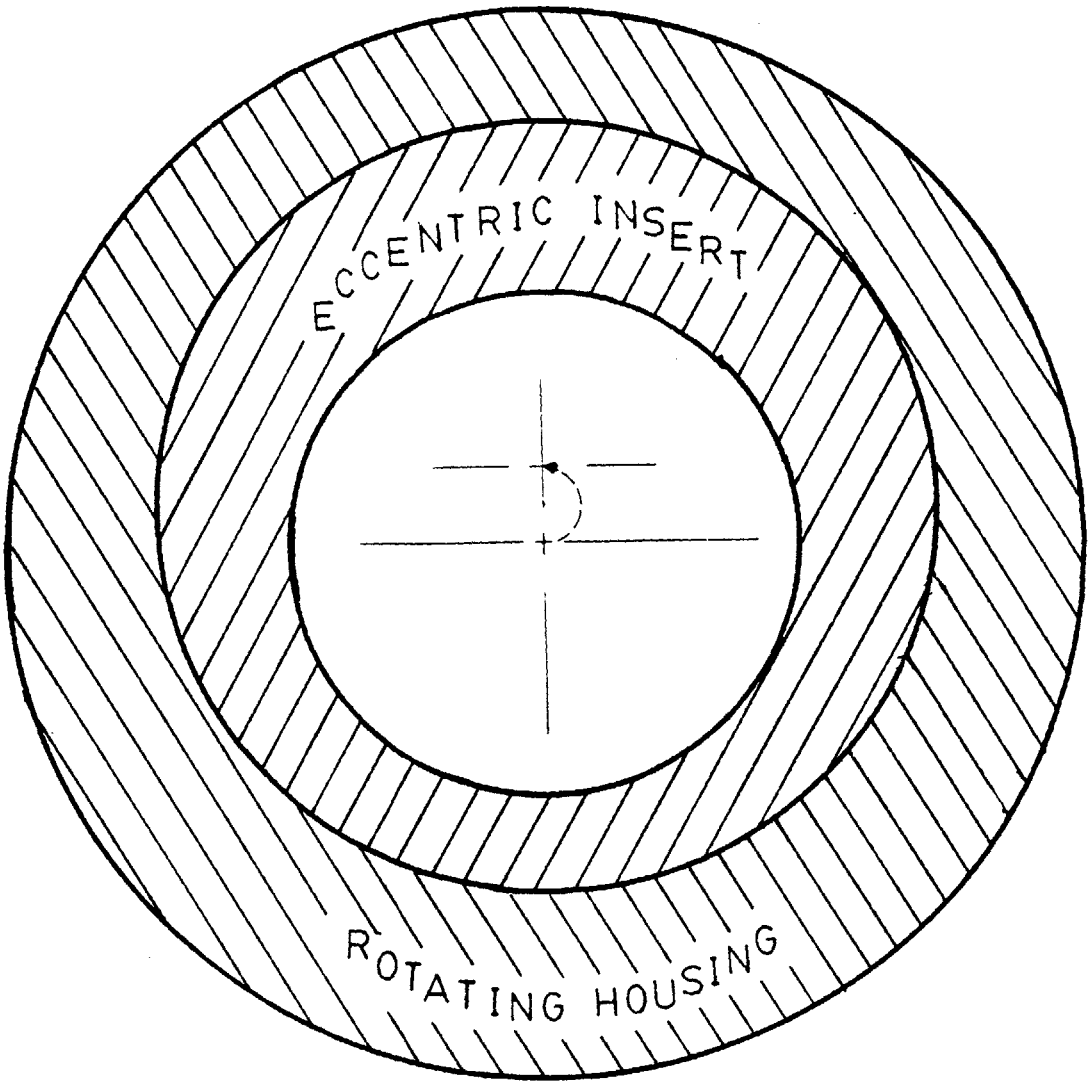

Figure 26 - Mechanism for producing variable whirl eccentricity.

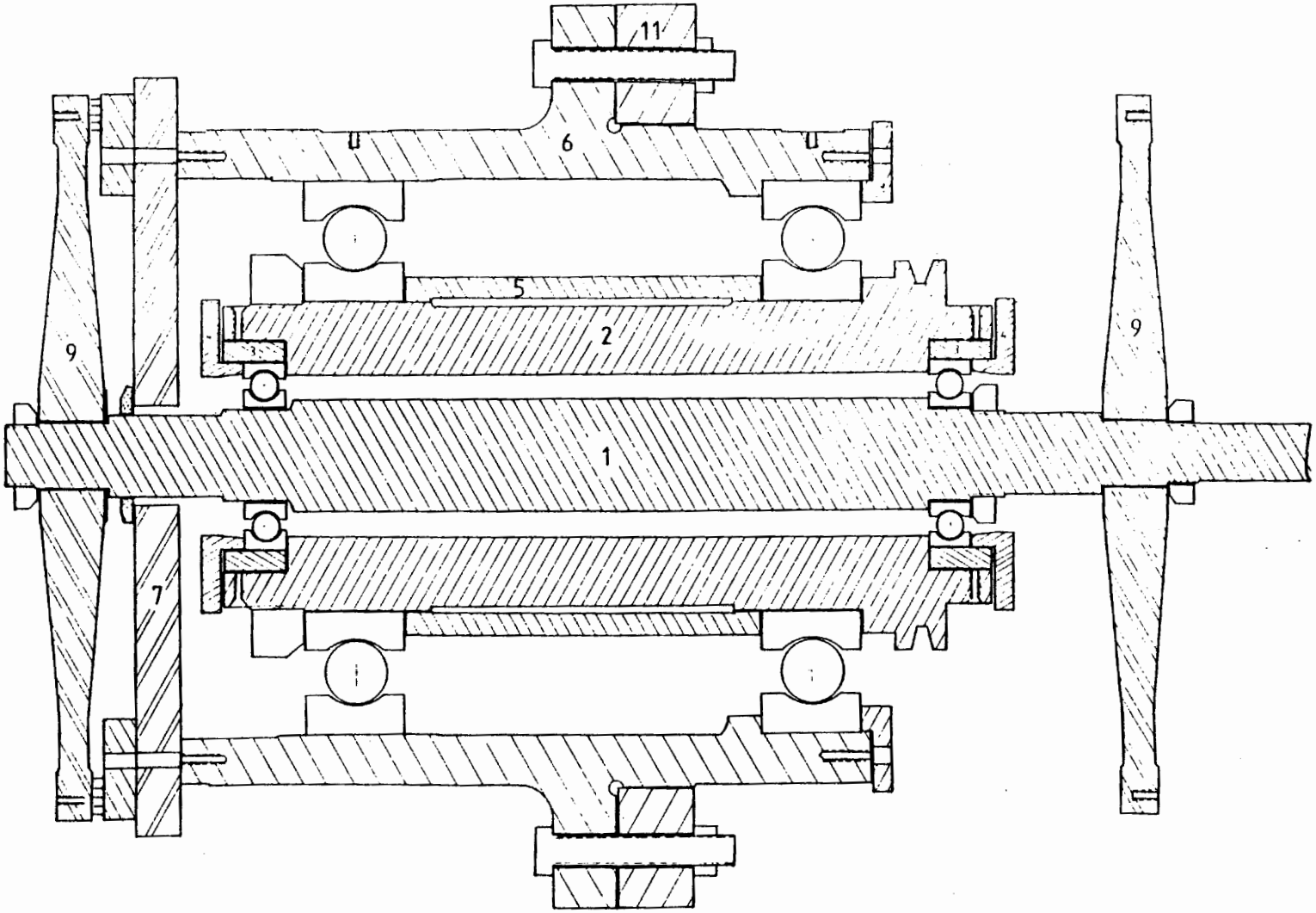

Figure 27 - Assembly cross-section of rotating rig.

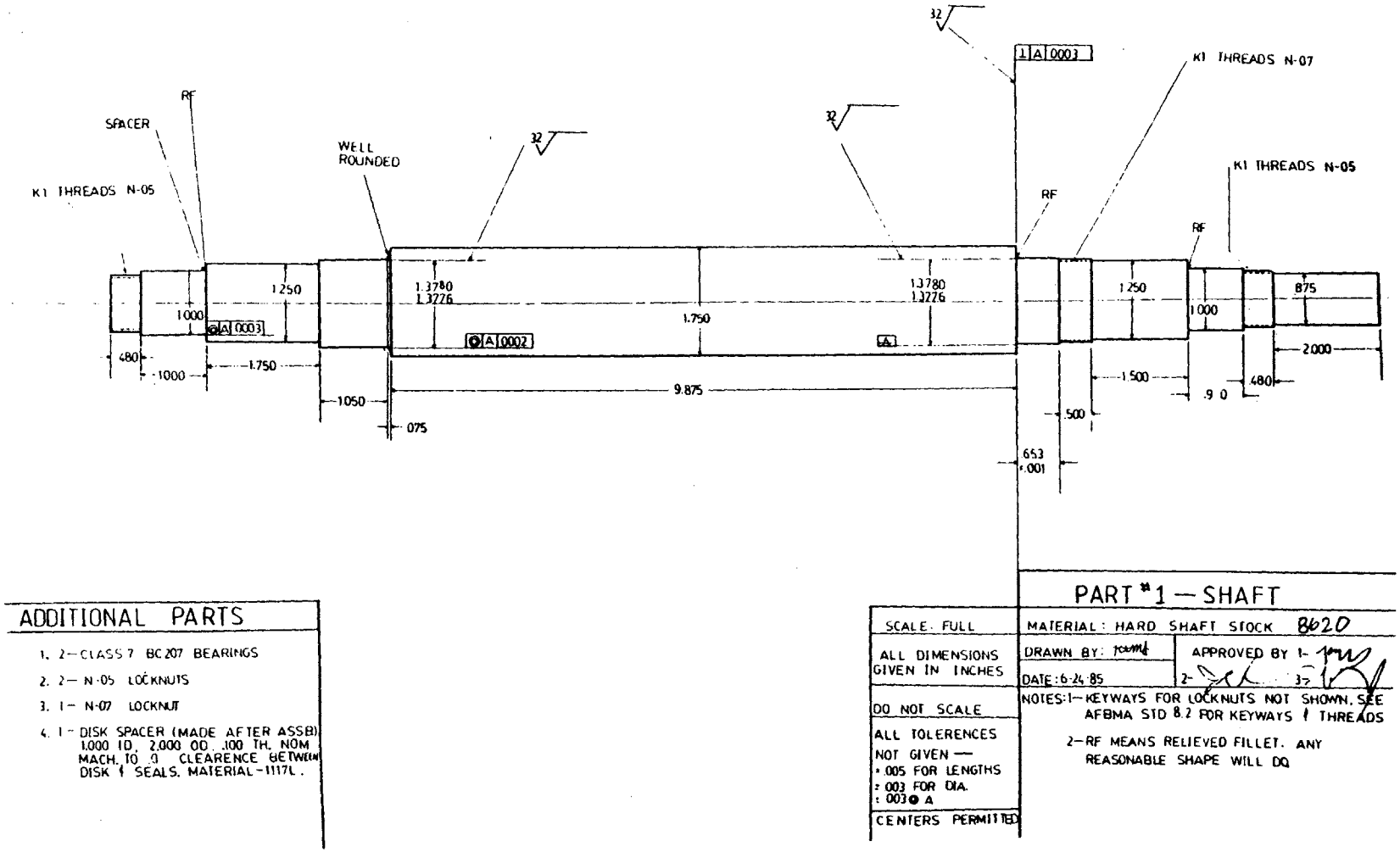

Figure 28 - Rotating Rig Part #1.

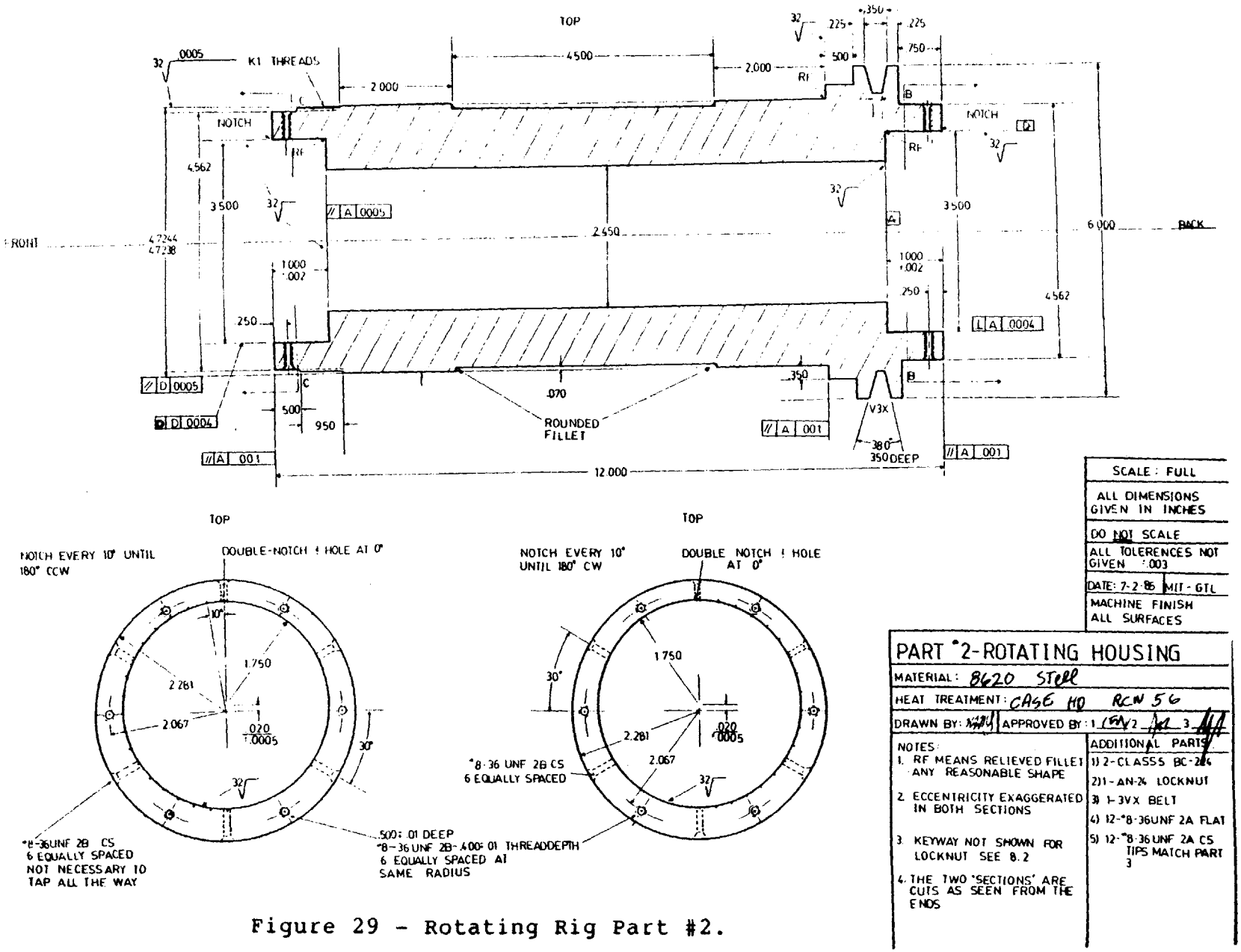

Figure 29 - Rotating Rig Part #2.

SCALE : FULL	
ALL DIMENSIONS GIVEN IN INCHES	
DO NOT SCALE	
ALL TOLERENCES NOT GIVEN .003	
DATE: 7-2-86	MIT - GTL
MACHINE FINISH ALL SURFACES	

PART #2-ROTATING HOUSING

MATERIAL: 8620 STEEL

HEAT TREATMENT: CASE HD RCN 56

DRAWN BY: [illegible] APPROVED BY: 1 [illegible] 2 [illegible] 3 [illegible]

NOTES:
1. RF MEANS RELIEVED FILLET IN ANY REASONABLE SHAPE
2. ECCENTRICITY EXAGGERATED IN BOTH SECTIONS
3. KEYWAY NOT SHOWN FOR LOCKNUT SEE 8.2
4. THE TWO 'SECTIONS' ARE CUTS AS SEEN FROM THE ENDS

ADDITIONAL PARTS:
1) 2-CLASS S BC-284
2) 1-AN-24 LOCKNUT
3) 1-3VX BELT
4) 12-*8-36UNF 2A FLAT
5) 12-*8-36 UNF 2A CS TIPS MATCH PART 3

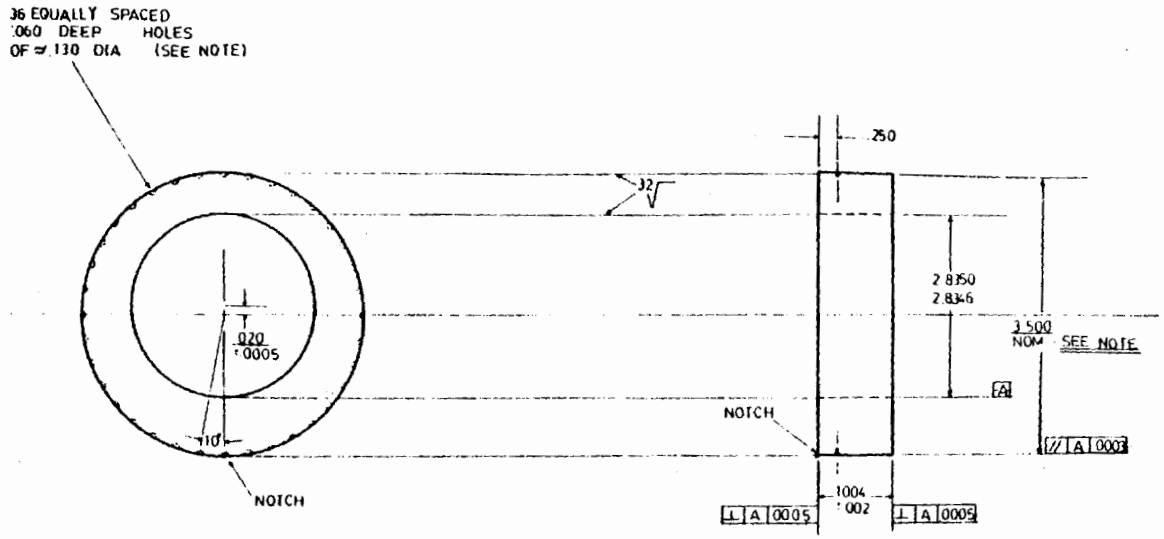

Figure 30 - Rotating Rig Part #3.

	PART #3—ECCENTRIC INSERT
	MATERIAL: 8620 CASE HR
	TREATMENT: 50 mil RWC 56
# OF PARTS: 2	DATE 7-7-85 | DRAWN BY: [illegible] | MIT-STL-
SCALE FULL	APPROVED BY 1 2 3
ALL DIMENSIONS GIVEN IN INCHES	NOTES: 1) THE OUTSIDE DIAMETER 3500 NOM SHOULD BE MADE TO MAINTAIN A CLOSE SLIDING FIT EACH OF THE TWO INSERTS SHOULD BE MADE AFTER PART 2 IS FINISHED. EACH INSERT SHOULD BE MADE WITH OD .0000 TO .0003 SMALLER THAN CORESPONDING PART 2 ID'S
DO NOT SCALE	2) EXAGGERATED ECCENTRICITY
	3) HOLES CAN BE MADE WITH DIFFERENT GEOMETRY, BUT MUST MATCH SCREW TIPS

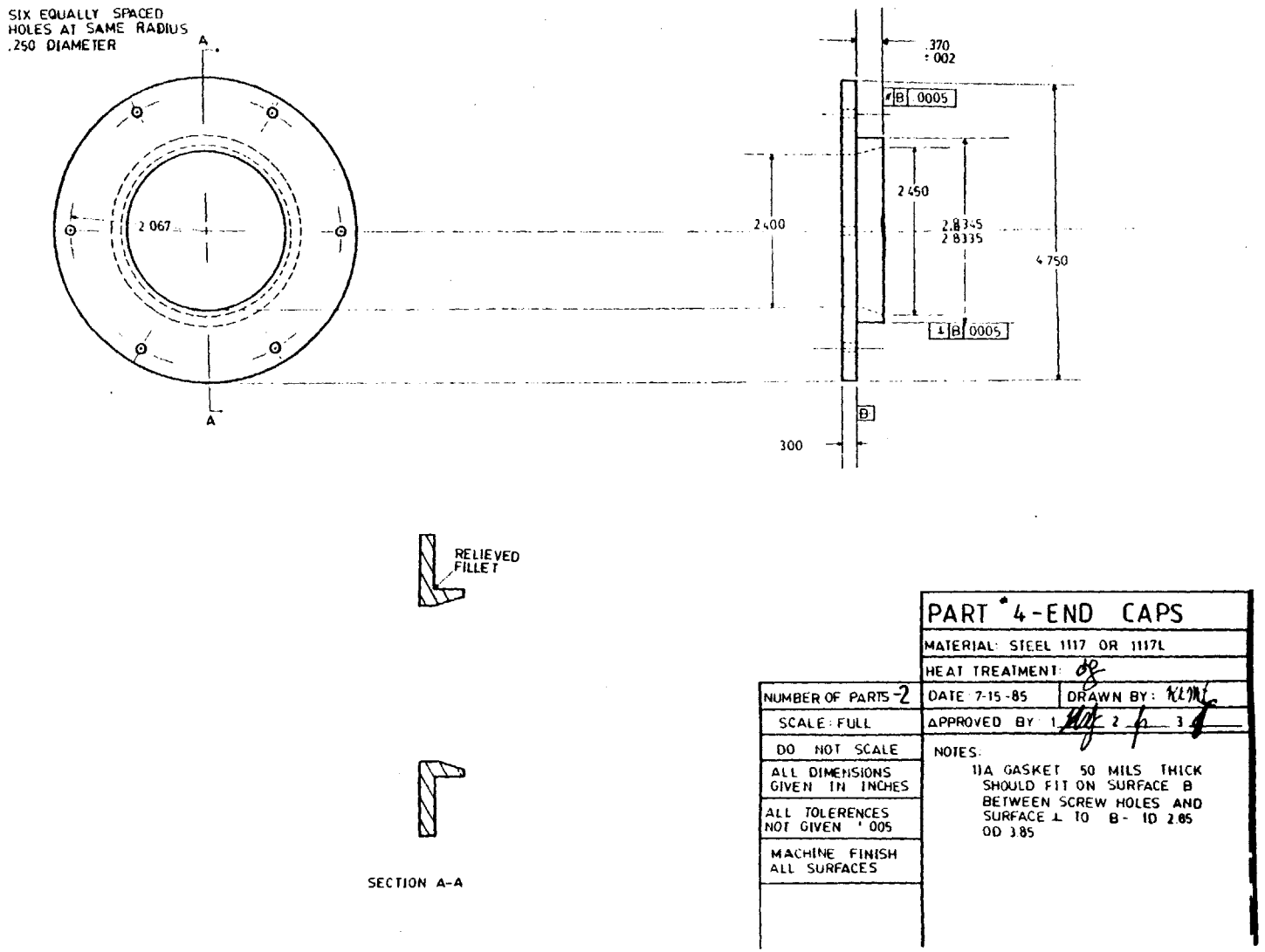

Figure 31 - Rotating Rig Part #4.

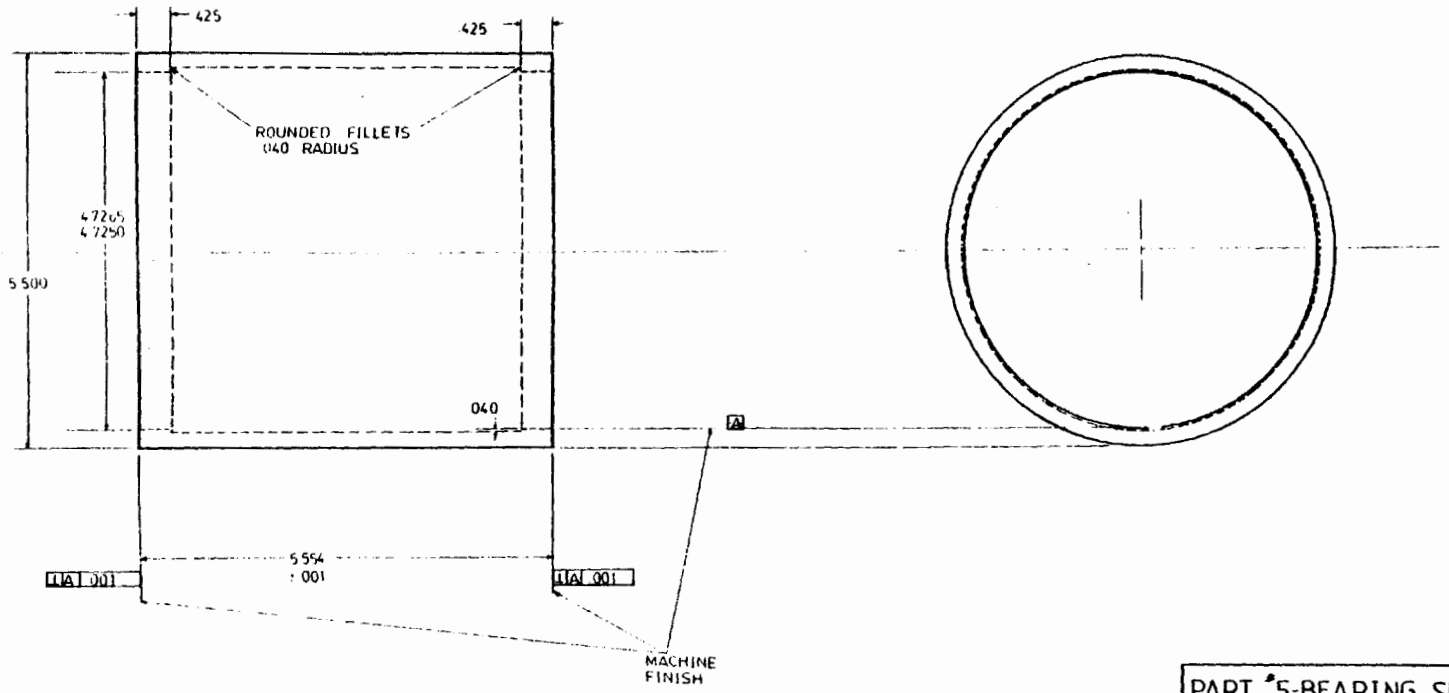

PART #5-BEARING SPACER

MATERIAL 1117L OR SIMILAR STEEL

HEAT TREATMENT: NONE

DATE: 7-15-85 | DRAWN BY: [illegible] | MAT-GTL

APPROVED BY: 1 2 3

TAP & DRL

AFD 30°

SCALE FULL
DO NOT SCALE
ALL TOLERENCES NOT GIVEN ±.010
ALL DIMENSIONS GIVEN IN INCHES
MACHINE FINISH 125 A

Figure 32 - Rotating Rig Part #5.

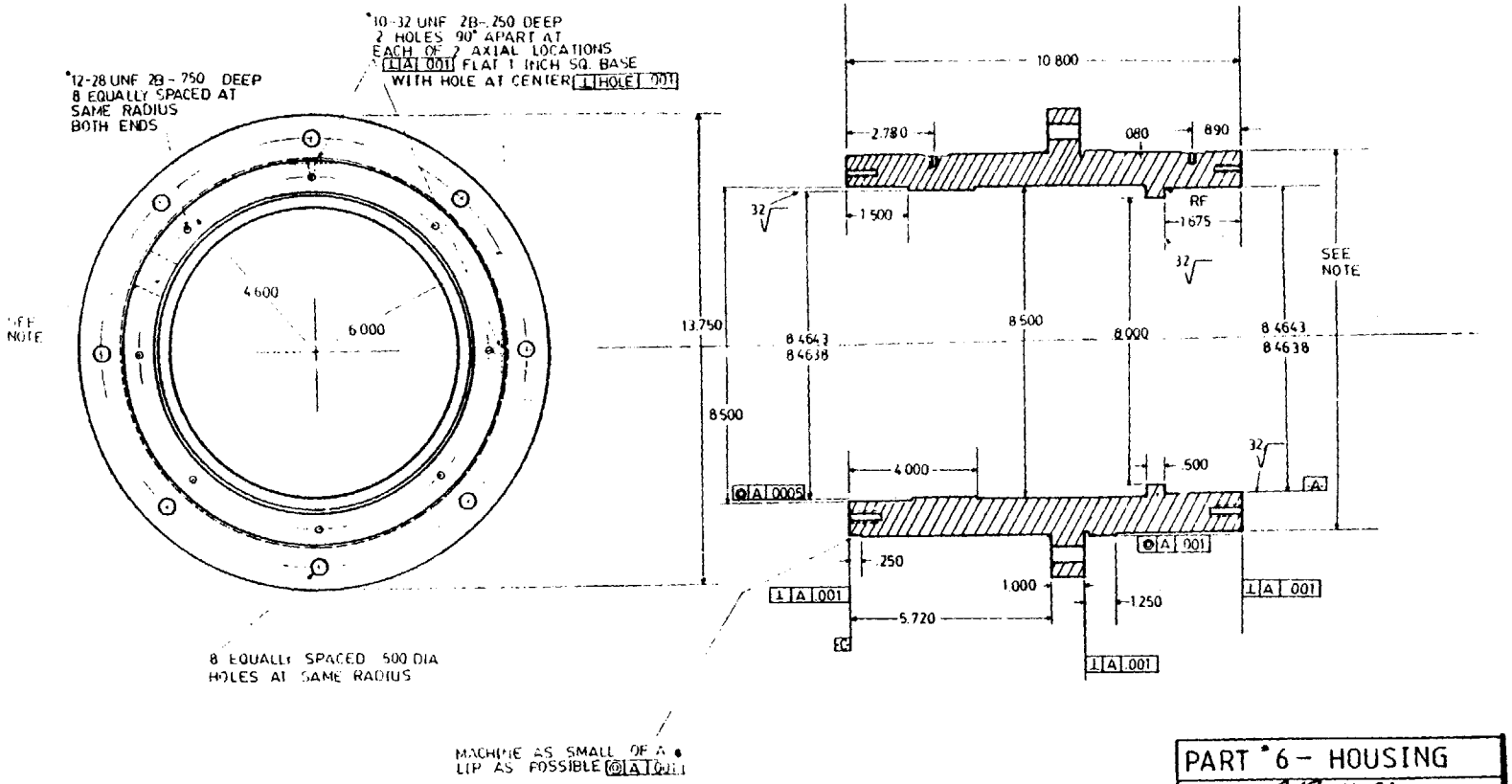

PART *6 - HOUSING	
MATERIAL: TWP 1018L	
HEAT TREATMENT: SR-2	
DATE: 7-20-85	DRAWN BY: WM
APPROVED BY: 1 BM 2 ✓ 3 ✓	

ALL DIMENSIONS GIVEN IN INCHES	NOTES 1) MAKE HOUSING 10.000 MIN. A THICKIER WALL UP TO 10.500 OD IS BETTER. 2) RF MEANS RELIEVED FILLET 3) 1.000 DIA HOLE RADIALLY INWARD // TO -C- 1.000 FROM -C- DO NOT PUT SO AS TO INTERFERE WITH TAPPED HOLES FROM THE END
ALL TOLERENCES NOT GIVEN ±.005	
ADDITIONAL PARTS 16 *12-28-2A FLAT	
[illegible] SCALE	

Figure 33 - Rotating Rig Part #6.

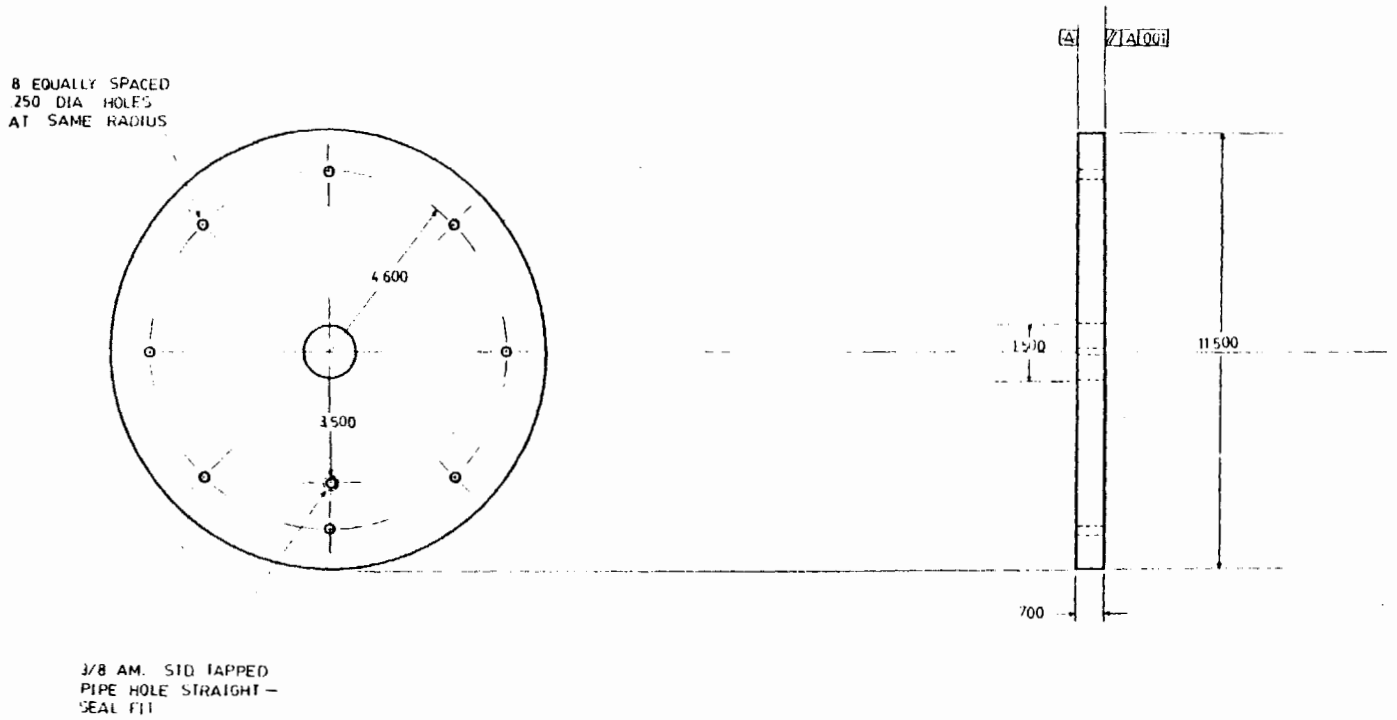

Figure 34 - Rotating Rig Part #7.

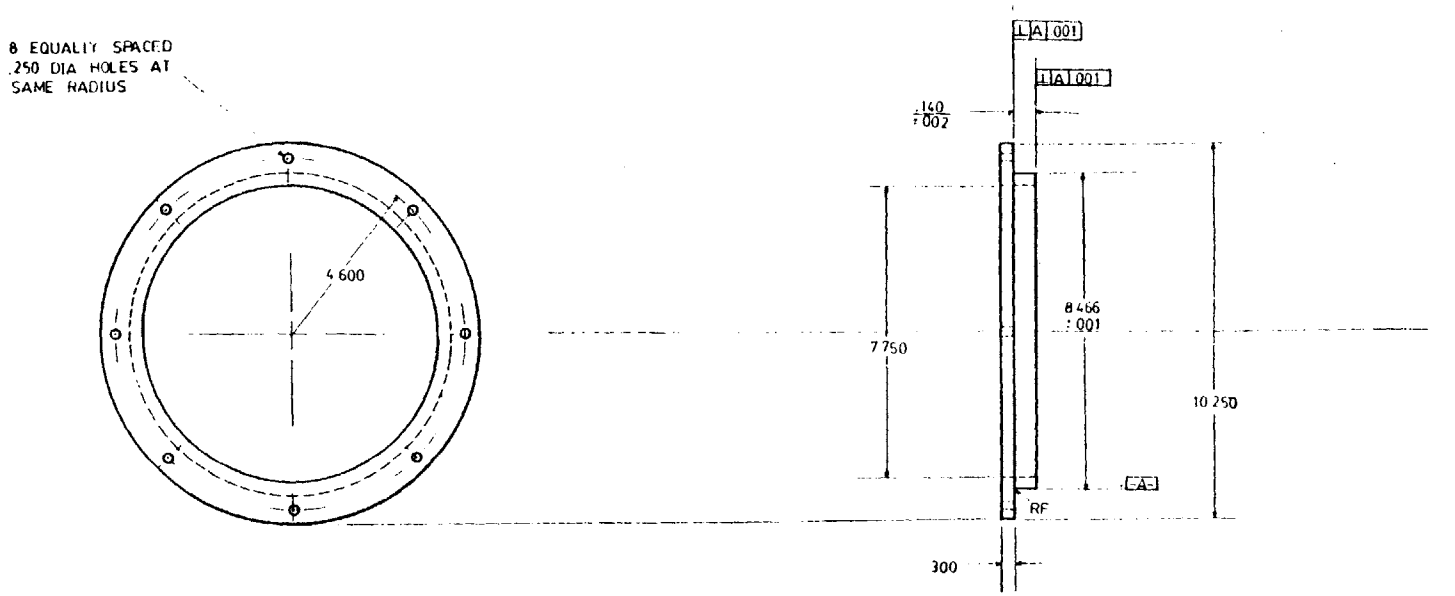

PART 8 BEARING PLATE

MATERIAL: 1018L - FM

HEAT TREATMENT: NONE

DATE 7-17-85 | DRAWN BY: [illegible] | MIT-GTL

APPROVED BY: 1 [illegible] 2 [illegible] 3 ____

DO NOT SCALE
ALL DIMENSIONS GIVEN IN INCHES
ALL TOLERENCES NOT GIVEN ± .005
MACHINE FINISH ALL SURFACES

NOTES

1) RF MEAN RELIEVED FILLET ANY REASONABLE SHAPE

2) A 50 MIL GASKET SHOULD BE MADE TO FIT BETWEEN PLATE AND HOUSING.

Figure 35 - Rotating Rig Part #8.

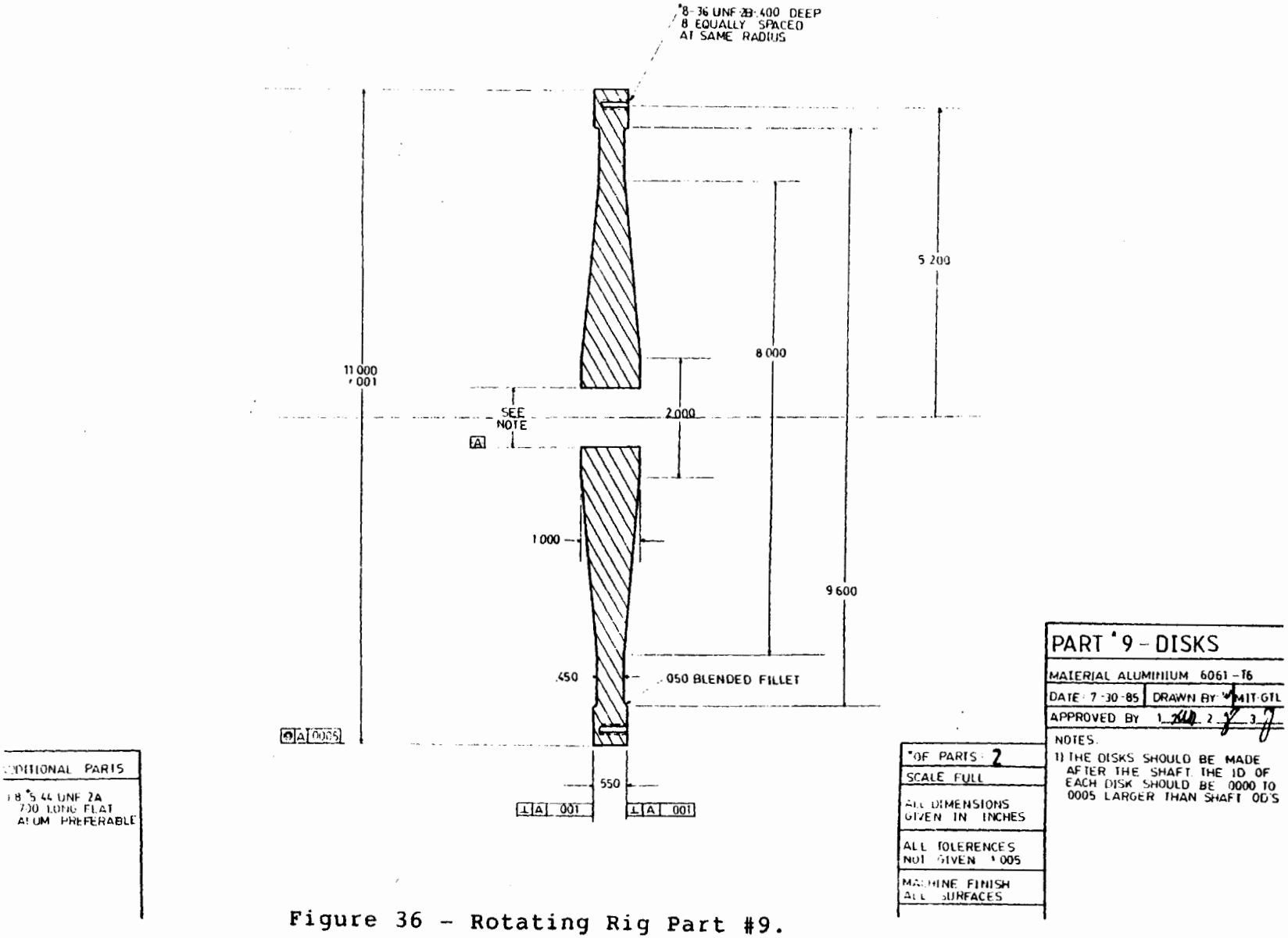

Figure 36 - Rotating Rig Part #9.

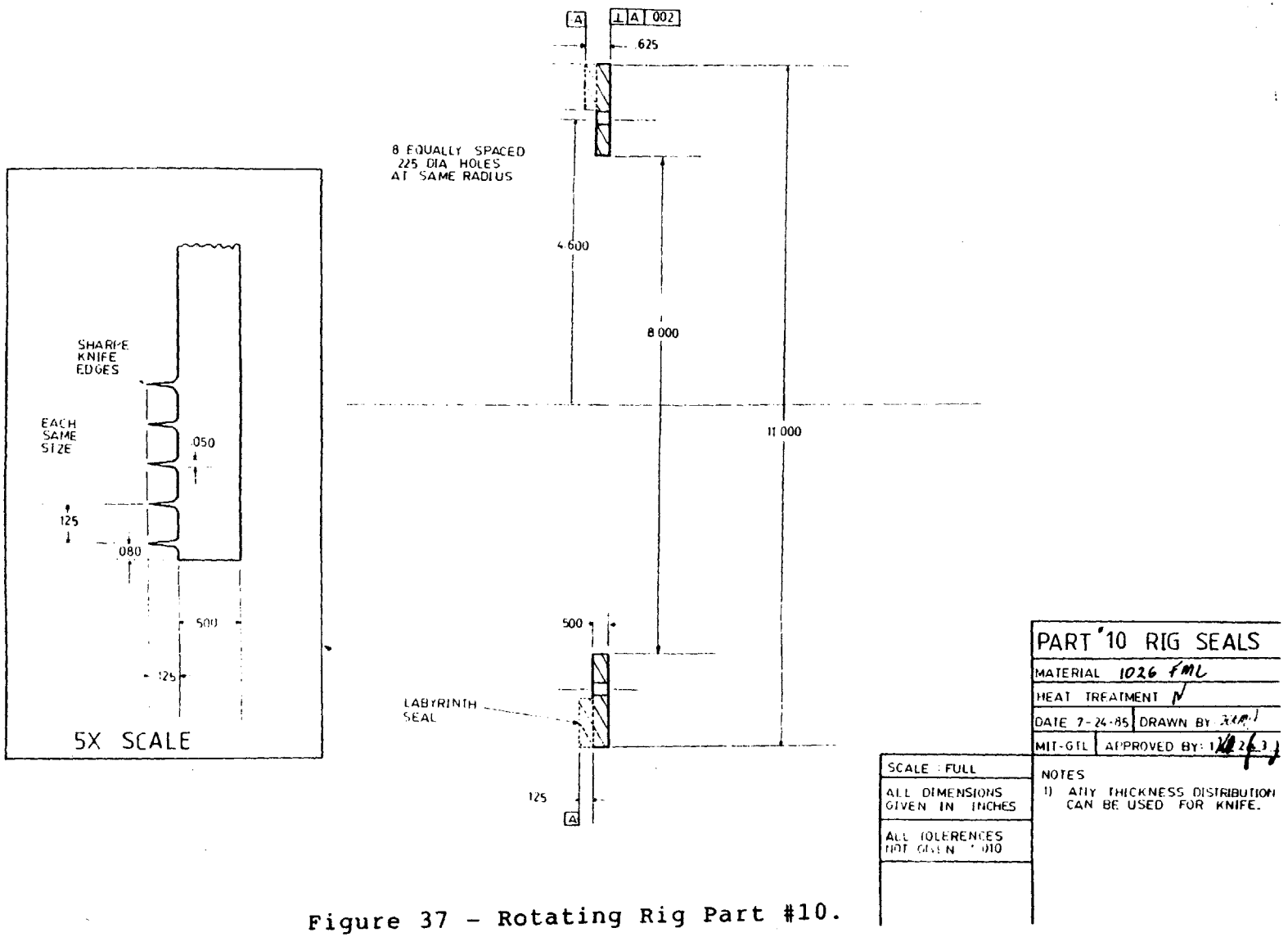

Figure 37 - Rotating Rig Part #10.

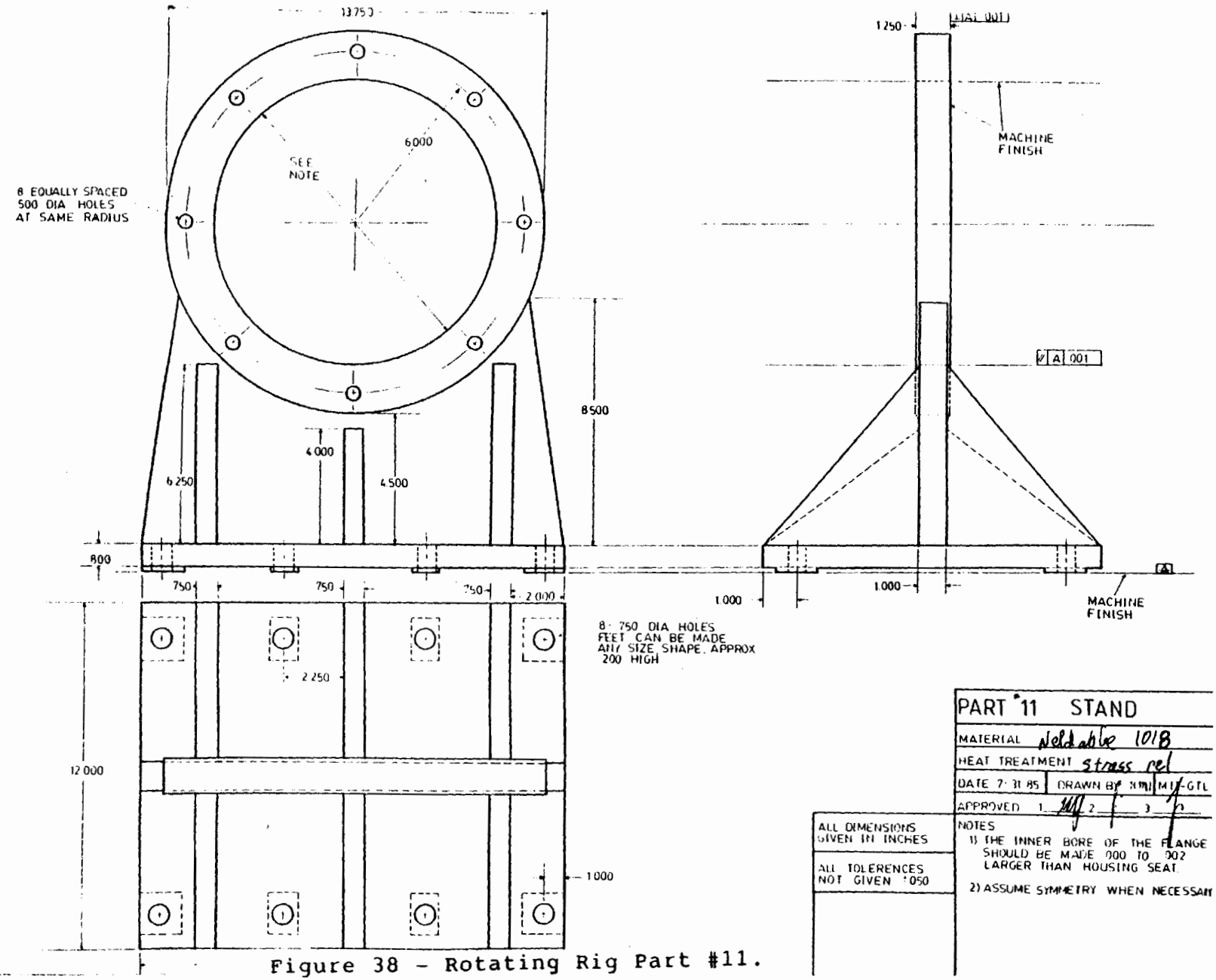

Figure 38 - Rotating Rig Part #11.

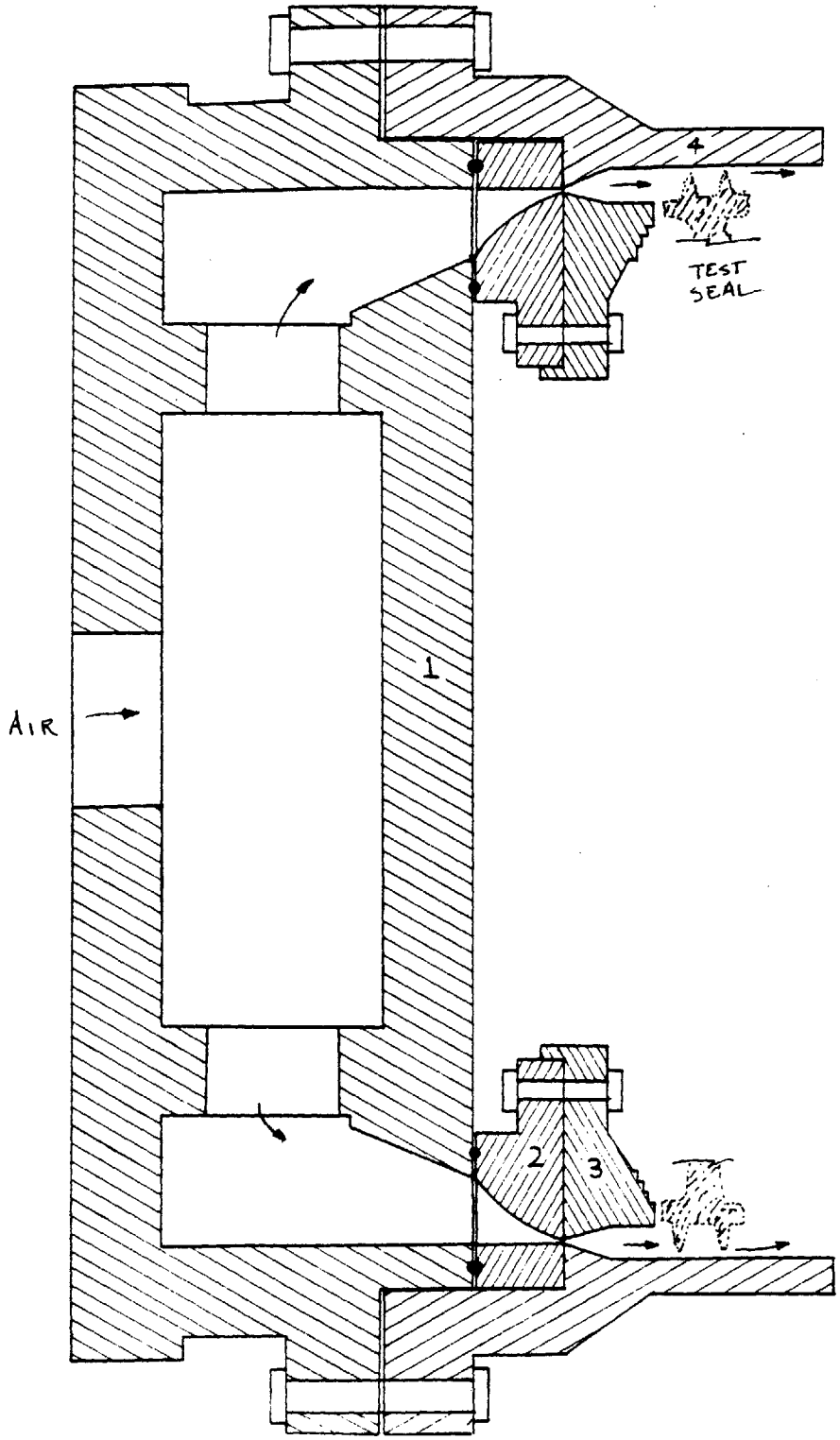

Figure 39 - Assembly cross section of air supply.

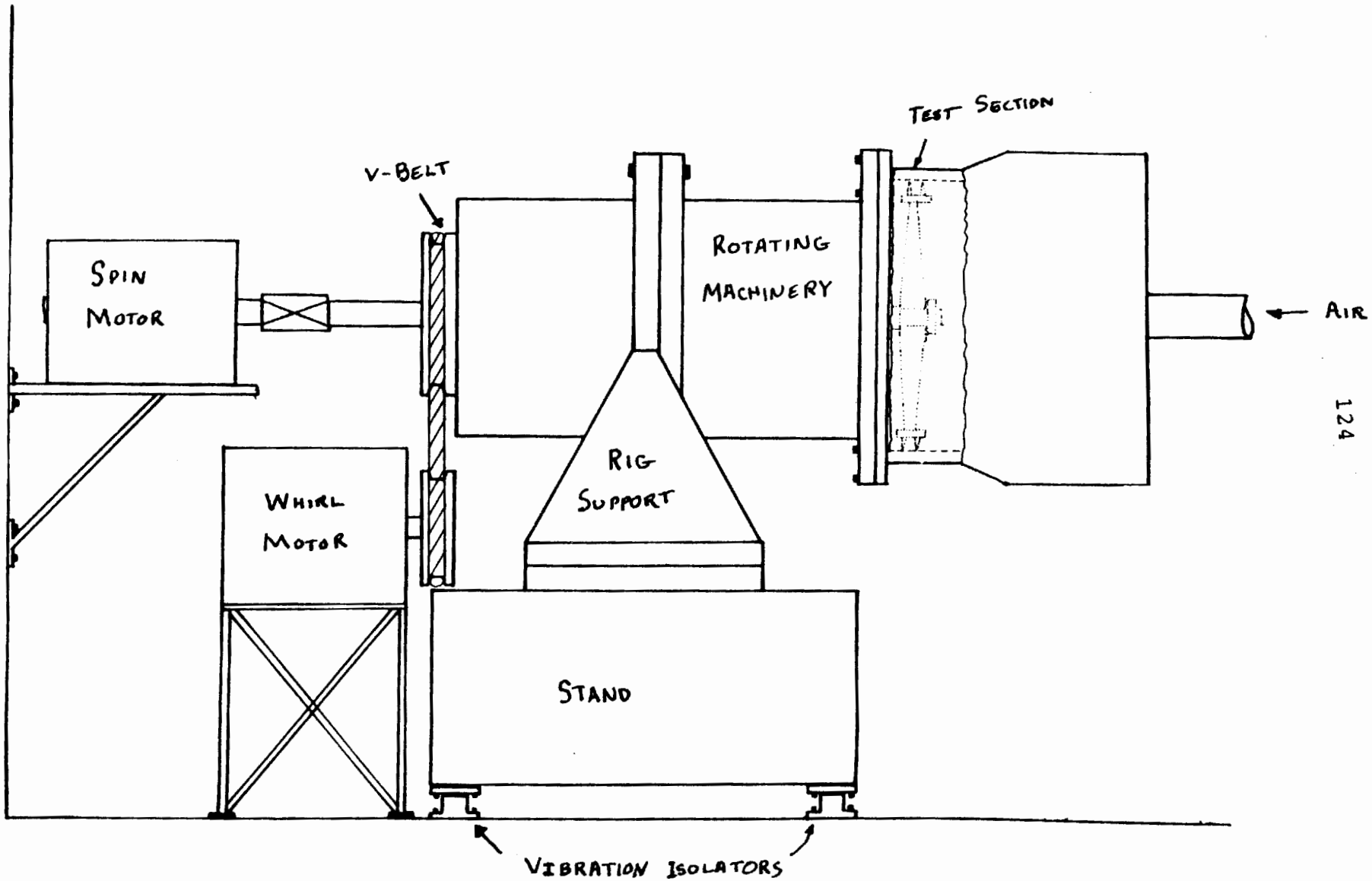

Figure 40 - Side view of labyrinth seal test facility.

CHAPTER 6

INSTRUMENTATION

6.1 INSTRUMENTATION REQUIREMENTS

The measurement of many physical quantities must be made in order to calculate, correlate and compare the spring and damping characteristics for this single gland seal to the predictions of the Kostyuk-Iwatsubo theory. In Chapter 4 the results of the theory were presented in terms of amplitude and gap relative phase of the pressure perturbations. This form was chosen, since these will be the type of measurements made. The quantities to be measured are the following:

1. The static pressure inside the gland as a function of angle and time.
2. The motion of the seal. This includes the whirl amplitude and angular velocity as well as the spinning angular velocity. Note that the relative phase between the minimum gap and the pressures must be known.
3. The inlet conditions, P_i, V_i, T.
4. The average swirl velocity, V^*, and pressure P^*, inside the gland.
5. The flow rate through the test seal, $\dot{Q}$.
6. The rig vibration level.

The facility requirements, as given in the last chapter, are intimately connected with the capabilities of commercially available transducers. The major constraint in this regard was imposed by the sensitivity and accuracy on the time resolved pressure measurements.

6.2 PRESSURE MEASUREMENTS

Recall that for the baseline case presented in Chapter 4 the amplitude of the minimum pressure perturbation $|\hat{\xi}|\ P^*$ was $5 \times 10^{-4}\ P^*$. With the facility scaling this turns out to be approximately 100 pa (0.015 psi). To obtain sufficient resolution it is necessary to measure within 10 pa (0.0015 psi) at most. Since the average pressure P^* is 223 kpa (34.90 psi), it is implied that relative variations of 0.0086% would have to be measured. Transduces-amplifies systems able to measure such high pressures with the required sensitivity are not readily available. Due to this state of affairs a scheme employing relative pressure measurements was derived. This technique to be described was found to be more satisfactory than simply using absolute or atmospheric transducers.

The reference pressure is obtained by running tubes from pressure taps in the seal gland into a reference pressure manifold, supplying the reference pressure P^*. Then tubes are run to each of the differential transducers. Therefore the net reading from the transducers would just be the unsteady perturbation component $|\hat{\xi}|\ P^* \cos(\phi+\Omega t)$. The average value should be zero. A porous material is placed in the manifold to dampen any unwanted fluid resonances. Theoretically one transducer at any angular location within the gland would suffice. However, for purposes of redundancy and to measure the spatial non-uniformity within the

gland, four equally spaced transducers will be used. At maximum whirling speed the theory suggest that the first harmonic would be at 50 hz. However, transducers with a greater frequency response are desirable to detect the higher harmonics associated with geometric imperfections traveling at shaft spinning speed (100 hz x n). Due to this an upward limit of 1 khz was set. To accurately measure such high frequencies, flush mounted membrane transducers are required. The kind chosen was Kulite XCS-190 5 psid flush mounted pressure transducers with a sensitivity of 45 mv/psi. These are active strain gauge/membrane devices. The power for the bridges and the signal amplification is supplied by four Pacific Instruments 8650 signal conditioning amplifiers. High frequency components (over 1 kz), due mainly to turbulent fluctuations, can be filtered by these amplifiers or this can be accomplished later in digital mode by the data acquisition software. The other pressure measurements, which are steady state, are made by a single 100 psi transducer along with an automatic switching, multi-port scanivalve.

6.3 SEAL KINEMATIC MEASUREMENTS

In theory, the motion of the seal is precisely controlled by the rotating machinery. However, in practice one would expect some deviations due to machining tolerances, normal operating vibrations, etc. Therefore direct measurements of the seal motion is necessary. To make these measurements,

two Bently-Nevada CSN-5 proximeter systems are placed on orthogonal axes in the plane of rotation of the test disk. This system is capable of measuring the whirl path to less than 0.0025mm (0.0001 in). The relative phase is found by using a time synchronization technique.

The speeds of the shaft and the rotating housing are measured by frequency counters pricking up a once per rev impulse from small magnets implanted in each. This information may be used in a closed loop control system to more precisely control the speed of the two motors.

6.4 VELOCITY MEASUREMENTS

Two of the most important non-dimensional parameters found in the theory involved the average tangential velocity in the seal, σ, and the change in this velocity component, Γ. Therefore, it is necessary to measure this component in the test plenum as well as in the gland. To obtain these measurements a two probe hot wire anemometer will be placed at each of the two stations. The 10 mil wires are oriented normal to the plane of maximum velocity and have a 45° angle between them. Again, the excitation and amplification/ conditioning is handled by Pacific Inst. 8650 amps.

6.5 VIBRATION MEASUREMENTS

The vibration measurements, primarily intended for machine health monitoring, are made by attaching 4 Endevco 7702-50 accelerometers to the outer casing of the machine. Two

transducers each are placed in two parallel planes 90° apart. If possible the vibration signals will be used to back out the aerodynamic forces on the seal. If the vibration spectra is measurably different at different flow rates then the rotor dynamic coefficients K_{ij} and C_{ij} can be calculated.

6.6 FLOW MEASUREMENTS

The flow rate through the seal could be calculated with direct measurements of P_i and P^*. However, the accuracy may not exceed 10%. Therefore an independent measurement will prove useful. Two flow meters will be used. One low loss turbine flow meter will be used to yield the flow entering through the 2 inch supply line. The other meter, a calibrated ASME orifice/pressure loss device, will be used to measure the flow that bypasses the test seal and escapes through the two rig seals. By subtracting the leakage from the total the air flow rate through the test seal is obtained.

6.7 DATA ACQUISITION SYSTEM

The output from the amplifiers is digitized by a 12 bit 32 channel Lecroy Analog to Digital converter (ADC). The sampling rate for the unsteady measurements will be 10 Khz. These digital data will be dumped into a Lecroy 880DA buffer system. Then the data will be fed into the 30 meg disk of an IBM-PC-AT. A statistical analysis suggest that measurements

should be taken for about 60 whirl orbits and a phase lock averaging technique should be employed in reducing the pressure perturbation data. Therefore, measurements should be made for approximately 20 ms. Not all of the data acquisition software for performing these tasks has been procured.

CHAPTER 7

CONCLUSIONS

7.1 SUMMARY

The importance of the aeroelastic forces generated by whirling labyrinth seals on the stability of rotor/bearing systems was described. All of the pertinent literature concerning this problem and the closely related problem of acoustic-elastic instability producing high cycle fatigue of the sealing knives was presented.

A lumped parameter model based on those of Kostyuk and Iwatsubo was presented. A simplified set of coupled non-linear ordinary differential equations was obtained by transforming to rotating coordinates. The equations were linearized and a set of linear algebraic equation obtained by assuming single period harmonic behavior. These continuity and momentum equations were non-dimensionalized and a solution for the pressure perturbation $\hat{\xi}$ was presented. Three limiting cases were given first by setting certain of the driving terms to zero. Then the results of a design study, whose purpose was to obtain the range of the various variables necessary to corroborate the theory experimentally, was presented. The results were given both in terms of amplitude and phase of the pressure perturbation and the non-dimensional rotordynamic coefficients. Closed form approximations were obtained for these under the assumption that $|\sigma(1-W)| \ll 1$. Based on this study, facility

requirements were set and a detailed mechanical design was given. Finally, the necessary instrumentation to measure the various physical quantities was presented.

7.2 RECOMMENDATIONS FOR FURTHER WORK

The major goal of this work was to obtain a facility capable of measuring the aeroelastic forces generated by spinning whirling labyrinth seals. Tests should be conducted on straight-through convergent and divergent seals under a sufficient range of inlet conditions necessary to check the quantitative accuracy of this type of lumped parameter model. The hypothesis put forward in Chapter 4 that "custom tailored" seals can lead to universally stable seals should be verified experimentally.

Further analytical and computational efforts should concentrate on the nonlinear behavior of such seals. Preliminary theoretical results, based on solving (2.30) and (2.31) more exactly, suggest nonlinearities could play a significant role when the shaft's rotational speed is nearly twice the first lateral critical speed. Computational methods for solving this system are dependent on devising an appropriate scheme for imposing the proper periodic boundary condition on P and V. One method which appears to hold promise in this respect is any one of the many discrete fourier transform methods. In these periodicity is imposed automatically. Even though recent developments in the direct numerical simulation of high Reynolds number, cavity

flows (47) show promise, such methods are not sufficiently economical to allow them to be used as a design tool at the present time.

Recently, some turbomachines have shown "unbalanced response" at high flow rates. One possible explanation of this is that a noncircular spinning seal is somewhat equivalent to a whirling seal except that the pressure perturbations within the glands are locked to rotor speed instead of the rotors natural frequency. This would appear to be a forced vibration in this context. This should be checked thoroughly.

REFERENCES

1. Martin, H.M., "Labyrinth Packing", Engineer, January 10, 1908, pp. 35-38.

2. Stodola, A., Steam and Gas Turbines, 6th edition, McGraw-Hill, Vol. 1, 1927, pp. 189-194.

3. Sneck, H.J., "Labyrinth Seal Literature Survey", Journal of Engineering for Power, October 1974, pp. 579-581.

4. General Electric Flow Data Book, Vol. 1, Section 405.2, May 1982, pp. 3-21.

5. Ehrich, F.F., "Identification and Avoidance of Instabilities and Self-Excited Vibrations in Rotating Machinery", ASME Paper 72-DE-21, October 1979.

6. Ehrich, F.F., and Childs, D., "Self-Excited Vibration in High Performance Turbomachinery", Mechanical Engineer, May 1984, pp. 66-79.

7. Bisplinghoff, R.L., and Ashley, H., Aeroelasticity, Addison-Welsey, 1956, pp. 381-384.

8. Childs, D.W., "The Space Shuttle Main Engine High Pressure Fuel Turbopump Rotordynamic Instability", Journal of Engineering for Power, January 1978, pp. 48-57.

9. Ek, M.C., "Solution of the Subsynchronous Whirl Problem in the High-Pressure Hydrogen Turbomachines of the SSME", AIAA/SAE 14th Joint Propulsion Conference, Las Vegas, NV, July 25-27, 1979.

10. Jeffcoat, H.H., "The Lateral Vibration of Loaded Shafts in the Neighborhood of a Whirling Speed", Phil. Mag., No. 6, 1919, pp. 304-314.

11. Nordman, "Modal Analysis in Rotordynamics", Chapter 1, Dynamics of Rotors, Stability & System Identification, Springer-Verlag, New York, 1984.

12. Dugundji, J., Duong, C.N. and Chang, Y.P., "Formulation of Labyrinth Seal Effects in Rotor Dynamic Analysis", Presented at 11th ASME Design Eng. Conference on Vibration and Noise, September 27-30, 1987, Boston, MA.

13. Den Hartog, J.P., Mechanical Vibrations, 4th edition, McGraw-Hill, 1956, pp. 295-297.

14. Thomas, H.J., "Instabile Eigenschwingungen von Turbinenlaeufern Angefacht durch die Spaltstroemung in Stopfubuchsen und Bechauchflung (Unstable Natural Vibrations of Turbine Rotors Induced by the Clearance Flows in Glands and Blading)", Bull. de L'A.I.M. 71 No. 11/12, pp. 1039-1063.

15. Alford, J.S., "Protecting Turbomachinery From Self-Excited Rotor Whirl", Journal of Engineering for Power, October 1965, pp. 333-344.

16. Ehrich, F.F., "Aeroelastic Instability in Labyrinth Seals", Journal of Engineering for Power, October 1968, pp. 369-374.

17. Vance, J.M., and Murphy, B.T., "Labyrinth Seal Effects on Rotor Whirl Instability", Institute of Mechanical Engineers, 1980.

18. Kostyuk, A.G., "A Theoretical Analysis of the Aerodynamic Forces in the Labyrinth Glands of Turbomachines", Teploenergetica, 1972, Vol. 19, No. 11, pp. 29-33.

19. Iwatsubo, T., "Evaluation of Instability Forces of Labyrinth Seals in Turbines or Compressors", NASA C.P. 2133, 1980, pp. 139-169.

20. Iwatsubo, T., "Flow Induced Force of Labyrinth Seal", NASA C.P. 2250, 1982, pp. 205-222.

21. Gans, B.E., Prediction of the Aero-Elastic in a Labyrinth Type Seal and its Impact on Turbomachinery Stability, Eng. Thesis, Department of Mechanical Engineering, M.I.T., 1983.

22. Kurohashi, Y., and Inoue, T., "Spring and Damping Coefficients of Labyrinth Seals", Proceedings, Institution of Mechanical Engineers, 1980.

23. Celorio-Villasenor, A., Analysis of Disturbing Aerodynamic Forces in Labyrinth Seals, S.M. Thesis, Department of Aeronautics and Astronautics, M.I.T., 1984.

24. Kameoka, T., and Abe, T., "A Theoretical Approach to Labyrinth Seal Forces", Work Shop on Rotor Dynamic Stability, Texas A&M Univ., May 1984, pp. 28-30.

25. Lee, O.W.K., Prediction of Aerodynamic Force Coefficients in Labyrinth Seals, S.M. Thesis, Department of Aeronautics and Astronautics, M.I.T., February 1984.

26. Childs, D.W., and Scharrer, J.K., "An Iwatsubo Based Solution for Labyrinth Seals: Comparison to Experimental Results", Journal of Gas Turbines and Power, April 1986, Vol. 108, pp. 325-331.

27. Sisto, F., and Rajakumar, C., "A Parametric Study of Turborotor Excitation Forces Generated by Labyrinth Seals", ...

28. Martinez-Sanchez, M., Lee, O.W.K., and Czajkowski, E., "Prediction of Force Coefficients for Labyrinth Seals. Work Shop on Rotordynamic Stability," Texas A&M University, May 1984, pp.

29. Benckert, H., and Wachter, J., "Investigation of the Mass Flow and the Flow Induced Forces in Contactless Seals of Turbomachines", Proceedings of the 6th Conference on Fluid Machinery, Budapest 1979, pp. 57-66.

30. Benckert, H., and Wachter, J., "Flow Induced Coefficients of Labyrinth Seals", NASA C.P. 2133, May 1980.

31. Spurk, J.H., and Keiper, R., "Selbssterregte Schwingungen bei Turbomachinen Infolge der Labyrinth-Stromung", Ingenur- Archjiv, 1974.

32. Leong, Y.M.M.S., and Brown, R.D., "Circumferential Pressure Distributions in a Model Labyrinth Seal", NASA C.P. 2133, 1980, pp. 222-232.

33. Hauck, L., "Measurement and Evaluation of Swirl-Type Flow in Labyrinth Seal of Conventional Turbine Stages", NASA C.P. 2250, 1982, pp. 242-259.

34. Urlicks, K., Clearance Flow Generated Transverse Forces at the Rotors of Thermal Turbomachines, NASA translation tech mem. TM-77292, October 1983, Ph.D. Dissertation, Munich Technical University, 1975.

35. Wohlrab, R., Experimental Determination of Gap Flow Conditioned Forces at Turbine Stages and their Effects on the Running Stability of Simple Rotors, NASA translation tech mem. TM-77293, October 1983, Ph.D. Dissertation, Munich Technical University, 1975.

36. Childs, D.W., "Testing Seals for Rotordynamic Coefficients", NASA Publication CP-2250, 1982.

37. Wright, D.V., "Labyrinth Seal Forces on a Whirling Rotor", Proceedings of the Applied Mechanics, Bioengineering and Fluids Engineering Conference, Houston, TX, June 20-22, 1983, pp. 19-31.

38. Wright, D.V., "Air Model Tests of Labyrinth Seal Forces on a Whirling Rotor", ASME Paper 82GT-3458.

39. Patera, T., Computational Fluid Dynamics, Chapter 6 Viscous Computations, to be published, M.I.T. Press 1987, Class Notes.

40. Abbot, D.R., "Advances in Labyrinth Seal Aeroelastic Instability Prediction and Prevention", ASME Journal of Engineering for Power, Vol. 103, April 1981, pp. 308-312.

41. Srinivasan, A.V., Arnold, R.A. and Dennis, A.J., "Aeroelastic Instabilities in Labyrinth Air Seal Systems", ASME Paper 84-GT-169, June 1984.

42. Lewis, D.A., Platt, C.E. and Smith, E.B., "Aeroelastic Instability in F100 Labyrinth Air Seals", AIAA/ASME/SAE 14th Joint Propulsion Conference Paper 78-1087, Las Vagas, NV, July 25-27, 1978.

43. Morse, P.M., Ingard, K.U., Theoretical Acoustics, McGraw-Hill, 1968, pp. 309-312.

44. Ingard, K.U., Personal Communication.

45. Lomakin, A.A., "Die Berechung der Krútischen Drehzahl und der Bedingungingen fuer Sicherung der dynamischen Stabilitatet des Laeufers von hydrauischen Hochruck-Maschinenunter Beruecksichtigung der Kraefte, die in der Dichtunger entstenen. (Calculation of Critical Speeds and the condition to insure the dynamic stability of hydrolic high-pressure machine rotors, taking into consideration the forces generated in the seals.)", Energomasinostroenie 4, No. 4, 1-5, 1958.

46. Kiesewetter, H.S., "Beruehrungsfreie Dichtungen," (Non-contact seals), VDJ Publishers, Duesseldorf 1973,

47. Gustafson, K., and Halasi, K., "Cavity Flow Dynamics at Higher Reynolds Number and Higher Aspect Ratio," J. Comp. Physics, Vol. 70, No. 2, June 1986, pp. 271-283.

48. Shapiro, A.H., The Dynamics and Thermodynamics of Compressible Fluid Flow, Volume I & II, Ronald Press, New York, 1953.

49. Liepman, H.W., and Roshko, A., Elements of Gas Dynamics, John Wiley & Sons, New York, 1957.

50. Schlichting, H., Boundary Layer Theory, McGraw-Hill, New York, 1955.

51. White, F.M., Viscous Fluid Flow, McGraw-Hill, 1974.

52. Rosenow, W., and Chow, H.T., Heat Mass and Momentum Transfer.

53. AFBA Standard #12-A73 Specifications, Gill Press, 1974, pp. 143.

54. Nissan, A.H., and Bresan, V.P., "Swirling Flow in Cylinderrs," A.I.Ch.E. Journal, Vol. 7, No. 4, Dec. 1961, pp. 543-547.

55. Ward-Smith, A.J., Pressure Losses in Ducted Flows, Butterworths, London, 1971.

56. Komotori, K., "A Consideration on the Labyrinth Packing of Straight Through Type," Nihom Kikai Gakkai Transactions JSME, Vol. 23, No. 133, 1978, pp. 617-623.

57. Meyer, C.A., "The Leakage Through Labyrinth and Honecomb Seals," ASME paper 74-WA PTC-2, Nov. 1974.

APPENDIX A

EXTENSION OF MODEL

Several simplifications were made in Chapter 2 while deriving the governing equations. These were made in order to obtain a set of equations which contained the pertinent flow physics while eliminating any unnecessary algebraic complexity. Now certain extensions of the sub models will be presented, which could be incorporated into the continuity and momentum relations hence yielding a more exact set of equations.

Flow Over the Seal Knives

As stated in Chapter 2, the flow rate per unit seal circumference q_1 (1-D approx.) is

$$q_1 = \rho_1 \delta_1 \mu W_1 \tag{A.1}$$

where ρ_1 is the density, δ_1 the gap, W_1 the axial velocity and μ is the flow coefficient. An approximation for q_1 was presented in Chapter 2. The density was set to the average density before and after the gap and W_1 was calculated by using the incompressible Bernoulli equation. With these, q_1 was found to be

$$q_1 = \frac{\delta_1 \mu}{\sqrt{R_a T}} \left(P_i^2 - P^2\right)^{1/2} \tag{A.2}$$

In the analysis μ was take to be 0.65 (constant). In

reality μ is not exactly constant. μ can be expressed as the product of the contraction coefficient C_c times the "carry-over factor" β

$$\mu = C_c\beta \qquad (A.3)$$

C_c is in turn a function of the geometry near the knife tip and the axial Reynolds Number. Figure 41 shows C_c as a function of the gap aspect ratio for different Reynolds numbers.

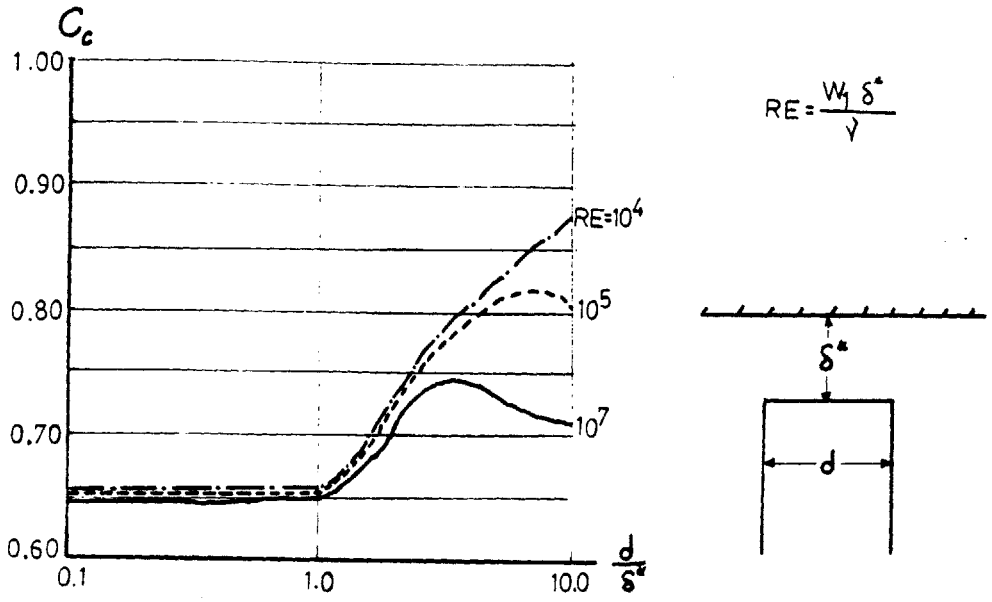

Figure 41 - Contraction Coefficient C_c vs. aspect ratio $\frac{\delta_1^*}{d}$ with Re used as parameters.

The carry-over factor β is very complicated and is generally

found by using empirical correlation such as those of Komotori (56) and Meyer (57). In essence, this number is a measure of the amount of kinematic energy not dissipated from the last constriction. For stepped or interlocking seals $\beta=1$ but for straight through types $\beta > 1$.

Equation (A.2) is very accurate when the axial Mach Number is sufficiently low. But when the pressure difference is high enough the last two seals Mach number may be too high for (A.2) to be used. In fact the flow in the last gap may be chocked. If the first analysis suggest $M > 0.6$ the following expressions for ρ_1 and W_1 should be used for those gaps.

$$W_1 = \sqrt{\frac{2\gamma}{\gamma-1}\left(\frac{P_o}{\rho_o}\right)\left[1 - \left(\frac{P}{P_o}\right)^{\frac{\gamma-1}{\gamma}}\right]} \qquad (A.4)$$

$$\rho_1 = \rho_o\left(1 + \frac{\gamma-1}{2} M^2\right)^{\frac{1}{\gamma-1}} \qquad (A.5)$$

Friction Factors

The change in swirl, induced by viscous shear stresses, was shown to be very important in the generation of aeroelastic forces. The stresses were expressed in terms of a Darcy friction factor using

$$\lambda = 0.3164\ Re^{-0.25} \qquad (A.6)$$

Another formula for smooth-straight ducts (Schlichting (50))

which is more accurate when $Re > 10^6$ is

$$\frac{1}{\sqrt{\lambda}} = 0.87 - \log\left(\frac{K_s}{R_h} + \frac{37.4}{Re\sqrt{\lambda}}\right) \qquad (A.7)$$

Secondary flows generated in curved piping will increase the average friction factor. A formula which accounts for this is

$$\frac{\lambda}{\lambda_o} = 1 + 0.075\ Re^{1/4}\left(\frac{R_h}{R}\right)^{1/2} \qquad (A.8)$$

where λ_o is the "straight" value and R_h and R are the hydraulic radius and curve radius respectively. If the Reynolds Number is very high or "casing treatments" are employed. Augmented friction factors should be used to account for roughness.

APPENDIX B

COMPUTER PROGRAMS

SINGSEAL.FOR

Given the inlet and exit conditions and geometry of the seal. SINGSEAL.FOR calculates the zeroth order solution in the seal gland and the non-dimensional parameters $\alpha, \varepsilon_1, \sigma, \Delta$ and Γ.

```
C    FILE NAME:SINGSEAL.FOR
C    DATE:1-5-87
C    BY:KNOX MILLSAPS
C    PURPOSE:THIS FILE CONTAINS A PROGRAM WHICH DOES A KOSTUAK-IWATSUBO
C    TYPY SOLUTION FOR A SINGLE LABYRINTH SEAL. THE PROGRAM IS FOR AIR.
C    ALL ROTORDYNAMIC COEFFICENTS ARE CALCULATED.
C
C   INPUT FILE 3 IS USED ONLY FOR GOEMETRIC DATA(ALL MKS UNITS)
C    RS=SEAL RADIUS, RL=AXIAL SPACE BETWEEN KNIVES, H=SEAL HIEGHT
C    DELST1=NOM. CLEAR. OF 1ST KNIFE, DELST2=NOM. CLEAR. OF 2ND KNIFE
C    R=RADIUS OF WHIRL,OMGS=SPIN ANGULAR VELOSITY, OMGW=WHIRL ANGULAR VEL.
C
C   INPUT FILE 4 IS USED ONLY FOR FLOW DATA (ALL MKS UNITS) PI=PRESSURE
C    BEFORE SEAL, PO=PRESSURE AFTER SEAL, TEMP=TEMPERATURE, VI=SWIRL VEL.
C    BEFORE SEAL(MEASURED CCW FROM X-AXIS)
C
        COMPLEX B(2,2), EHAT, ETAHAT, Z(2),IMG,DET
        OPEN(UNIT=3,FILE='GOEM.DAT',STATUS='OLD')
        OPEN(UNIT=4,FILE='FLOW.DAT',STATUS='OLD')
        READ(3,*) RS,RL,H,DELST1,DELST2,R,OMGS,OMGW
        READ(4,*) PI,PO,TEMP,VI
C
C   SET ALL CONSTANTS.
C
        RAIR=287.1
        GAMMA=1.4
C   CONTRACTION COEFFICIENT
        RMU=0.65
C   HYDRALIC DIAMETER=DH
        DH=4.0*H*RL/(2.0*H+2.0*RL)
C   VISCOSITY OF AIR= RNU
        RNU=0.0000145
        WRITE(5,*) 'RS=',RS,'RL=',RL,'H=',H,'DELST1=',DELST1
        WRITE(5,*) 'DELST2=',DELST2,'R=',R,'OMGS=',OMGS,'OMGW=',OMGW
        WRITE(5,*) 'PI=',PI,'PO=',PO,'VI=',VI
C   SOLVE FOR THE EQUILIBRIUM PRESSURE AND FLOW IN THE SEAL.
        D1=DELST1**2
        D2=DELST2**2
        D3=PI**2
        D4=PO**2
        PST=SQRT((D1*D3+D2*D4)/(D1+D2))
        ROST=PST/(TEMP*RAIR)
        WRITE(5,*) ' ROST=', ROST,'PST=',PST
        Q1ST=RMU*DELST1*SQRT((D3-PST**2)/(RAIR*TEMP))
        Q2ST=RMU*DELST2*SQRT((PST**2-D4)/(RAIR*TEMP))
        QST=Q2ST
C   GUESS THE EQUILBRIUM SWIRL TO BE THE INLET SWIRL AND ITERATE.
        VST=VI
1       CONTINUE
        CALL FRICSTAT(VST,DH,RNU,RLAM1)
        CALL FRICROT(VST,DH,OMGS,RS,RNU,RLAM2)
```

```
C
C  CALCULATE EQUILBRIUM SWIRL IN THE SEAL.
C
      VSTI=VST
      A=(ROST/8.0)*(RLAM1*RL-RLAM2*(RL+2.0*H))
      B1=QST+(ROST/4.0)*RLAM2*(RL+2.0*H)*OMGS*RS


      C=-QST*VI-(ROST/8.0)*RLAM2*(RL+2.0*H)*(OMGS*RS)**2
      VST=(-B1+SQRT(B1**2-4.0*A*C))/(2.0*A)
      WRITE(5,*) VST
      ERROR=ABS(VST-VSTI)
      WRITE(5,*) 'ERROR',ERROR
      IF(ERROR.LT.0.001) GO TO 2
      GO TO 1
2     CONTINUE
C
C  SET ALL NON-DIMENSIONAL PARAMETERS
C
      WRITE(5,*) 'LAM1=',RLAM1,'LAM2=',RLAM2
      WRITE(5,*) ' '
      EPS1=R/DELST1
      ALPHA=DELST2/DELST1
      CAPH=H/RS
      CAPL=RL/RS
      CAPD=DELST1/H
      CAPW=OMGW*RS/VST
      CAPS=OMGS*RS/VST
      DELQ=QST/(RMU*DELST1*ROST*SQRT(RAIR*TEMP))
      SIG=ROST*DELST1*VST/QST
      CGAM=1.0-(VI/VST)
C
C   IMG=I
C
      IMG=CMPLX(0.0,1.0)
      WRITE(5,*) 'PST=',PST,'ROST=',ROST,'QST=',QST,'VST=',VST
      WRITE(5,*) ' '
      WRITE(5,*) 'CAPH=',CAPH,'CAPL=',CAPL,'CAPD=',CAPD,'EPS1=',EPS1
      WRITE(5,*) ' '
      WRITE(5,*) 'ALPHA=',ALPHA,'DELQ=',DELQ,'GAM=',CGAM,'SIG=',SIG
      WRITE(5,*) ' '
      WRITE(5,*) 'CAPW=',CAPW,'CAPS=',CAPS
C
C   INPUT MATRIX COEFFICIENTS FOR SOLUTION
C
      B(1,1)= SIG*CAPL*(1.0-CAPW)*IMG/(GAMMA*CAPD)
     &  -(1.0+ALPHA**2)/DELQ**2
      B(1,2)=SIG*CAPL*IMG/CAPD
      B(2,1)=(CGAM/(DELQ**2)) - (SIG*CAPL/(8.0*GAMMA*CAPD*CAPH))*
     &  (RLAM1-RLAM2*(1.0+2.0*CAPH/CAPL)*(CAPS-1.0)**2)+
     &  CAPL*IMG/(DELQ**2*RMU**2*SIG*CAPD)
      B(2,2)=SIG*CAPL*(1.0-CAPW)*IMG/CAPD-1.0-(SIG*CAPL/(4.0*CAPH
     &  *CAPD))*(RLAM1+RLAM2*(1.0+2.0*CAPH/CAPL)*(CAPS-1.0))
      Z(1)=(SIG*CAPL*IMG*(1.0-CAPW)+(1.0-ALPHA))*EPS1
      Z(2)=-CGAM*EPS1
      CALL COMPLX2(B,Z,EHAT,ETAHAT,DET)
      STOP
      END
C*********************************************************************
      SUBROUTINE FRICSTAT(VST,DH,RNU,RLAM1)
C  THIS SUBROUTINE CALCULATES THE FRICTION FACTOR OF THE STATOR.
      SGN1=SIGN(1.0,VST)
      RE=ABS(VST*DH/RNU)
      RLAM1=SGN1*0.3164*RE**(-0.25)
      RETURN
      END
```

```
C*********************************************************************
      SUBROUTINE FRICROT(VST,DH,OMGS,RS,RNU,RLAM2)


C  THIS SUBROUTINE CALCULATES THE FRICTION FACTOR OF THE ROTOR.
      VREL=OMGS*RS-VST
      SGN2=SIGN(1.0,VREL)
      RE=ABS(OMGS*RS-VST)*DH/RNU
      RLAM2=SGN2*0.3164*RE**(-0.25)
      RETURN
      END
C*********************************************************************
      SUBROUTINE COMPLX2(B,Z,EHAT,ETAHAT,DET)
C    THIS SUBROUTINE SOLVES A 2*2 COMPLEX LIN ALG SYSTEM
C    B=COEFF. MATRIX,Z=RHS , EHAT AND ETAHAT ARE THE SOLUTION
      COMPLEX B(2,2), Z(2), EHAT, ETAHAT
      EHAT=(Z(1)*B(2,2)/B(1,2)-Z(2))/(B(1,1)*B(2,2)/B(1,2)-B(2,1))
      ETAHAT=(Z(1)-B(1,1)*EHAT)/B(1,2)
      DET=B(1,1)*B(2,2)-B(1,2)*B(2,1)
      RETURN
      END
C*********************************************************************
```

SSNDPP.FOR

Given the non-dimensional parameters of Chapter 4 as inputs SSNDPP calculates and plots the amplitude and phase of the pressure perturbations $\hat{\xi}$. It can also calculate and plot the non-dimensional rotordynamic coefficients $\overline{K_{ij}}$ and $\overline{C_{ij}}$.

```
C       FILENAME: SSNDPP.FOR
C       WRITTEN:KTMJ
C       DATE:1-20-87
C       PURPOSE: SINGLE SEAL NONDIMENSIONAL PRESSURE PERTURBATION.
C        THIS PROGRAM CALCULATES AND STORES THE NON DIM PRESSURE
C        PERT. USING ALL NON-DIM PARAMETERS EMPLOYING A SIMPLE KOS-
C        IWAT ANALYSIS. IT PLOTS 4 CURVES FOR 4 DIDFFERENT VALUES
C        OF THE CHOSEN PARAMETER EITHER ALPHA,DEL,GAMMA OR SIGMA IT
C        ALSO PLOTS THE NON DIM K'S AND C'S.
C
      DIMENSION W(41), AMP(41), PHS(41),XW(164),YP(164),NP(4),IOPT(4)
      DIMENSION YA(164), RKIIB(41), RKIJB(41), CIIB(41), CIJB(41)
      DIMENSION WR(82), NR(2), IOPT2(2)
      CHARACTER*20 PLTITL, TITLE1,TITLE2,TITLE3,TITLE4,TITLE5,TITLE6
      CHARACTER*20 TITLE7, TITLE8, TITLE9, TITLE10
      CHARACTER*9 DATE,TIME
C   READ IN WHICH IS USED AS PARAMETER.
C     RETURN FROM BELOW
2000  CONTINUE
      WRITE(5,*) 'READ IVARY AL=1, DEL=2, GAM=3, SIG=4, ROTOR=5'
      READ(6,*) IVARY
C
C   SET NOMINAL VALUES
C
      AL=1.0
      H=0.05
      RL=0.15
      D=0.05
      DEL=0.80
      GAM=.05
      SIG=0.2
C      WRITE(5,*) ' AL= ,H= ,RL= ,D=  '
C      READ(6,*) AL,H,RL,D
C      WRITE(5,*) 'DEL= , SIG=, GAM='
C      READ(6,*) DEL,SIG,GAM
      NLINE=4
      DO 1 I=1,4
      IOPT(I)=2
      NP(I)=41
      INDGR=55
1     CONTINUE
      IF(IVARY.EQ.1) GO TO 100
      IF(IVARY.EQ.2) GO TO 200
      IF(IVARY.EQ.3) GO TO 300
      IF(IVARY.EQ.4) GO TO 400
      IF(IVARY.EQ.5) GO TO 500
      GO TO 3000
C*****************************************
C  SET WHIRL ARRAY.
C*****************************************
100   CONTINUE
C     THIS BLOCK VARIES ALPHA
C     INPUT 4 VALUES OF ALPHA
C*****************************************
      WRITE(5,*) ' INPUT FOUR VALUES OF ALPHA.'
      READ(6,*) AL1,AL2,AL3,AL4
      AL=AL1
```

```
      DO 101 I=1,41
      W(I)=(I-1.0)*0.1-1.0
      WW=W(I)
      CALL SOLVE(WW,AL,H,RL,D,DEL,GAM,SIG,AM,PH)
      AMP(I)=AM
      PHS(I)=PH
      XW(I)=W(I)
      YA(I)=AMP(I)
      YP(I)=PHS(I)
101   CONTINUE
      AL=AL2
      DO 102 I=1,41
      W(I)=(I-1.0)*0.1-1.0
      WW=W(I)
      CALL SOLVE(WW,AL,H,RL,D,DEL,GAM,SIG,AM,PH)
      AMP(I)=AM
      PHS(I)=PH
      XW(41+I)=W(I)
      YA(41+I)=AMP(I)
      YP(41+I)=PHS(I)
102   CONTINUE
      AL=AL3
      DO 103 I=1,41
      W(I)=(I-1.0)*0.1-1.0
      WW=W(I)
      CALL SOLVE(WW,AL,H,RL,D,DEL,GAM,SIG,AM,PH)
      AMP(I)=AM
      PHS(I)=PH
      XW(82+I)=W(I)
      YA(82+I)=AMP(I)
      YP(82+I)=PHS(I)
103   CONTINUE
      AL=AL4
      DO 104 I=1,41
      W(I)=(I-1.0)*0.1-1.0
      WW=W(I)
      CALL SOLVE(WW,AL,H,RL,D,DEL,GAM,SIG,AM,PH)
      AMP(I)=AM
      PHS(I)=PH
      XW(123+I)=W(I)
      YA(123+I)=AMP(I)
      YP(123+I)=PHS(I)
104   CONTINUE
C
C  PLOT NDPP VS. W USING ALPHA AS PARAMETER.
C
      PLTITL(1:8)='      '
      PLTITL(9:16)='       '
      PLTITL(17:20)='    '
      TITLE1='AMP VS. W/ALPHA '
      TITLE2='PHS VS. W/ALPHA '
      DATE='      '
      TIME='      '
      CALL GRINIT(5,6,TITLE1)
      CALL GR_SET_TIME(DATE,TIME)
      CALL GRLINE(IOPT,NLINE,PLTITL,INDGR,XW,YA,NP)
      CALL GRINIT(5,6,TITLE2)
      CALL GR_SET_TIME(DATE,TIME)
      CALL GRLINE(IOPT,NLINE,PLTITL,INDGR,XW,YP,NP)
      GO TO 1000
```

```
C*************************************************************************
200     CONTINUE
C      THIS BLOCK VARIES DEL
C      INPUT 4 VALUES OF DEL
       WRITE(5,*) ' INPUT FOUR VALUES OF DEL.'
       READ(6,*) DEL1,DEL2,DEL3,DEL4
       DEL=DEL1
       DO 201 I=1,41
       W(I)=(I-1.0)*0.1-1.0
       WW=W(I)
       CALL SOLVE(WW,AL,H,RL,D,DEL,GAM,SIG,AM,PH)
       AMP(I)=AM
       PHS(I)=PH
       XW(I)=W(I)
       YA(I)=AMP(I)
       YP(I)=PHS(I)
201    CONTINUE
       DEL=DEL2
       DO 202 I=1,41
       W(I)=(I-1.0)*0.1-1.0
       WW=W(I)
       CALL SOLVE(WW,AL,H,RL,D,DEL,GAM,SIG,AM,PH)
       AMP(I)=AM
       PHS(I)=PH
       XW(41+I)=W(I)
       YA(41+I)=AMP(I)
       YP(41+I)=PHS(I)
202    CONTINUE
       DEL=DEL3
       DO 203 I=1,41
       W(I)=(I-1.0)*0.1-1.0
       WW=W(I)
       CALL SOLVE(WW,AL,H,RL,D,DEL,GAM,SIG,AM,PH)
       AMP(I)=AM
       PHS(I)=PH
       XW(82+I)=W(I)
       YA(82+I)=AMP(I)
       YP(82+I)=PHS(I)
203    CONTINUE
       DEL=DEL4
       DO 204 I=1,41
       W(I)=(I-1.0)*0.1-1.0
       WW=W(I)
       CALL SOLVE(WW,AL,H,RL,D,DEL,GAM,SIG,AM,PH)
       AMP(I)=AM
       PHS(I)=PH
       XW(123+I)=W(I)
       YA(123+I)=AMP(I)
       YP(123+I)=PHS(I)
204    CONTINUE
C
C  PLOT NDPP VS. W USING DEL AS PARAMETER.
C
       PLTITL(1:8)='      '
       PLTITL(9:16)='       '
       PLTITL(17:20)='    '
       TITLE3='AMP VS. W/DEL '
       TITLE4='PHS VS. W/DEL '
       DATE='       '
       TIME='       '
```

```
      CALL GRINIT(5,6,TITLE3)
      CALL GR_SET_TIME(DATE,TIME)
      CALL GRLINE(IOPT,NLINE,PLTITL,INDGR,XW,YA,NP)
      CALL GRINIT(5,6,TITLE4)
      CALL GR_SET_TIME(DATE,TIME)
      CALL GRLINE(IOPT,NLINE,PLTITL,INDGR,XW,YP,NP)
      GO TO 1000
C*********************************************************************
300   CONTINUE
C     THIS BLOCK VARIES GAMMA
C     INPUT 4 VALUES OF GAMMA
      WRITE(5,*) ' INPUT FOUR VALUES OF GAMMA.'
      READ(6,*) GAM1,GAM2,GAM3,GAM4
      GAM=GAM1
      DO 301 I=1,41
      W(I)=(I-1.0)*0.1-1.0
      WW=W(I)
      CALL SOLVE(WW,AL,H,RL,D,DEL,GAM,SIG,AM,PH)
      AMP(I)=AM
      PHS(I)=PH
      XW(I)=W(I)
      YA(I)=AMP(I)
      YP(I)=PHS(I)
301   CONTINUE
      GAM=GAM2
      DO 302 I=1,41
      W(I)=(I-1.0)*0.1-1.0
      WW=W(I)
      CALL SOLVE(WW,AL,H,RL,D,DEL,GAM,SIG,AM,PH)
      AMP(I)=AM
      PHS(I)=PH
      XW(41+I)=W(I)
      YA(41+I)=AMP(I)
      YP(41+I)=PHS(I)
302   CONTINUE
      GAM=GAM3
      DO 303 I=1,41
      W(I)=(I-1.0)*0.1-1.0
      WW=W(I)
      CALL SOLVE(WW,AL,H,RL,D,DEL,GAM,SIG,AM,PH)
      AMP(I)=AM
      PHS(I)=PH
      XW(82+I)=W(I)
      YA(82+I)=AMP(I)
      YP(82+I)=PHS(I)
303   CONTINUE
      GAM=GAM4
      DO 304 I=1,41
      W(I)=(I-1.0)*0.1-1.0
      WW=W(I)
      CALL SOLVE(WW,AL,H,RL,D,DEL,GAM,SIG,AM,PH)
      AMP(I)=AM
      PHS(I)=PH
      XW(123+I)=W(I)
      YA(123+I)=AMP(I)
      YP(123+I)=PHS(I)
304   CONTINUE
C
C  PLOT NDPP VS. W USING GAMMA AS PARAMETER.
C


      PLTITL(1:8)='      '
      PLTITL(9:16)='      '
      PLTITL(17:20)='    '
      TITLE5='AMP VS. W/GAMMA '
      TITLE6='PHS VS. W/GAMMA'
      DATE='      '
      TIME='      '
      CALL GRINIT(5,6,TITLE5)
      CALL GR_SET_TIME(DATE,TIME)
      CALL GRLINE(IOPT,NLINE,PLTITL,INDGR,XW,YA,NP)
      CALL GRINIT(5,6,TITLE6)
      CALL GR_SET_TIME(DATE,TIME)
      CALL GRLINE(IOPT,NLINE,PLTITL,INDGR,XW,YP,NP)
      GO TO 1000
```

```
C*****************************************************************
400     CONTINUE
C      THIS BLOCK VARIES SIGMA
C      INPUT 4 VALUES OF SIGMA
       WRITE(5,*) ' INPUT FOUR VALUES OF SIGMA.'
       READ(6,*) SIG1,SIG2,SIG3,SIG4
       SIG=SIG1
       DO 401 I=1,41
       W(I)=(I-1.0)*0.1-1.0
       WW=W(I)
       CALL SOLVE(WW,AL,H,RL,D,DEL,GAM,SIG,AM,PH)
       AMP(I)=AM
       PHS(I)=PH
       XW(I)=W(I)
       YA(I)=AMP(I)
       YP(I)=PHS(I)
401    CONTINUE
       SIG=SIG2
       DO 402 I=1,41
       W(I)=(I-1.0)*0.1-1.0
       WW=W(I)
       CALL SOLVE(WW,AL,H,RL,D,DEL,GAM,SIG,AM,PH)
       AMP(I)=AM
       PHS(I)=PH
       XW(41+I)=W(I)
       YA(41+I)=AMP(I)
       YP(41+I)=PHS(I)
402    CONTINUE
       SIG=SIG3
       DO 403 I=1,41
       W(I)=(I-1.0)*0.1-1.0
       WW=W(I)
       CALL SOLVE(WW,AL,H,RL,D,DEL,GAM,SIG,AM,PH)
       AMP(I)=AM
       PHS(I)=PH
       XW(82+I)=W(I)
       YA(82+I)=AMP(I)
       YP(82+I)=PHS(I)
403    CONTINUE
       SIG=SIG4
       DO 404 I=1,41
       W(I)=(I-1.0)*0.1-1.0
       WW=W(I)
       CALL SOLVE(WW,AL,H,RL,D,DEL,GAM,SIG,AM,PH)
       AMP(I)=AM
       PHS(I)=PH


       XW(123+I)=W(I)
       YA(123+I)=AMP(I)
       YP(123+I)=PHS(I)
404    CONTINUE
C
C  PLOT NDPP VS. W USING SIGMA AS PARAMETER.
C
       PLTITL(1:8)='      '
       PLTITL(9:16)='       '
       PLTITL(17:20)='    '
       TITLE7='AMP VS. W/SIGMA '
       TITLE8='PHS VS. W/SIGMA '
       TIME='      '
       DATE='      '
       CALL GRINIT(5,6,TITLE7)
       CALL GR_SET_TIME(DATE,TIME)
       CALL GRLINE(IOPT,NLINE,PLTITL,INDGR,XW,YA,NP)
       CALL GRINIT(5,6,TITLE8)
       CALL GR_SET_TIME(DATE,TIME)
       CALL GRLINE(IOPT,NLINE,PLTITL,INDGR,XW,YP,NP)
       GO TO 1000
C
C    THIS SECTION CALCULATES THE ROTORDYNAMIC COEFFICIENTS FOR THE
C    BASELINE CASE.
C*****************************************************************
```

```
  500     CONTINUE
          DO 501 I=1,41
          W(I)=(I-1.0)*0.1-1.0
          WR(I)=W(I)
          WR(I+41)=WR(I)
          WW=W(I)
          CALL SOLVE(WW,AL,H,RL,D,DEL,GAM,SIG,AM,PH)
          AMP(I)=AM
          PHS(I)=PH
  501     CONTINUE
          DO 502 I=1,40
          AF1W1=AMP(I)*COS(PHS(I))
          AF1W2=AMP(I+1)*COS(PHS(I+1))
          AF2W1=AMP(I)*SIN(PHS(I))
          AF2W2=AMP(I+1)*SIN(PHS(I+1))
          CIJB(I)=(AF1W1-AF1W2)/(W(I+1)-W(I))
          RKIIB(I)=AF1W1+W(I)*CIJB(I)
          CIIB(I)=(AF2W1-AF2W2)/(W(I)-W(I+1))
          RKIJB(I)=AF2W1-W(I)*CIIB(I)
  502     CONTINUE
          CIJB(41)=CIJB(40)
          CIIB(41)=CIIB(40)
          RKIJB(41)=RKIJB(40)
          RKIIB(41)=RKIIB(40)
          DO 503 I=1,41
          YA(I)=RKIIB(I)
          YA(41+I)=RKIJB(I)
          YA(82+I)=CIIB(I)
          YA(123+I)=CIJB(I)
          XW(I)=W(I)
          XW(41+I)=W(I)
          XW(82+I)=W(I)
          XW(123+I)=W(I)
  503     CONTINUE
  C


C     PLOT KXX, KXY, CXX, CXY
C
          PLTITL(1:8)='     '
          PLTITL(9:16)='      '
          PLTITL(17:20)='  '
          TITLE9='ROTORDYNM COEFF. '
          DATE=' '
          TIME='  '
          CALL GRINIT(5,6,TITLE9)
          CALL GR_SET_TIME(DATE,TIME)
          CALL GRLINE(IOPT,NLINE,PLTITL,INDGR,XW,YA,NP)
1000      CONTINUE
          GO TO 2000
3000      CONTINUE
          STOP
          END
C*******************************************************************************
          SUBROUTINE SOLVE(WW,AL,H,RL,D,DEL,GAM,SIG,AM,PH)
           COMPLEX RMG, EHAT, RNUM, DENM
           RMG=CMPLX(0.0,1.0)
           RNUM=(SIG*RL*(1.0-WW)*RMG+(1.0-(1.0/AL)))*(SIG*RL*(1.0-WW)*RMG/
     &     D-1.0) + GAM*SIG*RL*RMG/D
           DENM=(SIG*RL*(1.0-WW)*RMG/(1.4*D)-(1.0+AL**2)/DEL**2)
     &     *(SIG*RL*(1.0-WW)*RMG/D-1.0)-(SIG*RL*RMG/D)*(GAM/DEL**2 +
     &     RL*RMG/(DEL*0.65)**2/(SIG*D))
           EHAT=RNUM/DENM
           RE=REAL(EHAT)
           RIG=AIMAG(EHAT)
           AM=SQRT(RE**2 + RIG**2)
           PH=ATAN(RIG/RE)
           RETURN
           END
C*******************************************************************************
```

APPENDIX C

MECHANICAL DESIGN CALCULATIONS

Critical Frequencies for Rotating Rig

There are many possible modes of vibration for the rotating rig. But the only ones which could correspond the rotational frequencies (0-50 hertz whirling and 0-100 hertz spinning) are the bending and bouncing modes of the shaft/disks assembly. Figure 42 shows the model used for calculating the shaft/disk lateral vibration frequency.

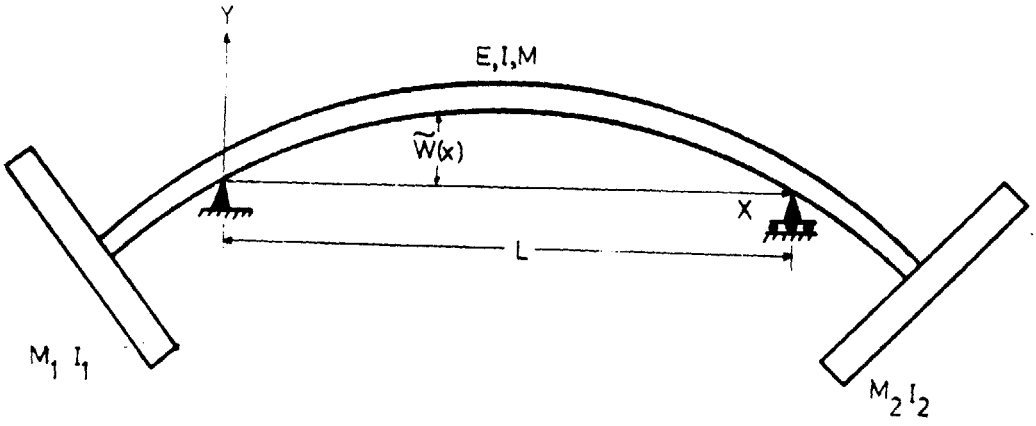

Figure 42 - Model of Shaft/Disk Assembly bending for calculation of bending frequency.

The frequency was found approximately by using Rayleigh's method which states,

$$\omega_n \sim \left[\frac{\text{Potential Energy}}{\text{Kinetic Energy}}\right]_{\text{assumed mode}}^{1/2} \qquad (C.1)$$

For the model this can be expressed as

$$\omega_n = \left[\frac{\int_o^l EI\left(\frac{d^2\tilde{\omega}}{dx^2}\right)^2 dx}{\int_o^l m\tilde{\omega}^2 dx + M_1\tilde{\omega}^2 + M_1\tilde{\omega}^2 + I_1\left(\frac{d\tilde{\omega}}{dx}\right)^2 + I_1\left(\frac{d\tilde{\omega}}{dx}\right)^2}\right]^{1/2} \qquad (C.2)$$

Assuming the shaft mode is $\tilde{\omega} = \sin\frac{\pi x}{L_1}$ and calculating the necessary properties from Part #1 the critical lateral frequency is found to be $\omega_n = 318.5$ Hz. The symmetric and unsymmetric bouncing modes were at a higher frequencies. These were found by treating the shaft as a rigid body and modeling the bearings as linear springs ($K_{Bearing} \sim 3 \times 10^6$ lb_f/in).

Stand Vibration

The stand to which the rotating rig/air supply is mounted is in turn supported by 4 (spring/damping) vibration isolators. The 3 degree of freedom model used for the calculation of vibration frequency is shown in Figure 43.

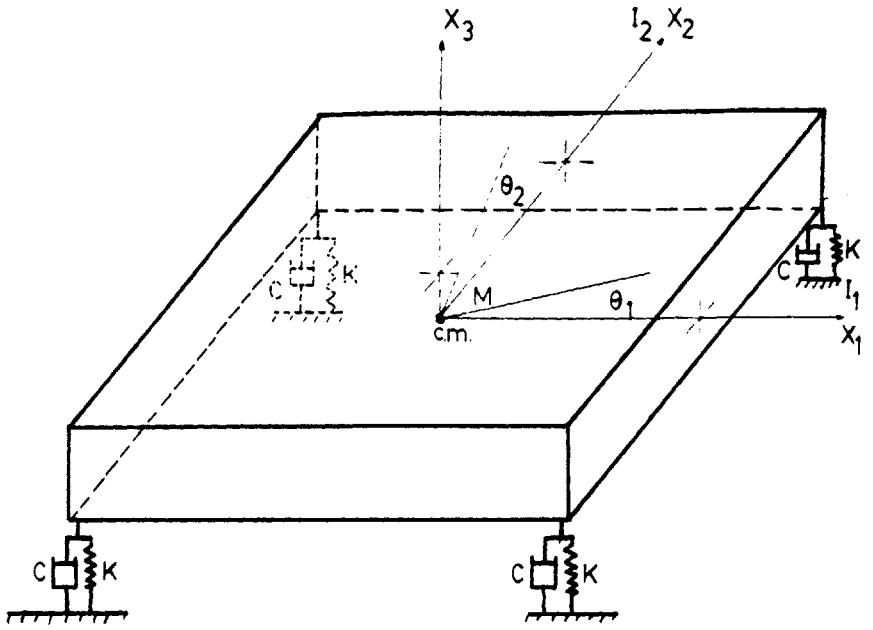

Figure 43 - Three degree of freedom model used for calculation of stand vibration modes.

This model was chosen in order to eliminate static and dynamic coordinate coupling in the equations of motion. It is fairly close to the actual case.

$$\text{I.} \quad M\ddot{X}_3 + 4C\dot{X}_3 + 4KX_3 = 0$$

$$\text{II.} \quad I_2\ddot{\theta}_1 + 2CL_1\dot{\theta}_1 + 4KL_1\theta_1 = 0 \qquad \text{(C.3)}$$

$$\text{III.} \quad I_1\ddot{\theta}_2 + 2CL_2\dot{\theta}_2 + 4KL_2\theta_2 = 0$$

Given the values of M, I_1, I_2, L_1, and L_2 vibration isolator were chosen to given 99.6% isolation.